[redacted]

Volume I of III

Unclassified Title

R-273

INTERPLANETARY NAVIGATION SYSTEM STUDY

by

J. H. Laning, Jr.
R. Battin
P. Bowditch
M. B. Trageser
R. L. Alonso
J. M. Dahlen
R. J. Magee
K. Nordtvedt
R. A. Scholten
H. H. Seward
W. E. Toth

April, 1960

[redacted]
TO
[redacted]

INSTRUMENTATION LABORATORY
MASSACHUSETTS INSTITUTE OF TECHNOLOGY
CAMBRIDGE 39, MASSACHUSETTS

Approved by: Roger B. Woodbury
Associate Director

N71-75177 (ACCESSION NUMBER) (THRU) [redacted]
170 (PAGES) None (CODE)
CR-122981 (NASA CR OR TMX OR AD NUMBER) (CATEGORY)
FACILITY FORM 602

60 W21 RN-5937

ABSTRACT

Navigation and control for Centaur interplanetary spacecraft are studied. The characteristics of interplanetary transfer trajectories to Mars and Venus and the accuracies and propellant requirements associated with interplanetary celestrial navigation were determined by analysis and machine computation. The design for a self-contained guidance and control system and studies on its components and environmental factors are presented. A discussion is given of digital computer techniques which are applicable to spacecraft navigation and control tasks.

TABLE OF CONTENTS

CHAPTER 1

GENERAL CONSIDERATIONS AND SUMMARY

by

Milton B. Trageser

TABLE OF CONTENTS

CHAPTER 1

GENERAL CONSIDERATIONS AND SUMMARY

Introduction

The objective of this study has been the formulation of practicable techniques and equipment characteristics for the navigation of interplanetary spacecraft to be launched by Centaur boosters beginning in 1964. It is clear that two fundamental conditions prevail, and these have directed the course of the investigation. First, a detailed description of spacecraft missions and configurations does not at present exist. Second, it is known that the accomplishment of the navigation and stabilization functions will require the development of a well-integrated guidance and control system.

In analytical work, therefore, we have focused our attention on orbital and navigational calculations which are applicable to interplanetary missions in general. Similiarly, in equipment studies we have evolved a self-contained guidance and control system (see Fig. 1-1) which could be packaged in a small cylindrical container and which would require little or no adaptation to permit integration with a wide variety of Centaur payload configurations.

Before presenting the results of the study, it is interesting to speculate on the various application of such a guidance and control system. It can be anticipated that interplanetary spacecraft within the domain of Centaur payloads and within the time period under consideration will probably conduct these missions by using one or a combination of the following operations:

1. the atmospheric injection of an aerodynamic vehicle on a trajectory of some specified maximum acceleration for landing on the planet,

2. the injection of the spacecraft into satellite orbit about the planet, more or less accurately,

3. the accurately guided passage of the spacecraft near the planet, perhaps for effective reconnaissance,

4. the accurately guided passage of the spacecraft near the planet with its later return to the earth or its vicinity for the landing of a recovery capsule or for the communication of large quantities of stored data at short range.

Preliminary analysis indicates that many probable guidance and control requirements for the above operations can very likely be met by a guidance and control system which would weigh 70 pounds and be packaged in a cylinder having a 11-inch diameter and a 22-inch length.

I Orbital Calculations

The results of extensive orbital calculations on transfer trajectories from the earth to Mars or Venus are presented in Chapter 2 of this report. The characteristics of these trajectories are given as contours on plots of launch date versus transit time. The data presented include the required orbital injection velocity, the location of the injection point, the approach velocity relative to the subject planet, and the communication range and angle from the sun at the time of approach.

All of these calculations have been carried out using a three dimensional solar system and elliptical planetary orbits. One can observe the significance of these effects by comparison of the 1962 and 1964 Mars trajectories, for example. These plots can not be overlaid without discrepancies of approximately two tenths of a year.

The studies indicate the desirability of considering some longer transit time trajectories for certain applications. For example, the payload into satellite orbit around Mars is much greater using a trajectory having an 0.85 year transit time rather than one requiring only 0.5 years due largely to the low relative velocity of approach to Mars for the longer transit orbit.

II Navigational Calculations

Several trajectories to Mars and Venus were used in the navigation optimization studies presented in Chapter 3. Using the angles between pairs of celestial bodies including the sun, the two nearest planets (including the moon), and the ten brightest stars, the inaccuracy in spacecraft position determination was calculated at regular times along the trajectory. The "best" combination of observations for each time was determined.

Numerous combinations of these optimum fixes were used in analysing the amount of maneuvering required and the resulting accuracies in the arrival at the subject planet. The relationship between the required maneuvers for a given navigational accuracy is shown.

The results obtained in this optimization program were substantially better than those reported in R-235* because of the greater generality permitted in the positional fix and the use of variable-time-of-arrival navigation. A maneuvering capability of 150 ft/sec. rms. is sufficient to obtain navigational accuracies of 15 to 50 miles rms at the destination. This accuracy is more than sufficient for most missions.

*Note: Throughout this report it is assumed that the reader has a familiarity with Instrumentation Laboratory Report R-235.

III Mission Performance

The 15 to 50 mile navigational accuracies established by the Chapter 3 studies enables the entry of experimental equipment into the atmospheres of Mars or Venus with very reasonable peak accelerations. The atmospheric entry calculations of Appendix A determine the peak drag acceleration associated with the atmospheric entry of a reasonable non-lifting aerodynamic vehicle for various velocities and points of aim. The 15 to 50 mile rms navigational errors establish the necessary atmospheric entry corridor widths of 60 to 200 miles in the point of aim if there is to be only a 0.025 probability for exceeding the specified peak accelerations and for failure to be captured by the planet. From Appendix A it is determined that these corridor widths are associated with peak accelerations of 3 to 8 earth g's for vehicles approaching Mars with a relative velocity of 10,000 feet per second. Similiarly, the specified peak accelerations for vehicles approaching Mars with a relative velocity of 20,000 feet per second are 8 to 16 g's. For Venus the corresponding peak accelerations are 15 to 45 g's for a velocity of 10,000 feet per second and 25 to 80 g's for a velocity of 20,000 feet per second.

The injection of a spacecraft into a satellite orbit about a planet can be accomplished with considerable accuracy. Obviously the location of the perigee can be established with the same order of accuracy as that with which the spacecraft can be guided to a specified point of aim. Since the velocity deviations from the nominal values at the points of aim, established in Chapter 3, are 100 to 200 feet per second, the ellipiticity of the satellite orbit can be established with an accuracy of better than 0.1 in the case of Mars. The orbital plane can have an accuracy of better than one degree.

Clearly the navigational accuracies quoted here are considerably better than needed for the effective deployment of television reconnaissance or other likely missions for near pass operations. The required accuracies, however, can be had through the use of the same guidance scheme with somewhat less propellant required for manuevers.

Round trip orbits and missions have been adequately covered in R-235. The results of the present navigation study indicate, however, that much less manuevering capability is required for the round trip orbits than indicated in R-235. This is the result of optimized fix and manuever programming.

IV Centaur Interplanetary Guidance and Control System

The guidance and control system shown in Fig. 1-1 and described in Chapter 4 is essentially a rescaled, modified, and improved version of the guidance and control system presented for the space probe in R-235. Its subsystems include a general purpose digital computer, a space sextant, an electro-mechanical assembly having flywheels, gyros, and an accelerometer, electronics for power supplies and the operation of accessories, and a thermal control. The subsystems are packaged within an environmentalized structural container. The system weighs 70 pounds and is essentially independent of the spacecraft of which it is a part. The spacecraft provides the supply of electrical energy for the operation of the system and the propulsive system to execute its manuevers.

As in R-235, the equipment is organized around a highly specialized general purpose digital computer. Much logical design technique, and circuit development for the appropriate type of computer has been carried on during the past year in connection with other Laboratory projects. A comprehensive discussion of this work is given in Appendix E of this report. Separately in Chapter 5 Section VI a discussion of the computer tailored for speacecraft is presented for contrast with the general discussion of Appendix E.

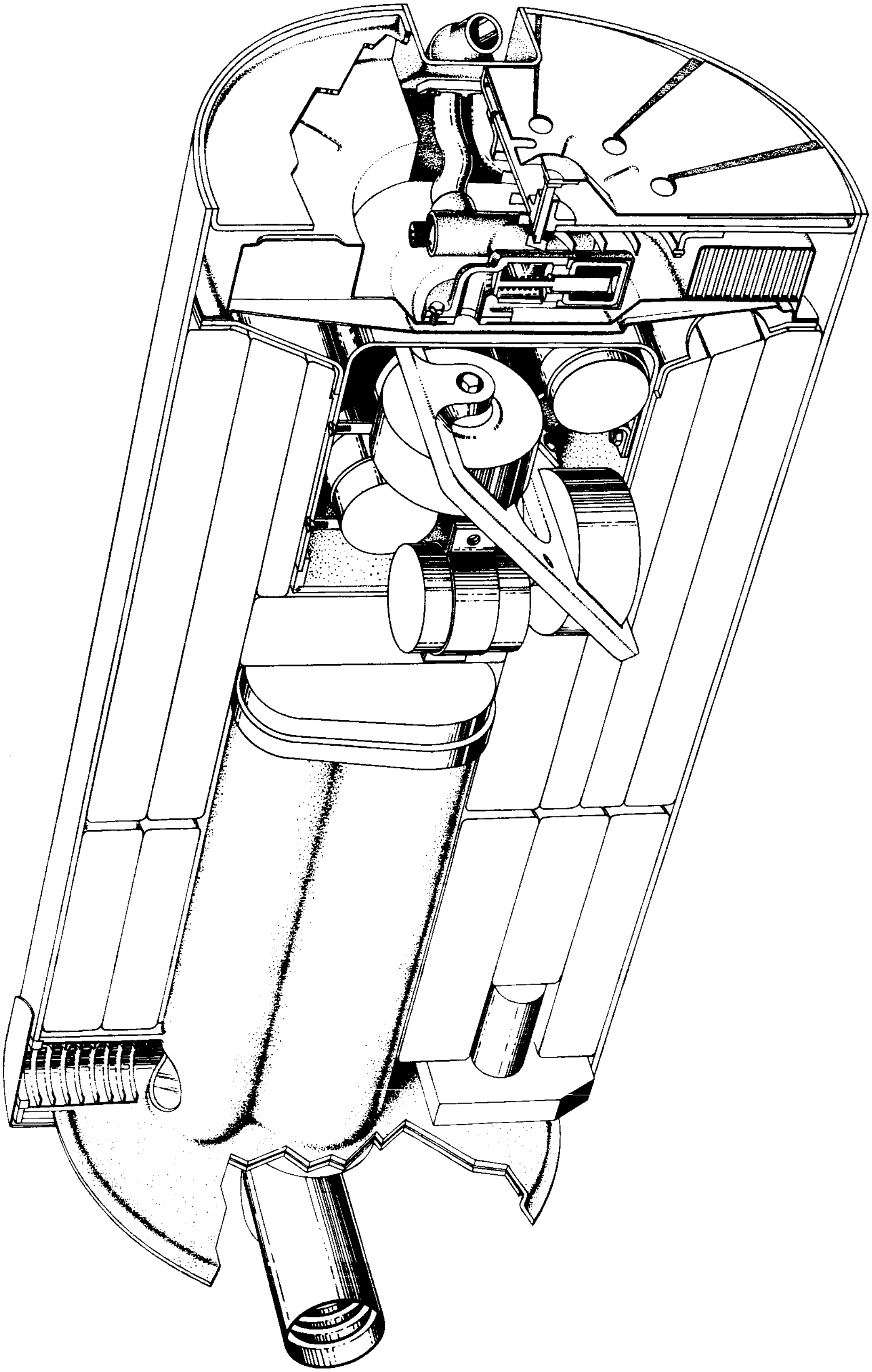

Fig. 1-1 CIGS--cutaway view.

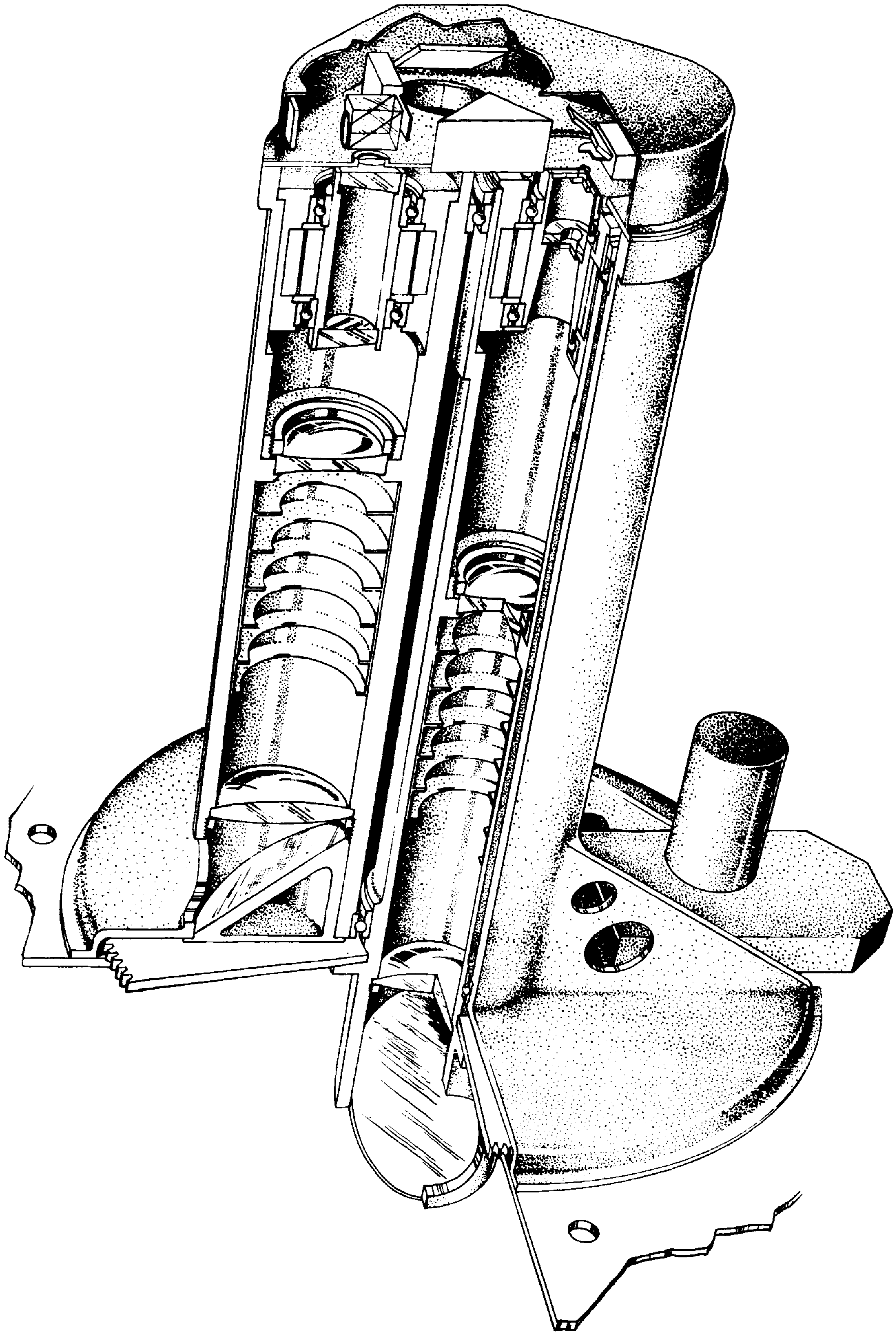

Fig. 1-2 Space sextant--cutaway view.

In addition to flywheel rescaling for a larger vehicle, other changes have been made from R-235 in order to make the operation of the guidance and control system more independent of the characteristics of the spacecraft of which it is a part. The solar vanes, an element which very strongly affects spacecraft configuration, have been replaced for angular momentum trimming by an iodine jet. The operation of this jet is described in Chapter 4 and its preliminary design is presented in Chapter 6. The use of torqued gyros for monitoring attitude changes instead of the use of flywheel revolution counting removes the need for accurate axis and moment of inertia information and results in a more accurate and versatile system.

The subsystem studies presented in Chapter 5 result in significant system improvement and development. The most prominent of these studies is the development of an improved space sextant design having greater accuracy, reliability, and simplicity. (see Fig. 1-2)

Much useful information on environmental problems has been presented in Chapter 7. Here the space and the booster environments are considered from the viewpoint of the guidance system engineer. Several novel ideas are presented including an "oily rag" concept for the oil vapor pressurization and lubrication of mechanisms which have precision and high speed moving parts and which are exposed to high vacuum.

Ref. Instrumentation Laboratory Report R-235, "A Recoverable Interplanetary Space Probe," prepared by the M. I. T. Instrumentation Laboratory in collaboration with the Avco Corporation, the Lincoln Laboratory of Massachusetts Institute of Technology, and the Reaction Motors Division of Thiokol Chemical Corporation, July 1959.

CHAPTER 2

ORBIT STUDIES

by

J. Halcombe Laning, Jr.

TABLE OF CONTENTS

CHAPTER 2

ORBIT STUDIES

This chapter is concerned with the theoretical analysis of interplanetary orbits in relation to propulsion requirements, approach velocities at Mars and Venus, and similar considerations. For the most part, the mathematical developments and techniques are those previously reported in Chapter 4 and Appendix A of Report R-235, to which the reader is referred for details. The principal changes in theory or in points of emphasis for this report relate to:

(a) enlargement of the region of search for orbits resulting from removal of the restriction that the payload return to Earth, and from increase in the maximum permissible velocity of departure from Earth,

(b) increased attention to the configuration of the planets at the time the vehicle arrives at Venus or Mars, insofar as it affects the communication link at that time,

(c) partial consideration of the geometry relating to injection.

Results of the analysis and calculations are generally presented in the form of contour maps, in which the coordinates are time of launch, T_L, and time of flight, T_F, and the contours represent constant values of the quantity under study. Results are partially interpreted in terms of the objectives of this report; however, the presentation is sufficiently general to admit other applications as well.

In Section I, an approach to the geometry of the injection problem is formulated as a background for some of the data shown later. Section II presents the main results of this chapter: plots covering Mars orbits for the period 1962-65 and Venus orbits for 1962-64 in some detail. Finally, in Section III is presented data relating specifically to the interesting prospect of placing a payload into an orbit about Mars or Venus. The calculation, though fairly approximate, gives a reasonably clear indication of the range of payload weights that can be expected with the vehicle presently under consideration.

I. Analysis of Injection Geometry for Interplanetary Orbits

The general problem considered in this section is the determination, for a specified interplanetary orbit, of a final stage burning point and a circular coasting orbit from (say) Canaveral which maximize the attainable post-injection payload. The derivation and subsequent calculations are made subject to the following procedures and assumptions:

(a) An elliptical interplanetary orbit from Earth to the destination planet is first determined, neglecting all gravitational fields except that of the Sun. This orbit is computed in three dimensions, using elliptical motions of all planets concerned.

(b) The nominal time of launch from Earth is taken to be that time at which the elliptical interplanetary orbit intersects the orbit of Earth. The velocity vector of the spacecraft relative to the Earth at this instant is denoted by $\bar{v}_r$.

(c) Injection takes place from a circular coasting orbit about a spherical rotating Earth.

(d) Motion of the spacecraft in the vicinity of Earth is assumed to be along a hyperbolic path relative to Earth, and such that the asymptotic value of the relative velocity vector is the vector $\bar{v}_r$ defined in (b) above.

(e) It is assumed that the actual time of launch can vary twelve hours or more from its nominal value without seriously affecting the interplanetary orbit parameters. As a result, it is assumed that the circular coasting orbit plane may be rotated arbitrarily about the North polar axis. Stated otherwise, once the desired spatial orientation of this plane is determined, it is assumed that the Earth may be so rotated as to bring the launch point into this plane at the nominal time of launch.

(f) Injection is presumed to occur via an instantaneous change of velocity from the circular coasting orbit to the hyperbola. This is assumed to occur in the horizontal plane so that this point is the vertex of the hyperbola.

(g) The point of injection is presumed to be independent of geographic restrictions; it may occur anywhere about the circle that is otherwise suitable*. It is assumed to take place during the first trip around the orbit, however.

Before proceeding, a few additional remarks in elaboration or qualification of these assumptions are in order. In the first place, the computations presume Canaveral as a specific launch point, and further designate one of three selected values (45°, 100°, 110°) for the azimuth direction of the coasting orbit through the

---

* Actually, shipboard tracking of the injection phase is postulated, but the calculation does not itself verify that injection occurs over an ocean area.

launch point. This in turn specifies the angle of inclination of the coasting orbit to the equatorial plane. In view of this, (e) above means that exactly one degree of freedom (namely, rotation about the polar axis) is available in fixing the plane of the coasting orbit. The combination of Canaveral and a specified value of azimuth can, of course, be replaced, without altering the results, by any other such combination that gives the same inclination angle. With regard to assumption (g), it has proved simpler computationally to determine the optimum location for injection around the coasting orbit and only afterwards to compute where this point lies on the Earth's surface. Thus, plots relating to injection location are presented, which can than be examined with the aid of a map.

Item (f) is a simplifying assumption which has the desirable effect of eliminating one rather awkward parameter from the calculations at relatively little cost. If one considers the problem of transition from a completely specified circular coasting orbit into a hyperbolic motion resulting in a specified asymptotic velocity vector, the one available parameter is the location around the circle at which the transition occurs. For each such location there is a readily computable impulsive velocity change, determined in both magnitude and direction, which will place the vehicle on a hyperbola with the desired terminal velocity. The theory is simple enough so that one would hope to obtain optimum results by purely analytic means; the author has not yet been able to do this. Rather simple numerical studies, however, have shown that for reasonable ranges of values of the parameters (magnitude and direction of the asymptotic velocity) the following interesting property is in evidence. Considering permissible injections to occur with a velocity impulse which lies either <u>in</u> or <u>above</u> the horizontal plane, the horizontal injection is always best. However, in a large class of cases, slightly improved results (i.e., a smaller required impulse) can be attained by allowing a small downward component to appear in the velocity impulse. At a nominal altitude of 126 miles, a velocity vector tilted a few degrees downward could perhaps be tolerated, if a lower limit of 100 miles altitude were acceptable in the post-injection phase. Since the velocity reduction does not appear to be large in any cases except those in which the required impulse itself seems too large to be acceptable, this possibility has not been followed through to any further conclusion.

With the preceding material as background, consider briefly the mathematical analysis of the injection problem: Given (a) from the interplanetary orbit calculation, the components v'_{rx}, v'_{ry}, and v'_{rz} of the asymptotic relative velocity vector, referred to an inertial set of axes in which x is in the direction of the vernal equinox, and the x, y plane is the ecliptic; (b) the launch point latitude and longitude ϕ_L, θ_L relative to the Earth; (c) an azimuth angle α_L of the velocity vector at launch. The requirements are:

(a) orientation of the circular orbital plane by rotation about the North polar axis (i.e., performing the equivalent act of determining the time of day of launch),

(b) location of the injection point, i, about the circular orbit,

(c) orientation of the plane of the hyperbola about the direction of $\overline{v}_r$ as an asymptote (this step is not independent of (a) and (b)),

such that the velocity impulse in transition from coasting orbit to hyperbola is minimized, subject to the assumptions made.

First resolve $\overline{v}_r$ into components associated with the Earth's polar axis equatorial plane, according to the relations

$$\left.\begin{aligned} v_{rx} &= v'_{rx} \\ v_{ry} &= v'_{ry} \cos \epsilon - v'_{rz} \sin \epsilon \\ v_{rz} &= v'_{ry} \sin \epsilon + v'_{rz} \cos \epsilon \end{aligned}\right\} \tag{2-1}$$

where ϵ is the angle of inclination of the ecliptic ($\cong 23.5^{\circ}$).

Let β be the angle made between the circular orbital plane and the equatorial plane, as shown in Fig. 2-1. Then β may be calculated from

$$\cos \beta = \cos \phi_L \sin \alpha_L \tag{2-2}$$

Now if the injection velocity impulse is constrained to lie in the horizontal plane, so that it occurs at the vertex of the hyperbolic path, there is a unique magnitude v_h required for the hyperbolic velocity immediately after injection in order to achieve a desired magnitude v_r of velocity asymptotically. This magnitude is

$$v_h = \sqrt{v_r^2 + \frac{2\mu}{r}} , \tag{2-3}$$

where r is the radius of the coasting orbit and μ is the gravitational constant of Earth. The impulse required to achieve v_h from the velocity

$$v_c = \sqrt{\frac{\mu}{r}} \tag{2-4}$$

of the coasting orbit is given by

$$\Delta v = \sqrt{v_h^2 + v_c^2 - 2 v_h v_c \cos \psi} , \tag{2-5}$$

where ψ is the angle (in the horizontal plane) between v_c and v_h. Since v_r is specified from the desired interplanetary orbit characteristics and r, the radius of the coasting orbit, is given, both v_c

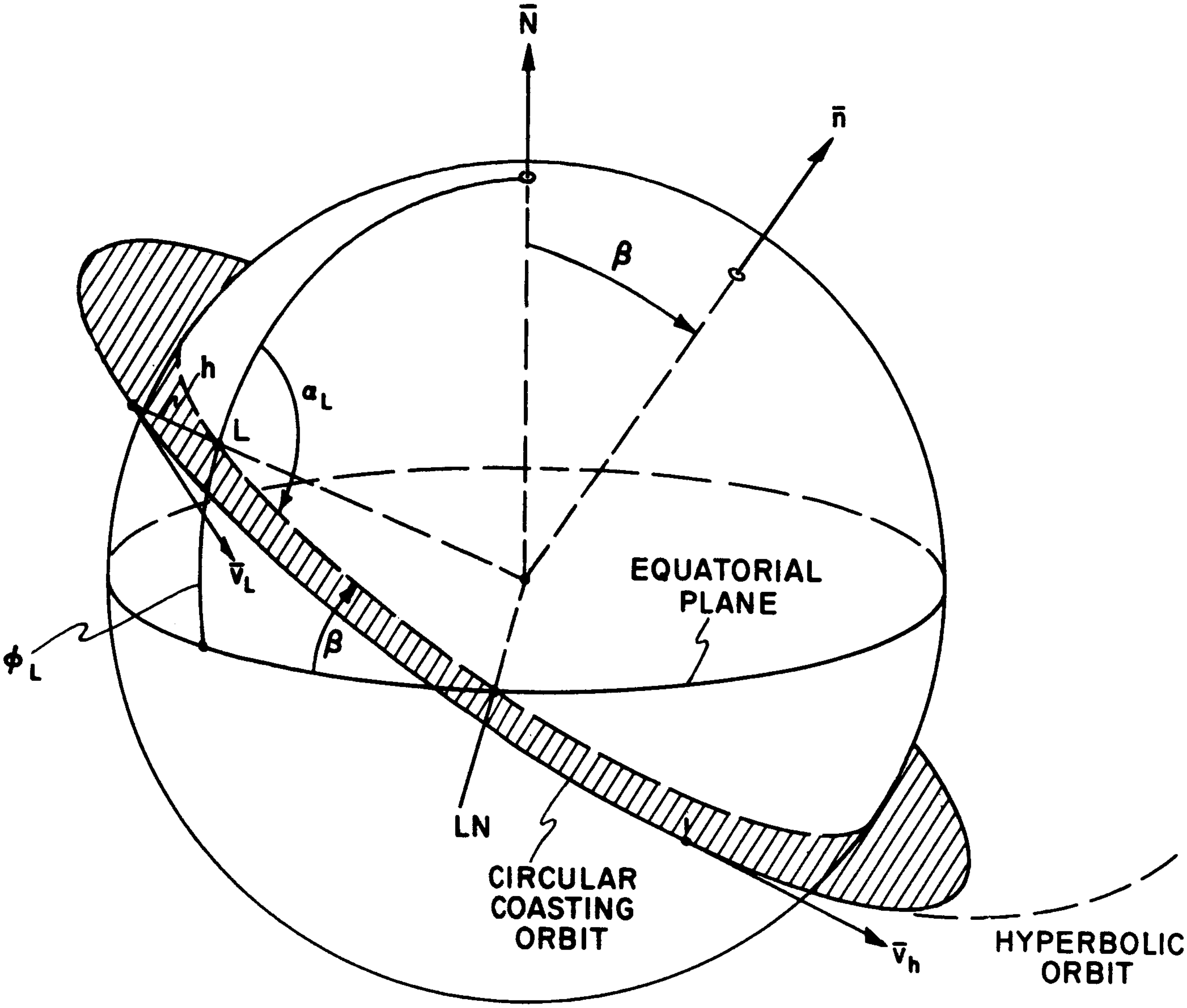

Fig. 2-1 Geometry of coasting orbit.

and v_h are determined. The only variable in Eq (2-5) that can be altered by selection of the orientation of the coasting orbital plane is the angle ψ; clearly ψ is to be made as small as possible if Δv is to be minimized.

At this point a relatively simple geometric construction permits solution of the minimization problem. ψ is the angle between the planes of the circular and hyperbolic orbits. Let the vector $\overline{n}$ (Fig. 2-1) be the unit vector normal to the coasting orbit and let γ (Fig. 2-2) be the angle from $\overline{v}_h$ to $\overline{v}_r$. If $\overline{v}_r$ is broken into components parallel and normal to the direction of $\overline{r}$, the radius vector common to the two planes (i.e., the vector drawn from the center of the Earth to the injection point), and if it is further noted that $\overline{r}$ is normal to $\overline{n}$, then

$$\overline{n} \cdot \overline{v}_r = v_r \cos \gamma \sin \psi . \tag{2-6}$$

Since γ depends only on v_r, Eq (2-6) states that $|\psi|$ is minimized by minimizing the scalar product $|\overline{n} \cdot \overline{v}_r|$; that is, by making the direction of $\overline{n}$ as close to orthogonal to $\overline{v}_r$ as is possible.

The vector $\overline{n}$ has one degree of freedom; it describes a cone about the North polar axis with the fixed angle β (Fig. 2-1). If we construct a plane through the center of the Earth and normal to $\overline{v}_r$, it is clear that this plane intersects the cone twice or not at all (or is tangent to it, in one isolated case). In the former case, there are two distinct directions of $\overline{n}$, the two lines of intersection, in which

$$\overline{n} \cdot \overline{v}_r = 0 . \tag{2-7}$$

In the latter case, $\overline{n} \cdot \overline{v}_r$ is made as small as possible by assigning $\overline{n}$ the direction of the trace on the cone which lies closest to the plane; that is, the trace whose projection onto the equatorial plane is 180° away from that of $\overline{v}_r$.

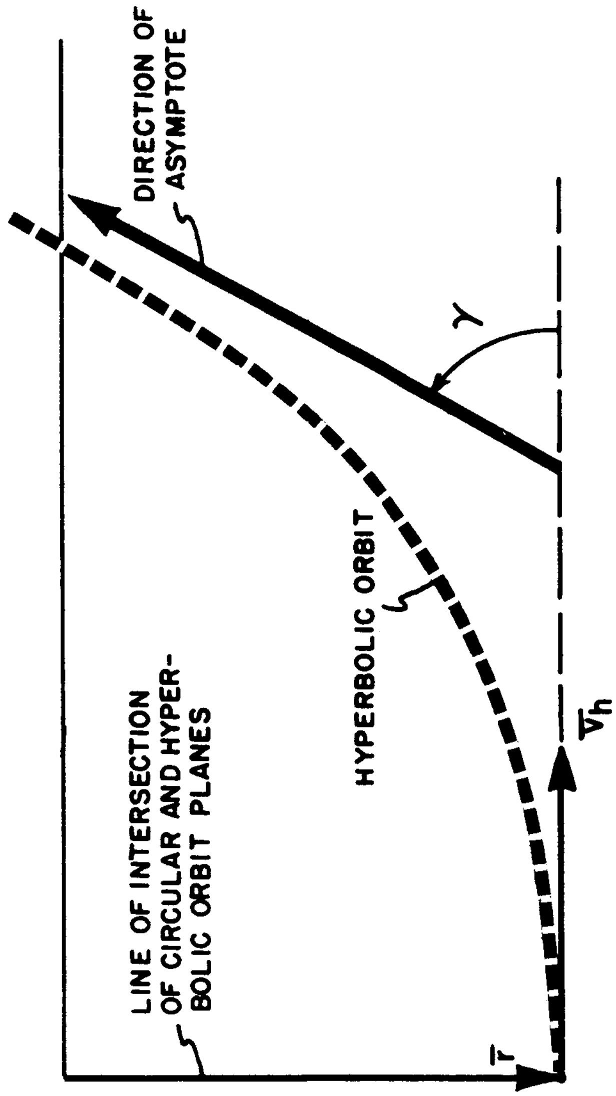

Fig. 2-2 Directions in hyperbolic orbit plane.

In the event Eq (2-7) is satisfied, we say that there exist two "optimum solutions". The corresponding angles ψ are both zero and hence the circular and hyperbolic orbit planes coincide. The two solutions are indeed distinct and lead to geographically distinct locations for injection.

Let δ be the angle between the North direction, $\overline{N}$, and $\overline{v}_r$. We assume, in what follows, that $\delta < \pi/2$. If Eq (2-7) possesses no solution, there exists a single "non-optimum" solution for which

$$\psi = \sin^{-1}\left[\frac{\cos(\beta + \delta)}{\cos \gamma}\right] . \tag{2-8}$$

Clearly for ψ to exist it is necessary that $\beta + \delta > \gamma$; if not, no horizontal injection is possible. In our computations, no cases have been noticed for which this test fails, however, such cases are quite possible theoretically.

For the non-optimum case, vectors $\overline{v}_r$, $\overline{N}$, and $\overline{n}$ are coplanar, as shown in Fig. 2-3. Let LN be the line of nodes for the coasting orbit with respect to the equatorial plane, as shown in the figure. Then the injection point is determined by the angle a in the figure, which may be computed from

$$a = \sin^{-1}\left[\frac{\sin \gamma}{\sin(\beta + \delta)}\right] \tag{2-9}$$

Fig. 2-4 illustrates the geometry of the optimum case. Here we find

$$a = \gamma \pm \cos^{-1}\left(\frac{\cos \delta}{\sin \beta}\right) . \tag{2-10}$$

in which the inverse cosine is understood to range between the values 0 and π, and the two signs correspond to the two distinct solutions.

Knowledge of the angle a for either the optimum or non-optimum case permits calculation of the total angle traversed in

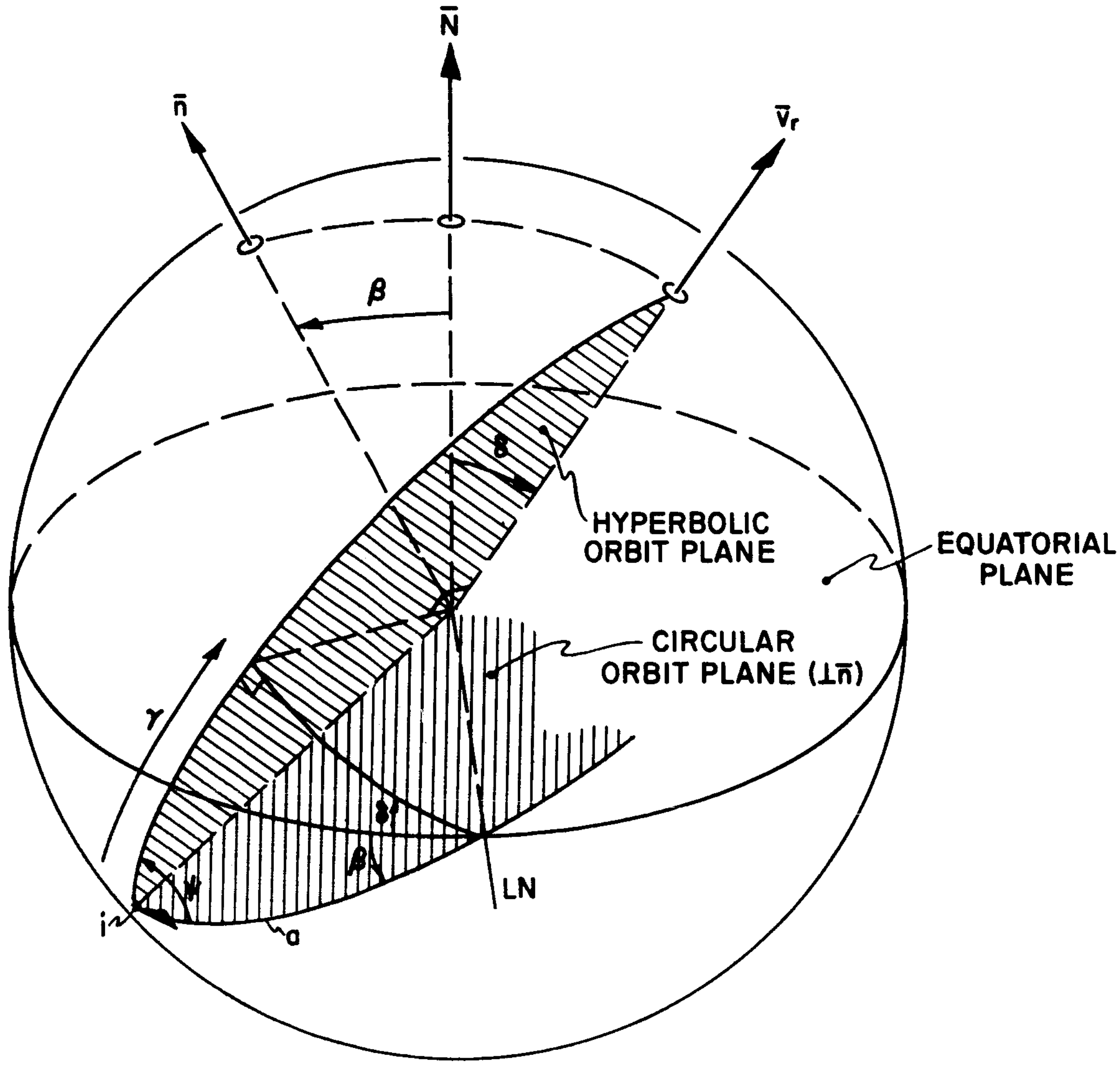

Fig. 2-3 Geometry of non-optimum injection.

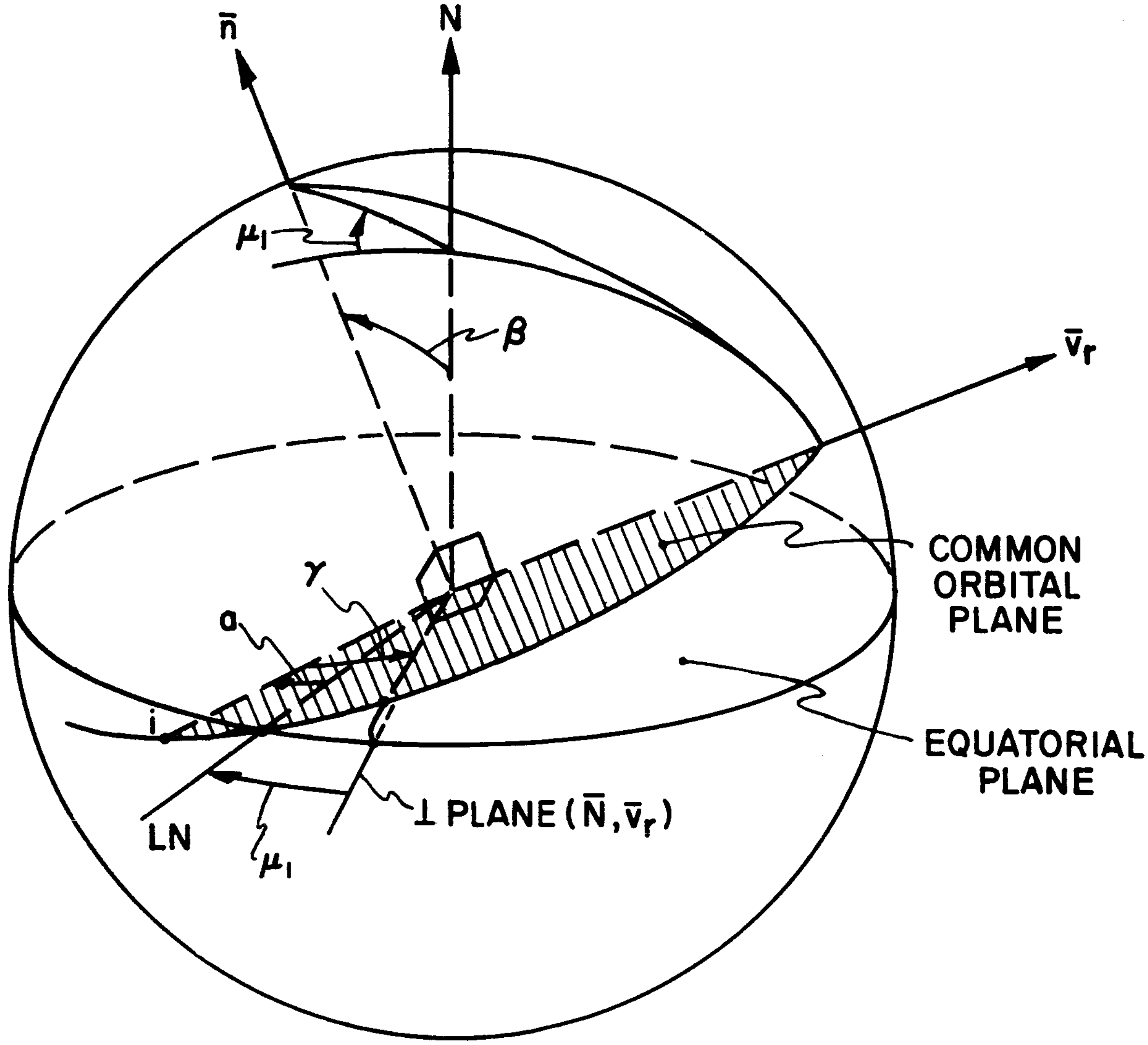

Fig. 2-4 Geometry of optimum injection.

circular orbit from launch to injection. This in turn permits computation of the required time, assuming motion at constant orbital speed. To this time has been added a correction of 200 seconds representing the approximate difference between the time actually required to climb into orbit and the time required to traverse the same distance at orbital speed. The rotation of the Earth during the period from launch to injection may then be computed and combined with the longitude traversed in a non-rotating coordinate system to yield the location of the injection point with respect to the Earth's surface.

As the final step in calculation, a quantity is computed which we call the "injection velocity", v_i, given by

$$v_i = v_c + \Delta v$$

$$= v_c + \sqrt{v_c^2 + v_h^2 - 2 v_c v_h \cos \psi} . \qquad (2\text{-}11)$$

This quantity is the same as v_h for optimum injection, and thus, under optimum conditions, depends only on v_r and not on launch azimuth. For non-optimum conditions, ψ is non-zero and v_i exceeds v_h by an amount that is a function of the particular coasting orbit selected. The quantity v_i is a direct measure of the total propulsion required to launch the spacecraft into the desired interplanetary orbit.

II. Interplanetary Orbit Data

As the first step in study of the feasible range of interplanetary orbits to Mars and Venus, a coarse orbits search was made for the purpose of outlining the general areas within which further detailed exploration was advisable. The independent variables used in this search, as in the detailed studies, were the date of launch and the time of flight. All orbital calculations were made on the basis of elliptical trajectories of both spacecraft and planets about the Sun, in three dimensions.

For the coarse search, the time of launch ranged from 1962.0 to 1967.0 at an interval length of 0.1 years, for both Mars and Venus. The time of flight values chosen were from 0.3 to 1.8 years, at an 0.1 year interval, for Mars, and from 0.1 to 1.0 years, at an interval of 0.05 years, for Venus. As a result of this search, five areas were outlined for detailed examination; they were chosen on the basis of the computed injection velocity, v_i, for the 110^o launch azimuth coasting orbit. Values of this velocity up to and including 42,000 feet per second were selected for investigation. As a result, each of these areas was covered with a series of contiguous rectangles within which orbits were computed, along with injection data for the 110^o, 45^o, and 100^o launch azimuths, at an interval of 0.02 years in both time of launch and time of flight. Due to lack of time, only four of these five areas were actually studied; they may roughly be described as the periods 1962.6 to 1963.7 and 1964.7 to 1965.8 for the planet Mars, and 1962.1 to 1963.2 and 1963.7 to 1964.7 for Venus. Altogether, approximately 6500 points were computed in this detail study. In the general region designated by the coarse search, one further Venus area, 1965.2 to 1966.3 remains to be studied, together with a fragment of an area of useful Mars orbits in the latter part of 1966.

A series of contour maps was selected as the means of displaying these data in a form which summarizes the key information relating to feasibility of various missions in an understandable way. These maps, which comprise the main body of the rest of this chapter, present plots in which launch date and time of flight are the axis coordinates. Within the areas for which data were computed (i.e., areas for which v_i does not exceed 42,000 fps), contours are drawn representing constant values of such quantities as relative velocity at the destination planet, injection velocity, and location of launch position.

The process whereby the contours were obtained involves linear interpolation between consecutive data points separated by 0.02 years (i.e., about 1 week) in either time of launch or time of flight. As finally presented, the data generally appears to be accurate to 1/16 inch or better; in the regions near 180° orbits the data points appeared to fluctuate by about this amount, whereas farther away from this region the data were quite smooth. Because of the pattern of rectangles chosen for defining the region of computation, it often happened in making the plots that a curve would pass through a region in which no data existed, only to reenter the data field at a later point. In these cases, the curves have been shown as continuing, but are composed of dashed lines to indicate that actual data points were not used.

One of the key questions concerning the relative merits of a self-contained navigation system versus one which operates primarily by a radiation link with Earth, is the feasibility of the radiation link at the time the destination planet is intercepted. Clearly those orbits which provide a severe limitation on the radiation link at intercept are more likely for consideration for a self-contained system. Granting that a communication link is necessary, in any event, at or about this time, its critical role may be somewhat reduced if it is required only to transmit scientific findings at a leisurely rate of information flow, rather than play a vital role in the control of the vehicle itself at this time. As a result, it was considered of interest to include the distance from Earth to the destination planet, as well as the apparent angle away from the Sun, in our studies.

These two quantities depend solely upon the configuration of the planets at the time of arrival at the destination. As a result, the distance R from Earth to Mars or Venus and the angle A_s made by the line of sight to the planet with the line of sight to the Sun, can conveniently be plotted as functions of the single variable $T_A = T_L + T_F$, which is the time of arrival. Plots of R and A_s are shown in Fig. 2-5 for Mars and Fig. 2-6 for Venus. To interpret these plots in relation to the contour maps shown later, it is necessary only to realize that a line of constant arrival time on the contour map is a straight line with a slope of -45^o; thus, for example, lines for the values R = 1.0 and 1.5 astronomical units are shown on the injection velocity contour of Fig. 2-8.

One of the principal differences between the present study and that done in R-235 lies in consideration of the injection problem as described in Section A of this chapter. Contour maps have been constructed representing constant values, every 30^o, of the longitude of the point of optimum injection, for one or more of the three values used for launch azimuth. To interpret these data in terms of geographic location, a map has been provided (Fig. 2-7) upon which are plotted the three coasting orbits. This was felt to be simpler and more manageable than separate longitude and latitude contours. From the contour plot, a value of longitude may be obtained, which is then used in conjunction with Fig. 2-7 to obtain geographic position.

Turning now to the main data, Fig. 2-8 to 2-21 cover the two areas of interest for Mars, and Fig. 2-22 to 2-32 the two Venus areas. The plotted contours represent selected values of injection velocity, v_i, velocity relative to the destination planet, and the first and second values of injection longitude, for various values of launch azimuth. No attempt has been made to include all of the possibilities in this presentation; rather, certain basic data are given for all four of the data sets, to which is added selected supplementary data for comparison.

The injection velocity, v_i, is the quantity computed in the previous section, eq. 2-11, and represents the total required velocity from launch to injection. It depends upon launch azimuth only in the event that the injection is non-optimum; otherwise, when the injection impulse occurs in the direction of the circular orbit velocity, v_i is identical to v_h and thus is a function only of v_r. For Mars orbits, injection has, generally, been found to be optimum. The contours of Fig. 2-8 divide naturally into two essentially disjoint areas, which are distinguished by the total angle travelled about the Sun from Earth to Mars. The lower region corresponds to the relatively faster trips which travel less than 180^o; the much larger upper region corresponds to orbits of greater than 180^o. Incidentally, no orbits were considered which travelled more than one complete revolution about the Sun. In the region generally near to 180^o, which separates the two areas of contours, the orbits are usually not close to the plane of the ecliptic because of the three dimensional character of the motion. As one result, the required velocities of departure from Earth become high, as is seen from the crowding of the injection velocity contours in this area. Another consequence is a tipping of the relative velocity vector v_r away from the equatorial plane by enough to prevent injection from being optimum. As a result, the injection velocity contours for different values of launch azimuth are found (e.g., Figs. 2-16 to 2-18) to differ primarily in the region near 180^o. Venus orbits, however, appear to include a somewhat greater proportion of non-optimum cases, as is seen by comparison of Figs. 2-27 to 2-29.

The velocity relative to the destination planet, shown in Figs. 2-9, 2-19, 2-24, and 2-30, is that computed from the elliptical solar orbits; i.e., that which would be the asymptotic value along the approach hyperbola. This quantity is of interest not only in determining feasibility of entering the planetary atmosphere

[redacted]

but also has an effect on the relation between navigation accuracy and fuel consumption in the final approach to the planet. In both instances it is advantageous that the relative velocity be low. Therefore, it is a pleasant surprise to note that, for Mars, the regions of low values for relative velocity at Mars appear to more or less coincide with a region of relatively low injection velocity required to achieve the orbit. Unfortunately, these areas in no manner coincide with a region in which the distance from Earth to Mars is low upon arrival. For Venus, however, most of the orbits fall within a region in which the distance from Earth is one astronomical unit or less at arrival.

There is relatively little to say about the contours of constant injection longitude, except to note that, in the case of non-optimum injection for which only one value of injection longitude exists, it has been designated as injection longitude 1. The region in which the curves are closely crowded together again corresponds to that of approximately 180° orbits. Only for the Mars 1962-63 case have injection longitudes been shown for other than the primary launch azimuth of 110°.

III. Orbital Payload Capabilities

One of the more intriguing possibilities for the type of vehicle considered in this report is that of placing a significant scientific payload into orbit about Mars or Venus. To explore this possibility, even though briefly, a rather approximate set of assumptions was made leading to the contour maps shown in Figs. 2-33 to 2-36. These contours show the payload weight which can be placed into orbit according to the relations which follow:

m_o = interplanetary payload (lbs)

= $2480 - 0.36\,(v_i - 36000)$

$\Delta v = \Delta v_n + \Delta v_o$

[redacted]

60WWRN - 5337

[redacted]

Δv_n = 300 fps = assumed constant velocity increment required for navigation

$$\Delta v_o = \sqrt{v_{rp}^{\,2} + \frac{2\mu_p}{r}} - \sqrt{\mu_p \frac{(1+\epsilon)}{r}}$$

= velocity increment required to enter an elliptical orbit of eccentricity ϵ and minimum radius r about a planet of gravitational attraction μ_p from a hyperbolic path with asymptotic relative velocity v_{rp}.

$$m_p = m_o \left\{ \left[(1+k) \ \exp\left(-\Delta v / I_{sp}\, g\right) \right] - K \right\}$$

= payload mass into orbit

where I_{sp} is the assumed specific impulse and where K is the ratio W_T/W_F of tank weight to fuel weight.

A fixed minimum orbital radius of 6000 miles was assumed with a value ϵ = 0.9 for eccentricity selected to make the required velocity impulse small. Two cases were considered, corresponding to low and high thrust vehicles:

Case A: I_{sp} = 200 sec., W_T/W_F = 0.1

Case B: I_{sp} = 300 sec., W_T/W_F = 0.25

It is seen from the plots that the two cases significantly affect the available payload capability, but that in either extreme a 500 lb capability would appear quite feasible.

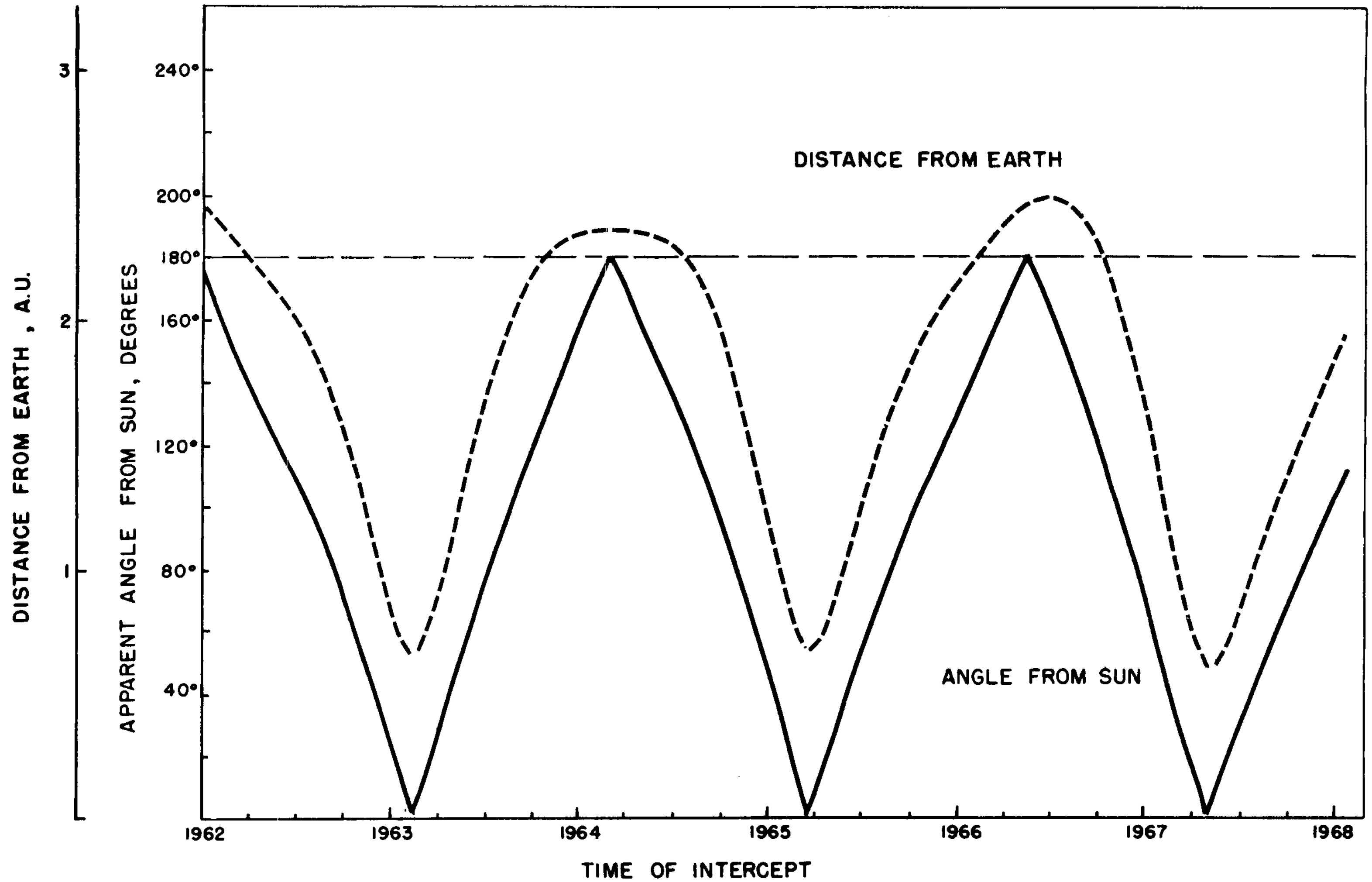

Fig. 2-5 Distance from Earth and apparent angle from sun at intercept with Mars.

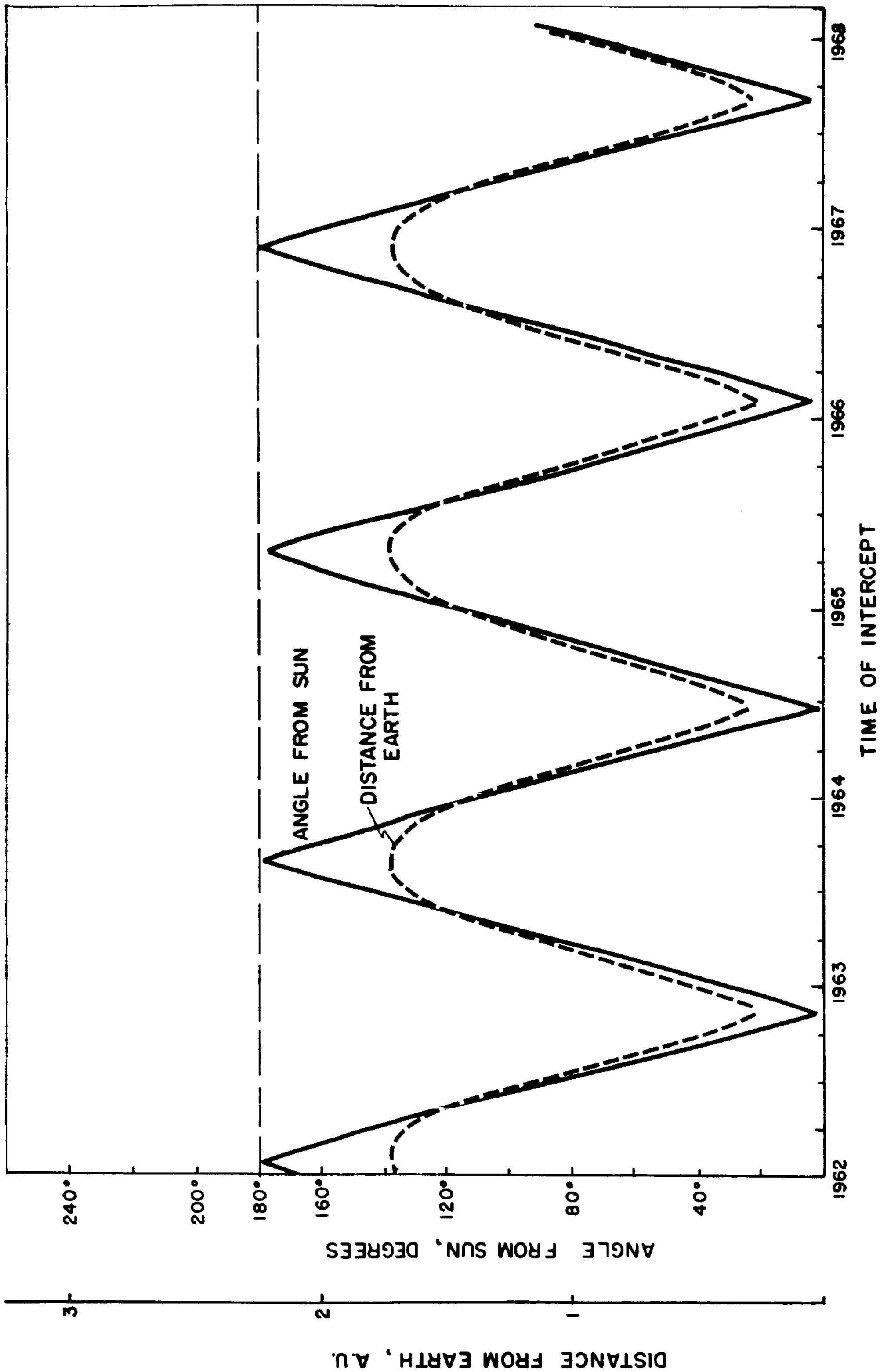

Fig. 2-6 Distance from Earth and apparent angle from sun at intercept with Venus.

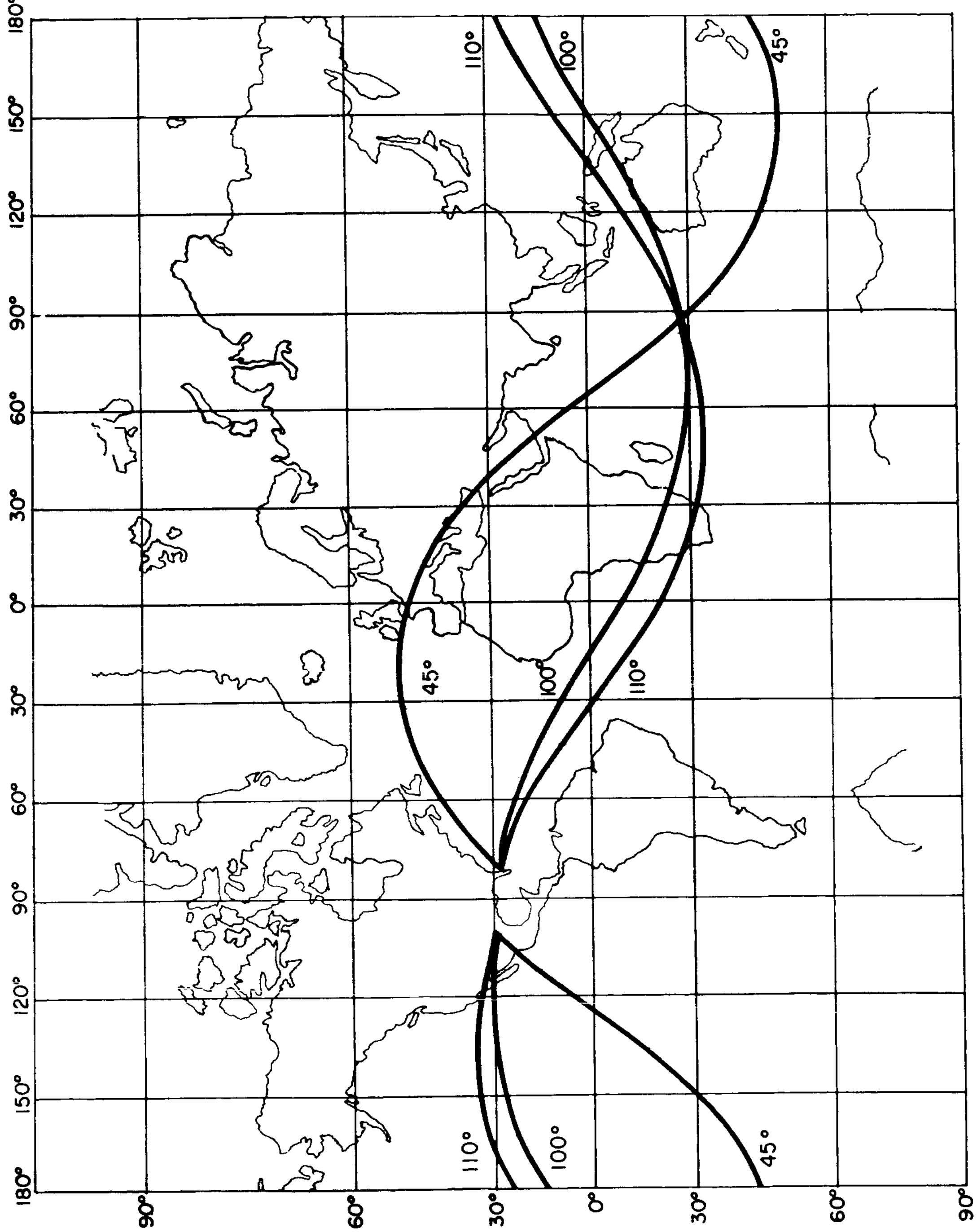

Fig. 2-7 Loci of points of injection.

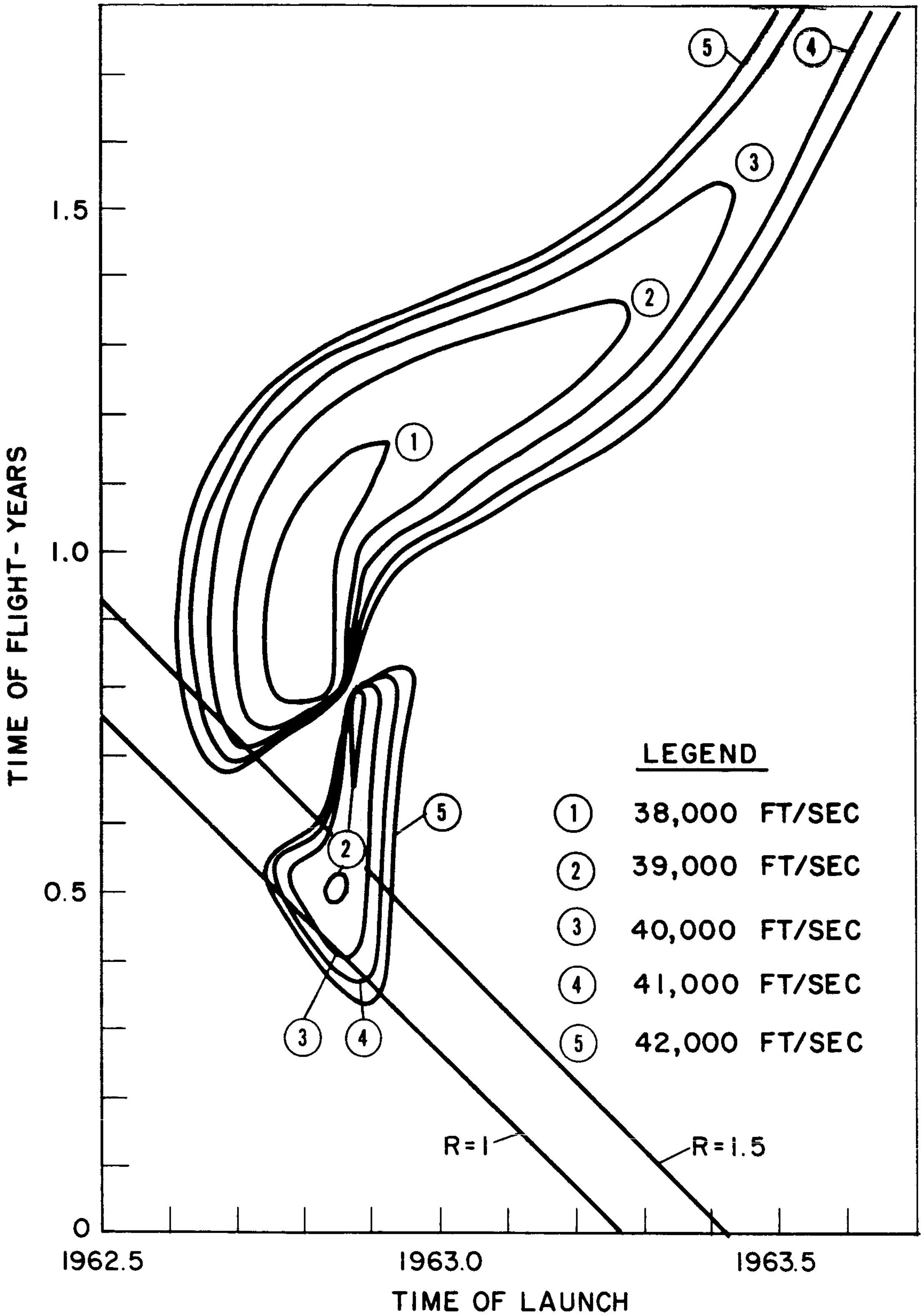

Fig. 2-8 Injection velocity--Mars 110° launch azimuth.

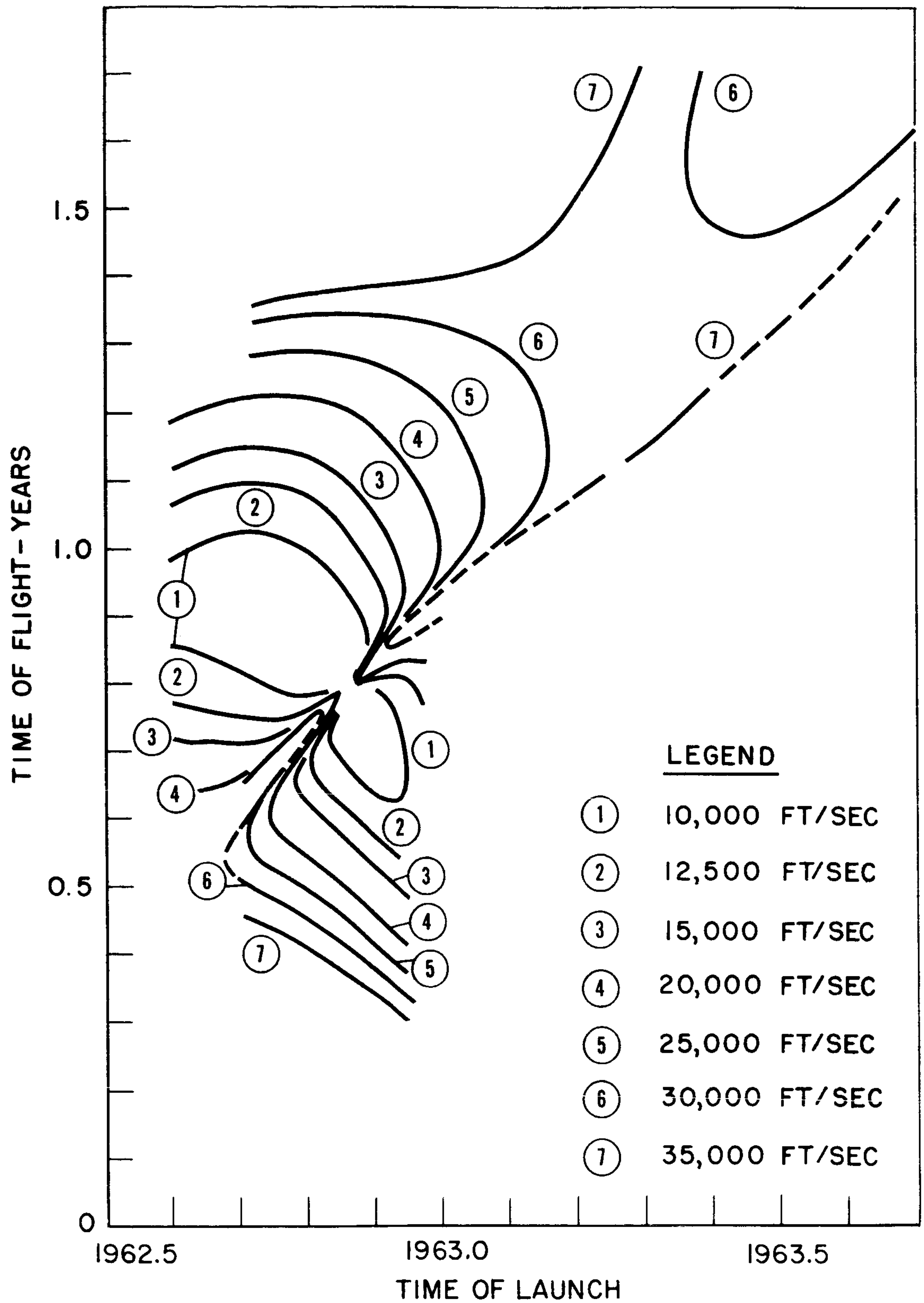

Fig. 2-9 Velocity relative to Mars.

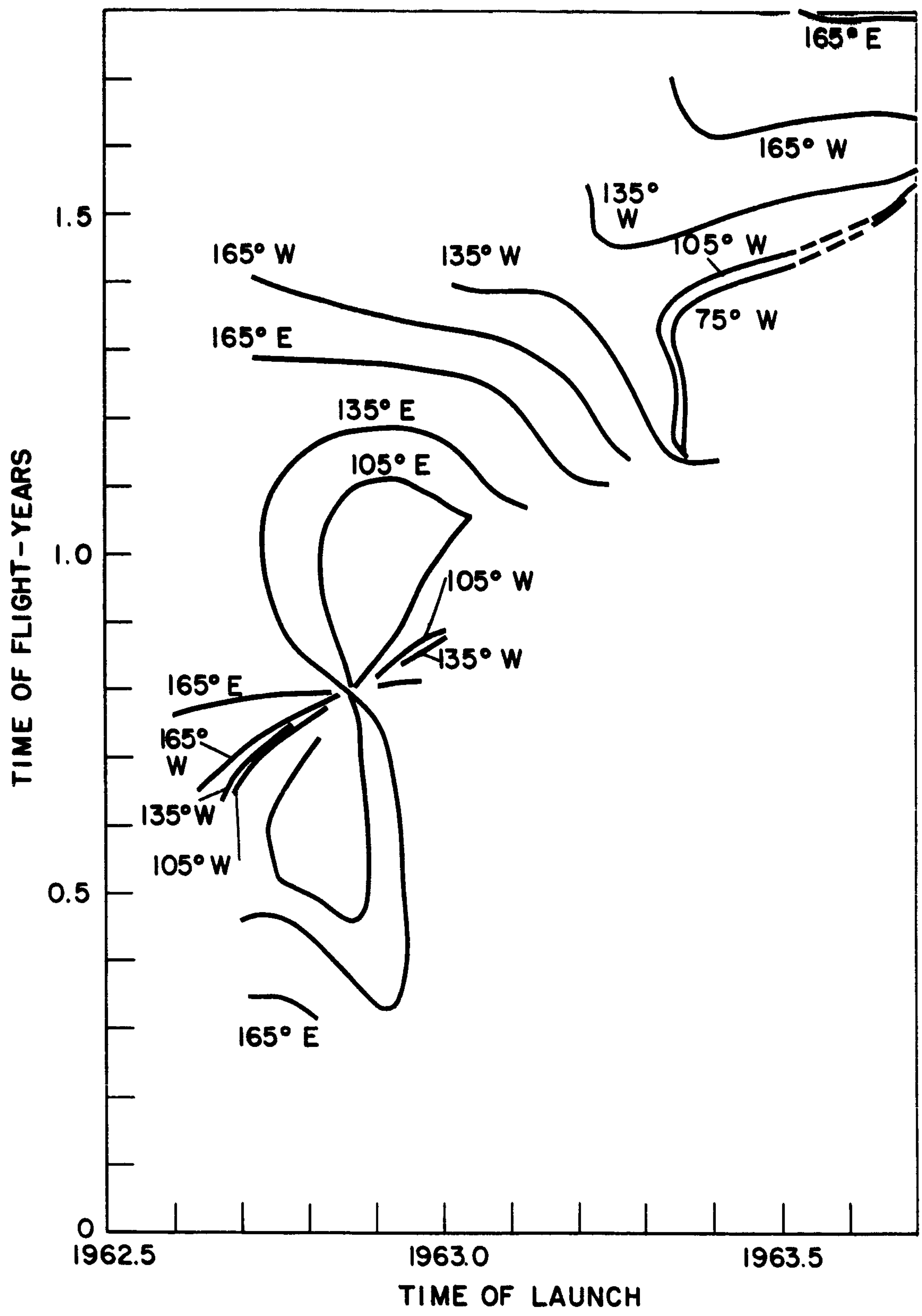

Fig. 2-10 Injection longitude 1--Mars 110° launch azimuth.

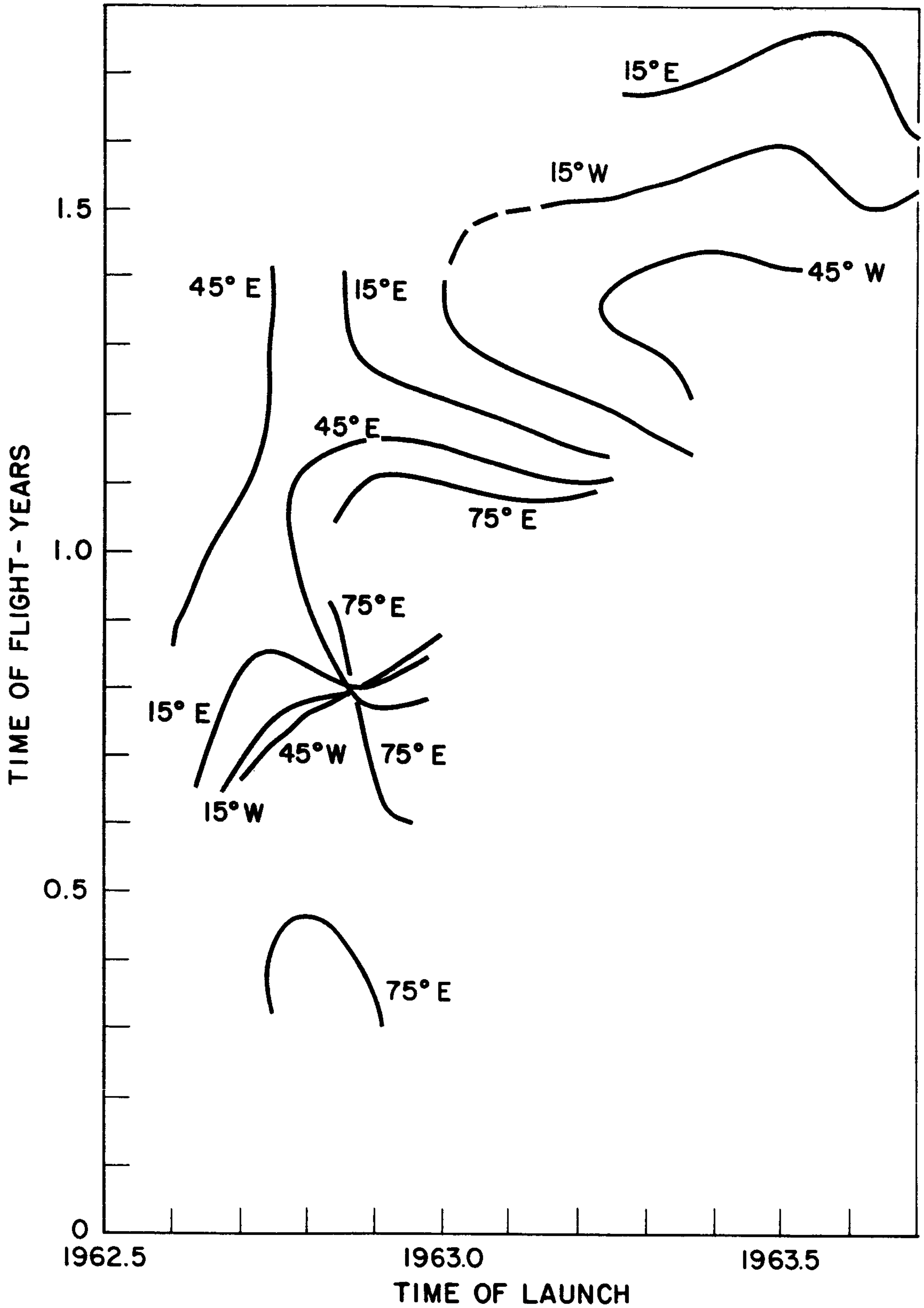

Fig. 2-11 Injection longitude 2--Mars 110° launch azimuth.

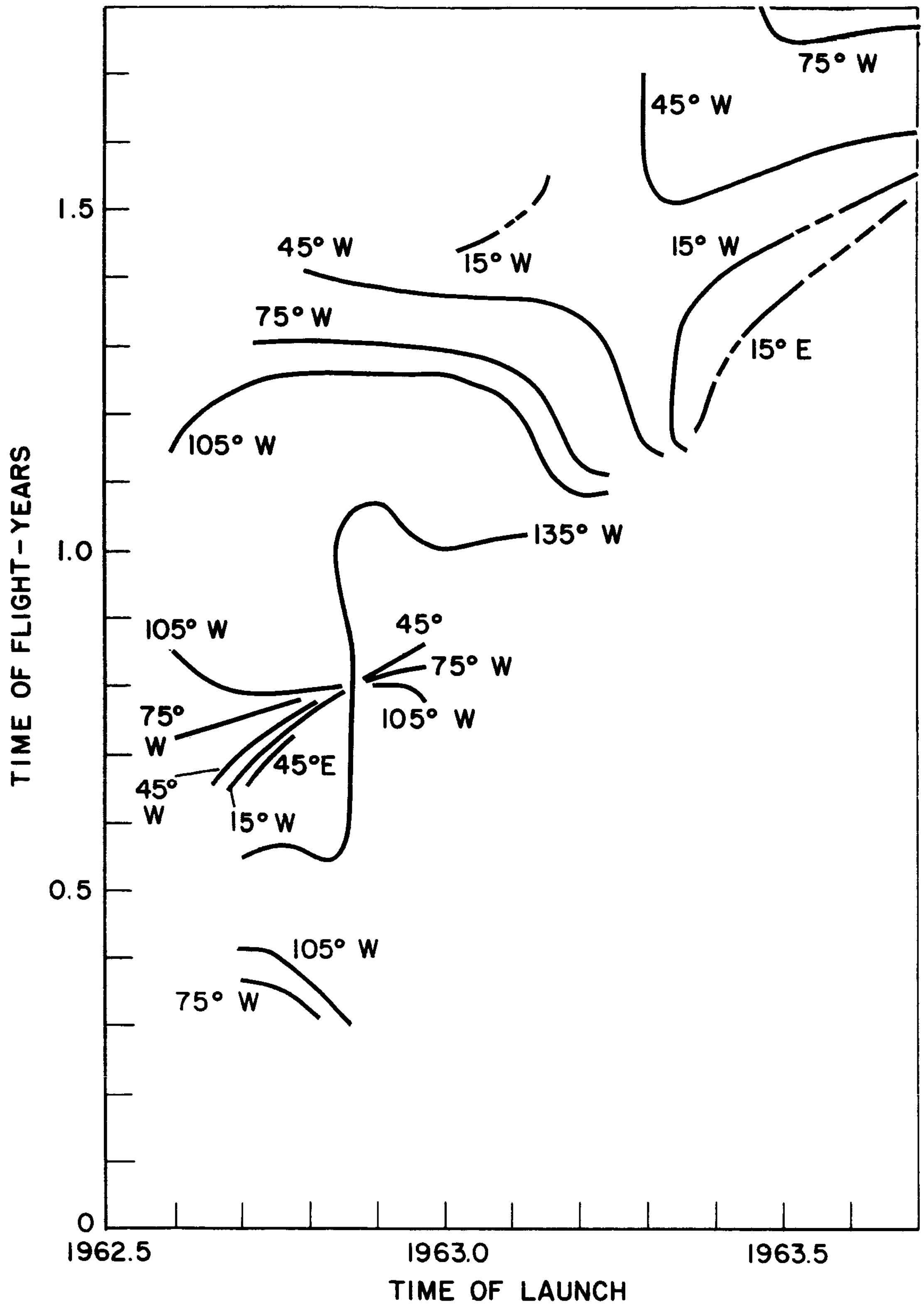

Fig. 2-12 Injection longitude 1--Mars 45° launch azimuth.

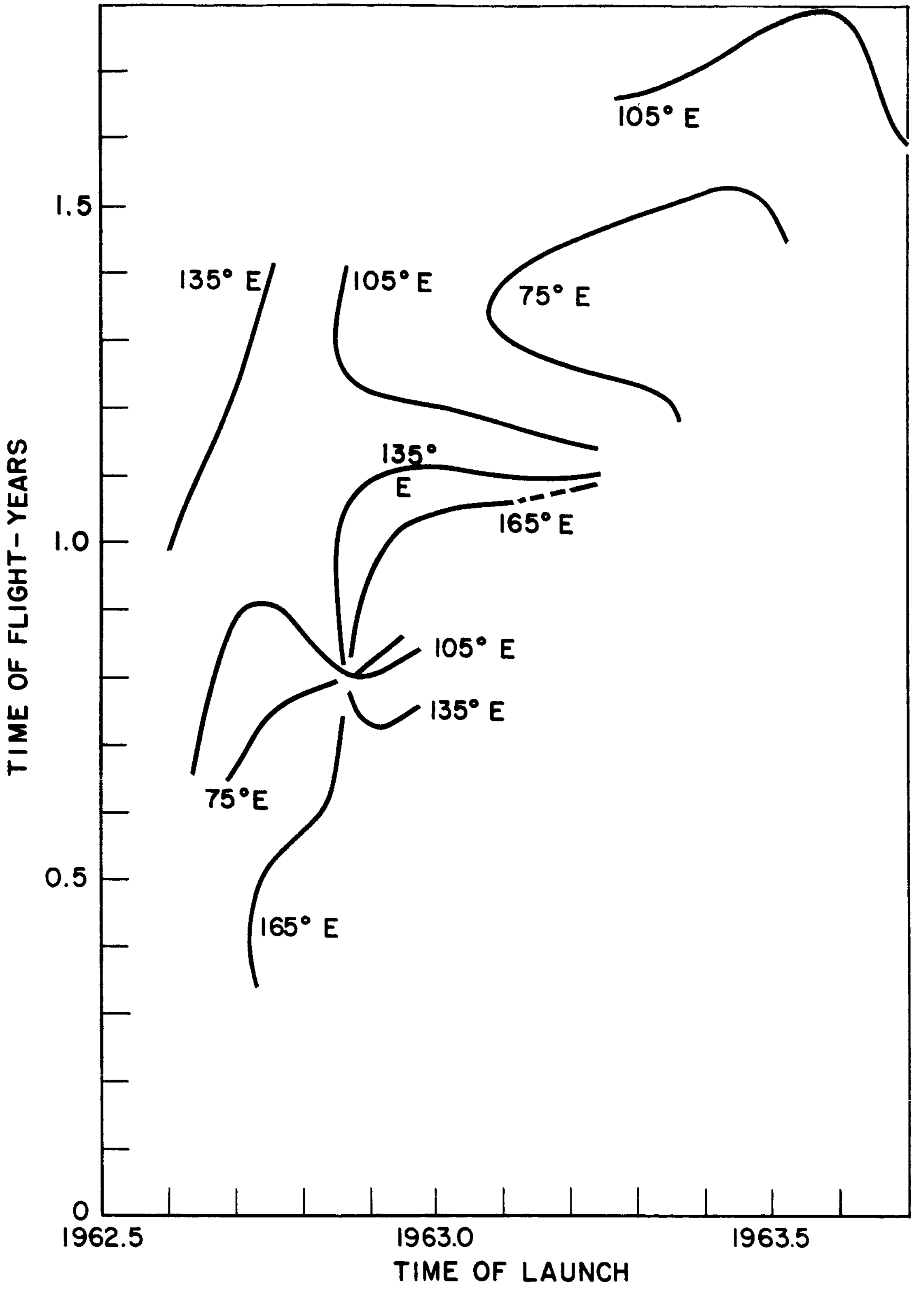

Fig. 2-13 Injection longitude 2--Mars 45° launch azimuth

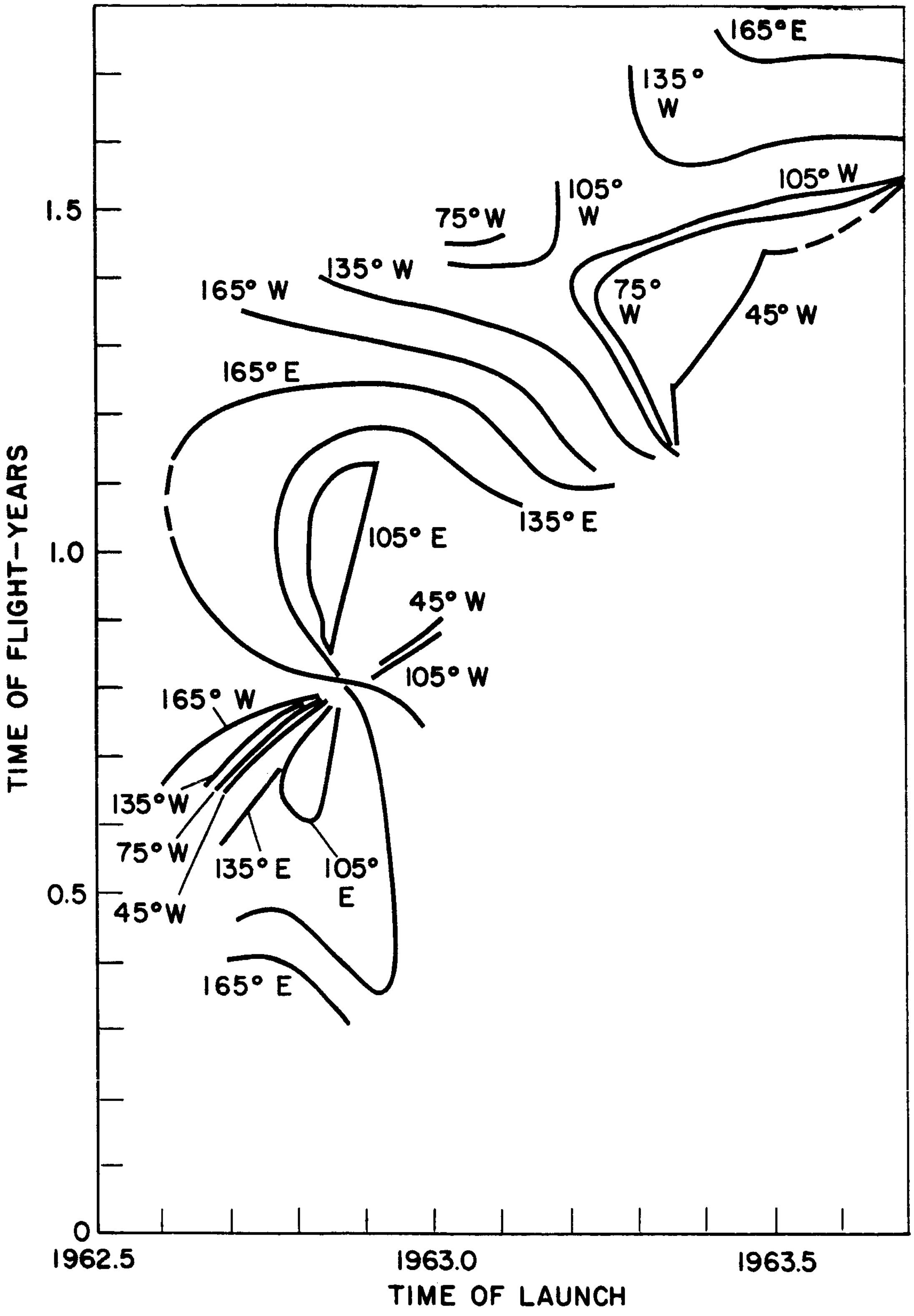

Fig. 2-14 Injection longitude 1--Mars 100° launch azimuth.

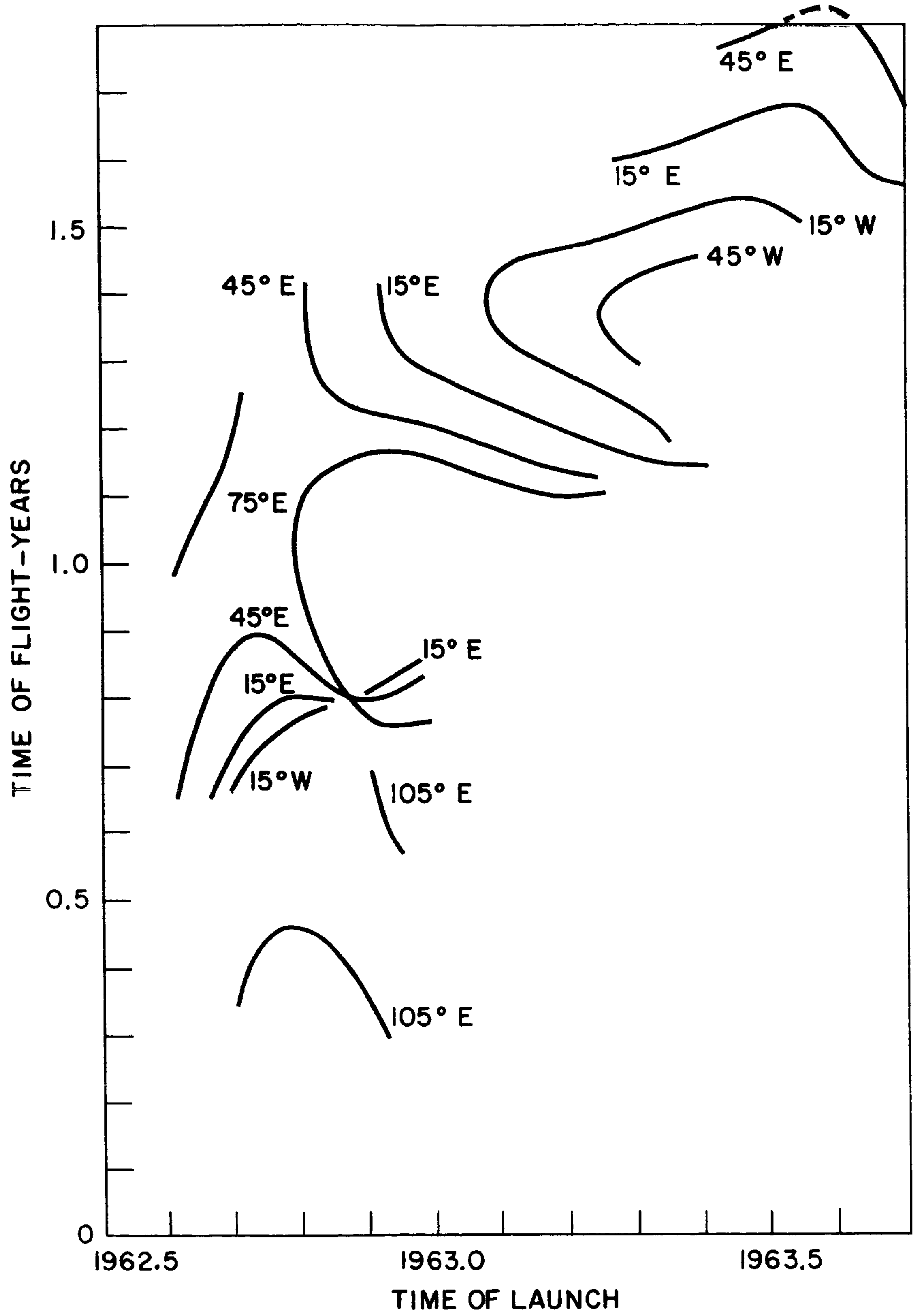

Fig. 2-15 Injection longitude 2--Mars 100° launch azimuth.

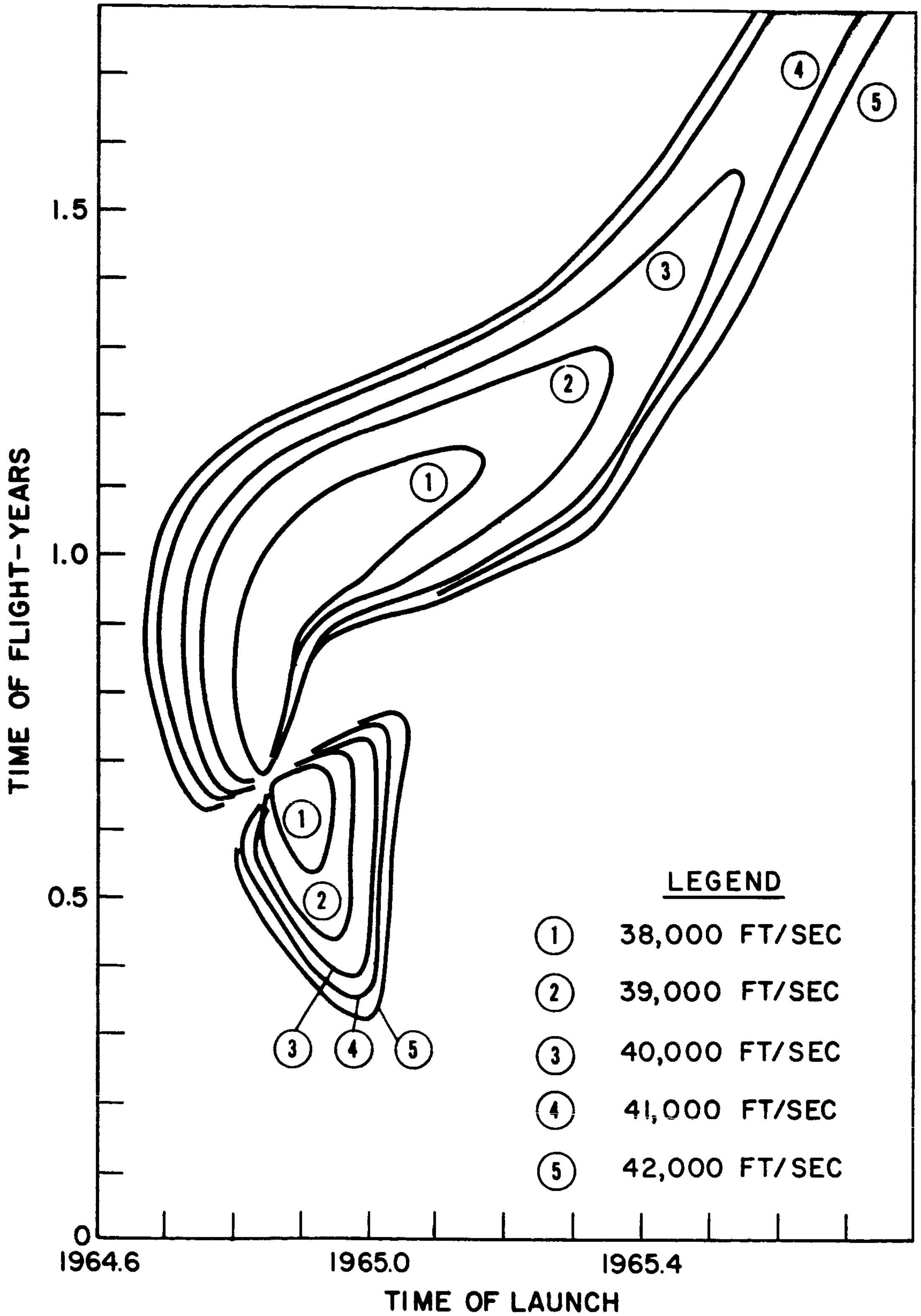

Fig. 2-16 Injection velocity--Mars 100° launch azimuth.

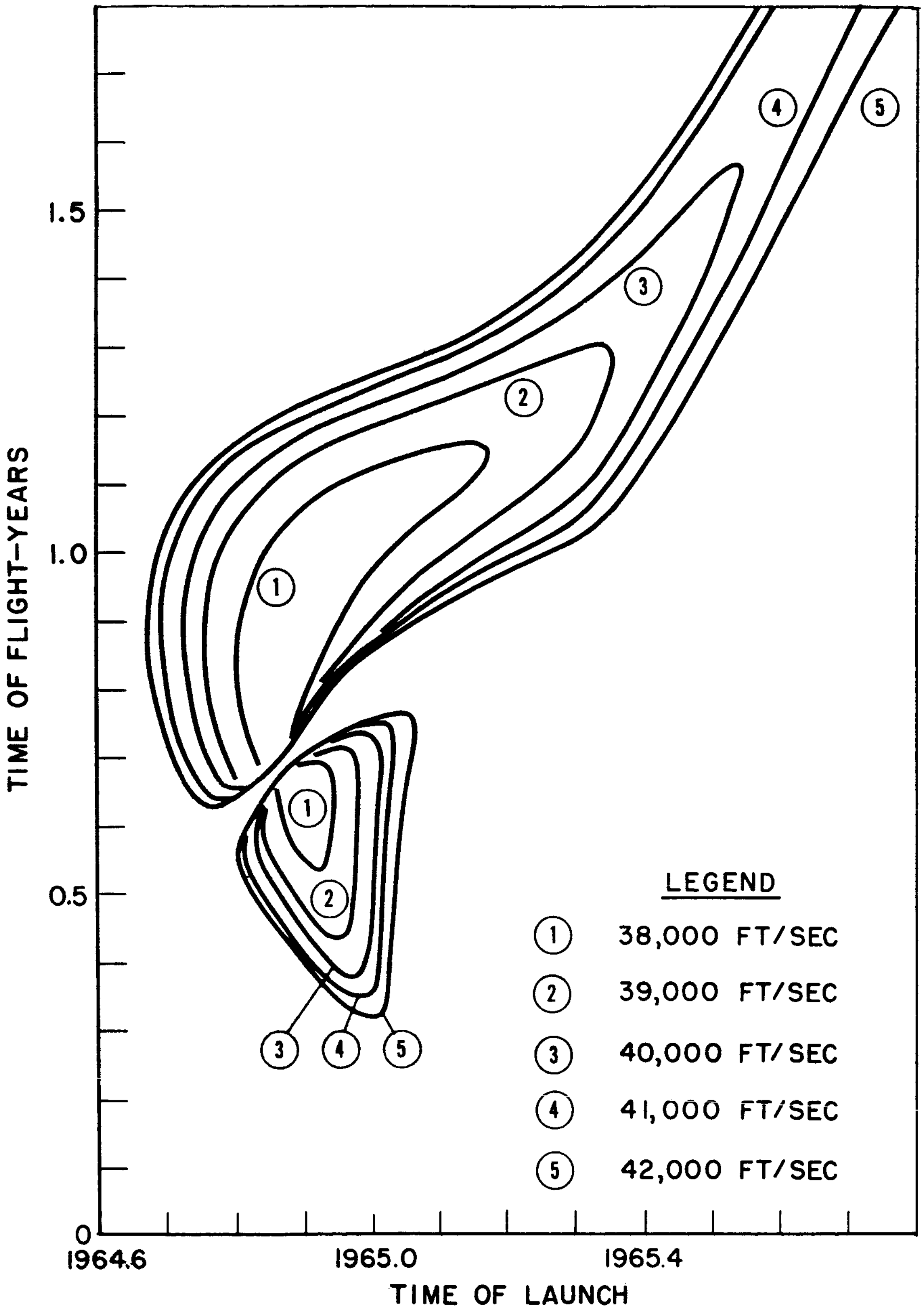

Fig. 2-17 Injection velocity--Mars 45^{o} launch azimuth.

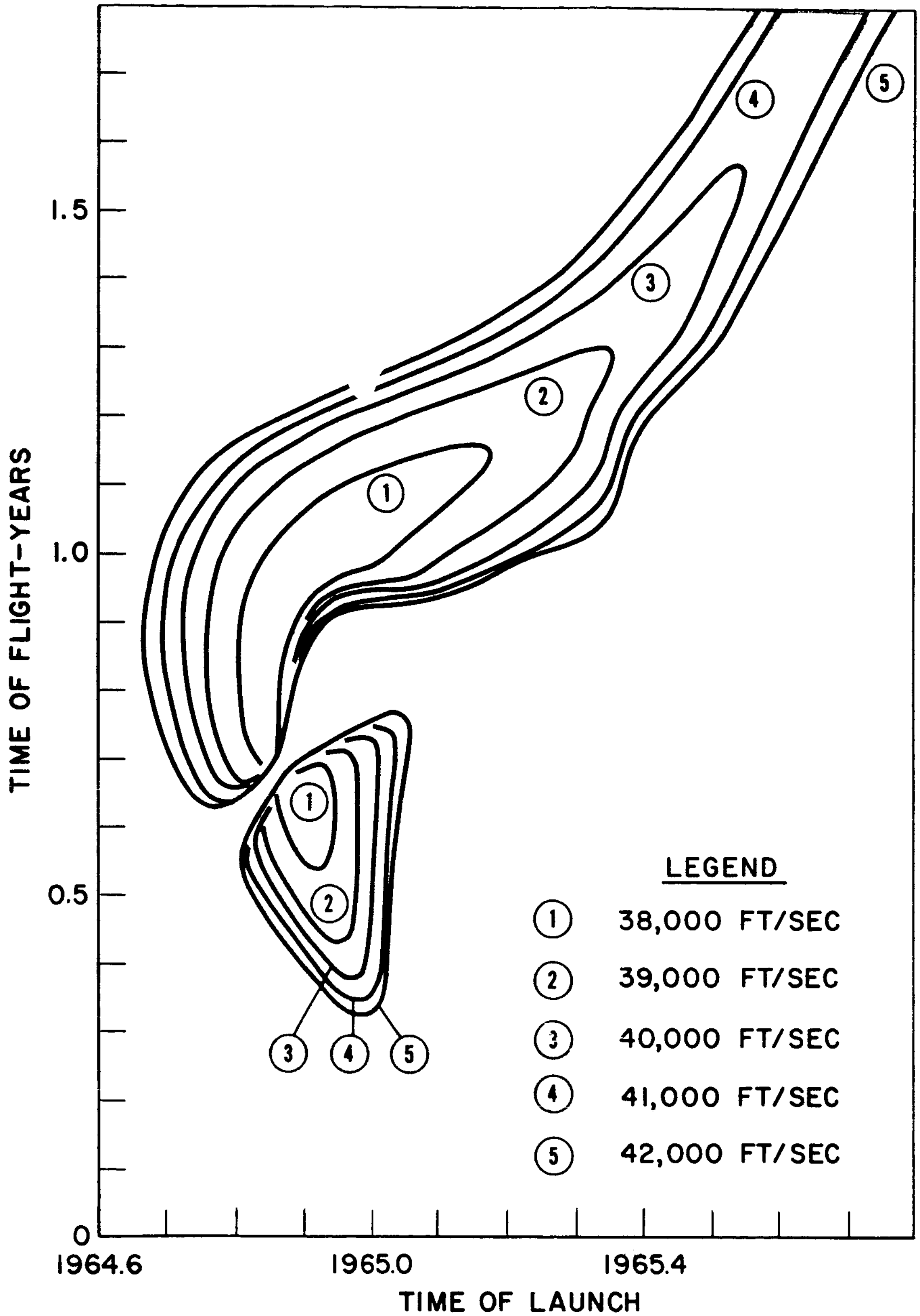

Fig. 2-18 Injection velocity--Mars 100° launch azimuth.

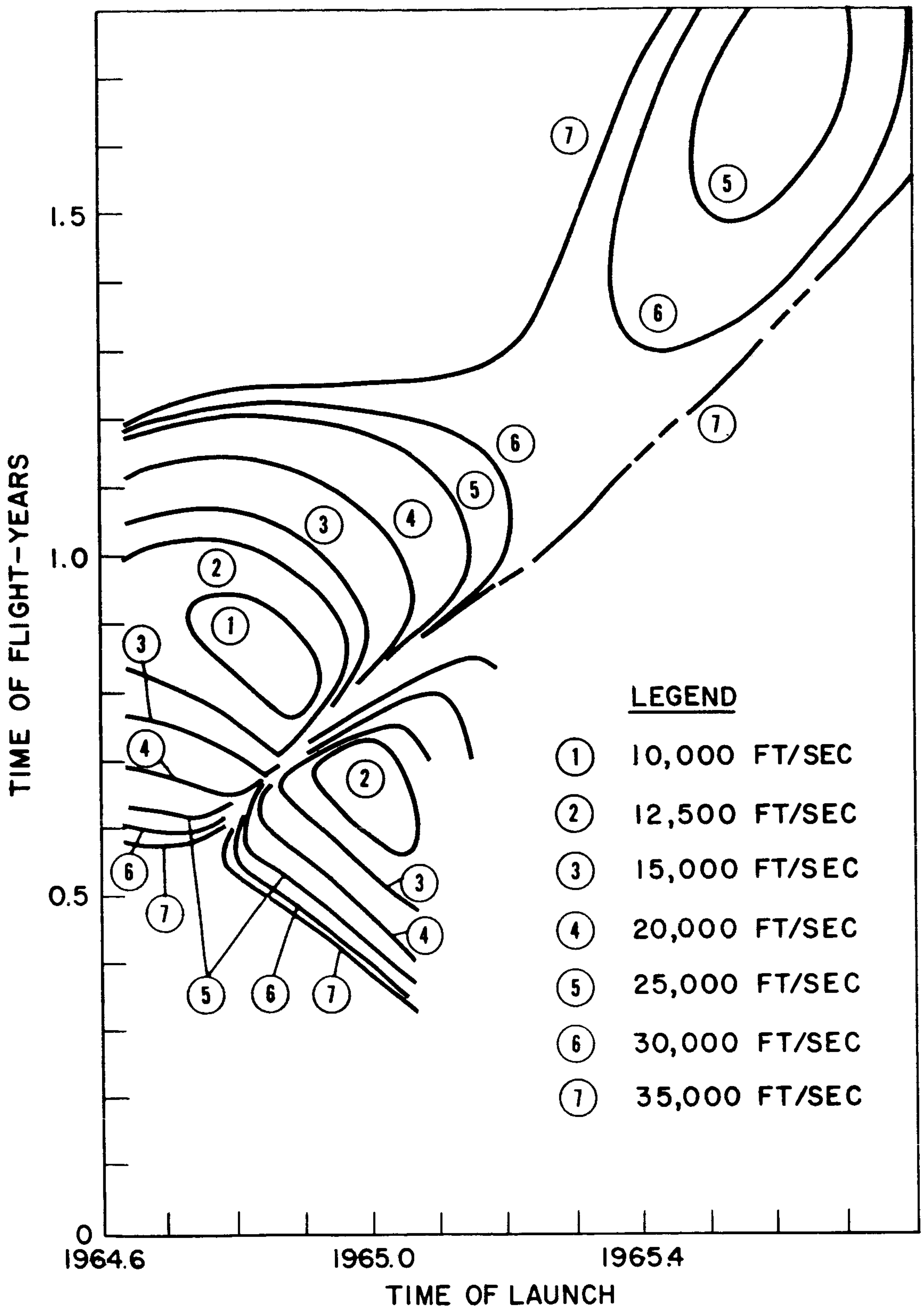

Fig. 2-19 Velocity relative to Mars.

60WWRN - 5337

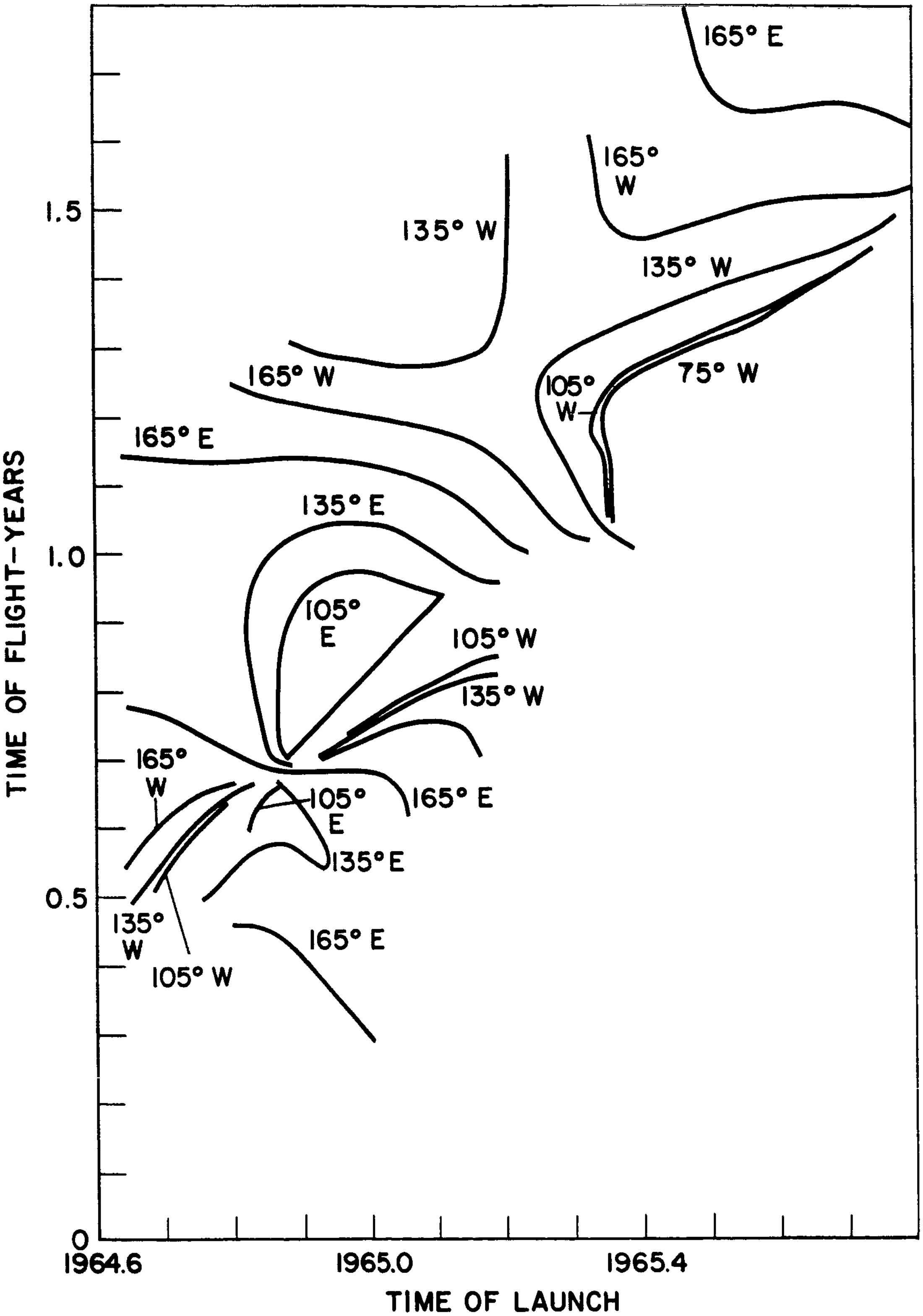

Fig. 2-20 Injection longitude 1--Mars 110° launch azimuth.

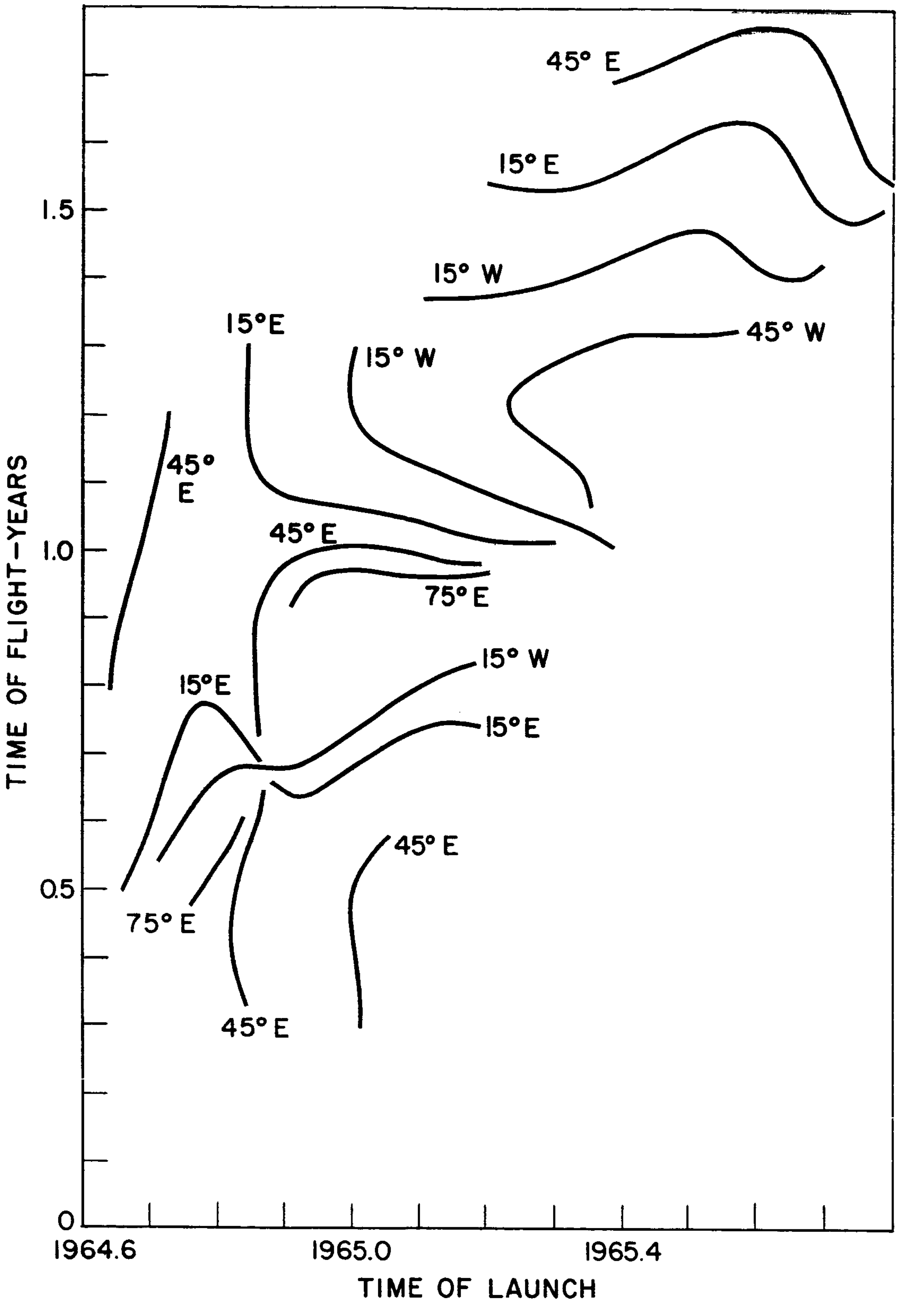

Fig. 2-21 Injection longitude 2--Mars 110° launch azimuth.

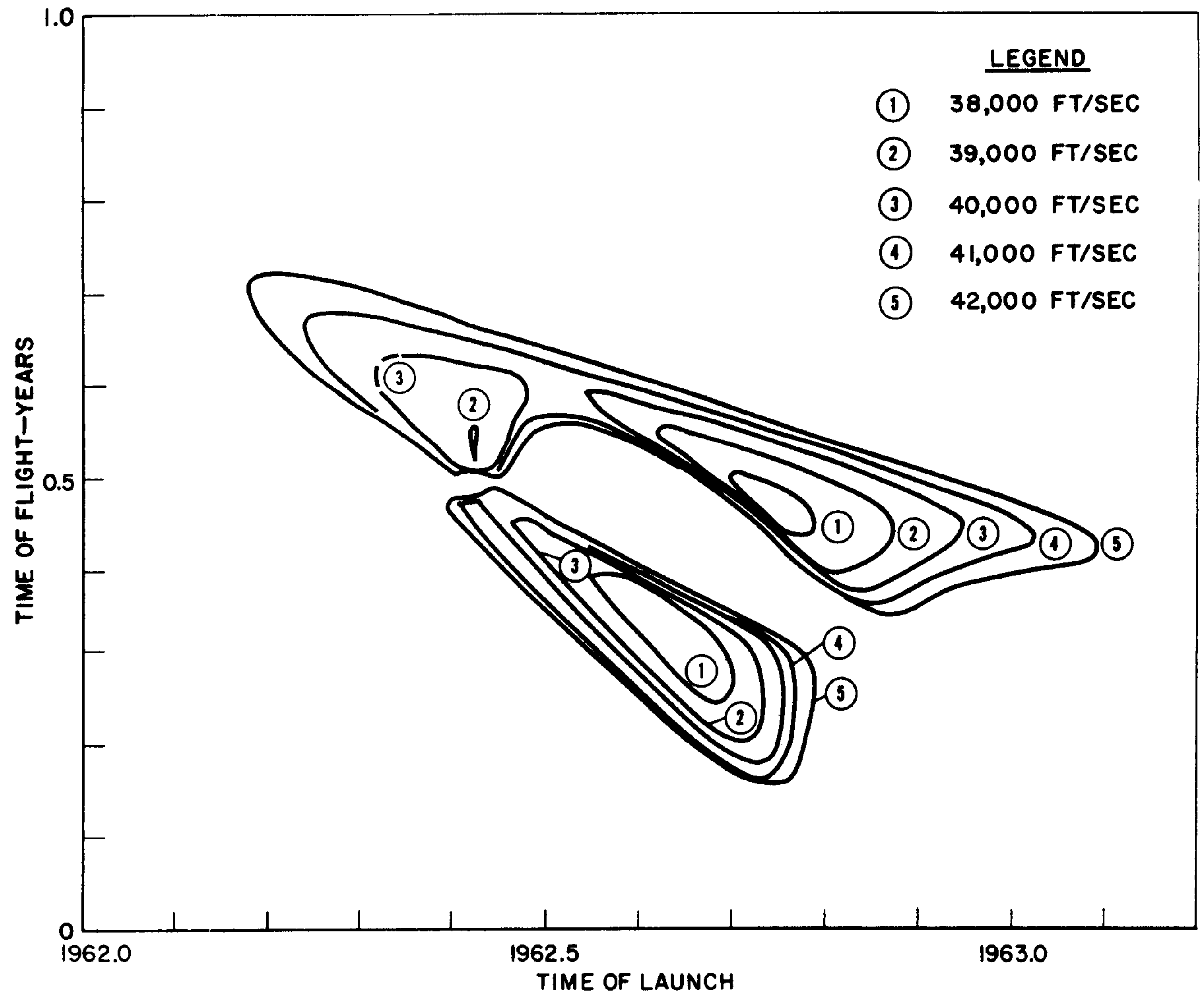

Fig. 2-22 Injection velocity--Venus 110^{o} launch azimuth.

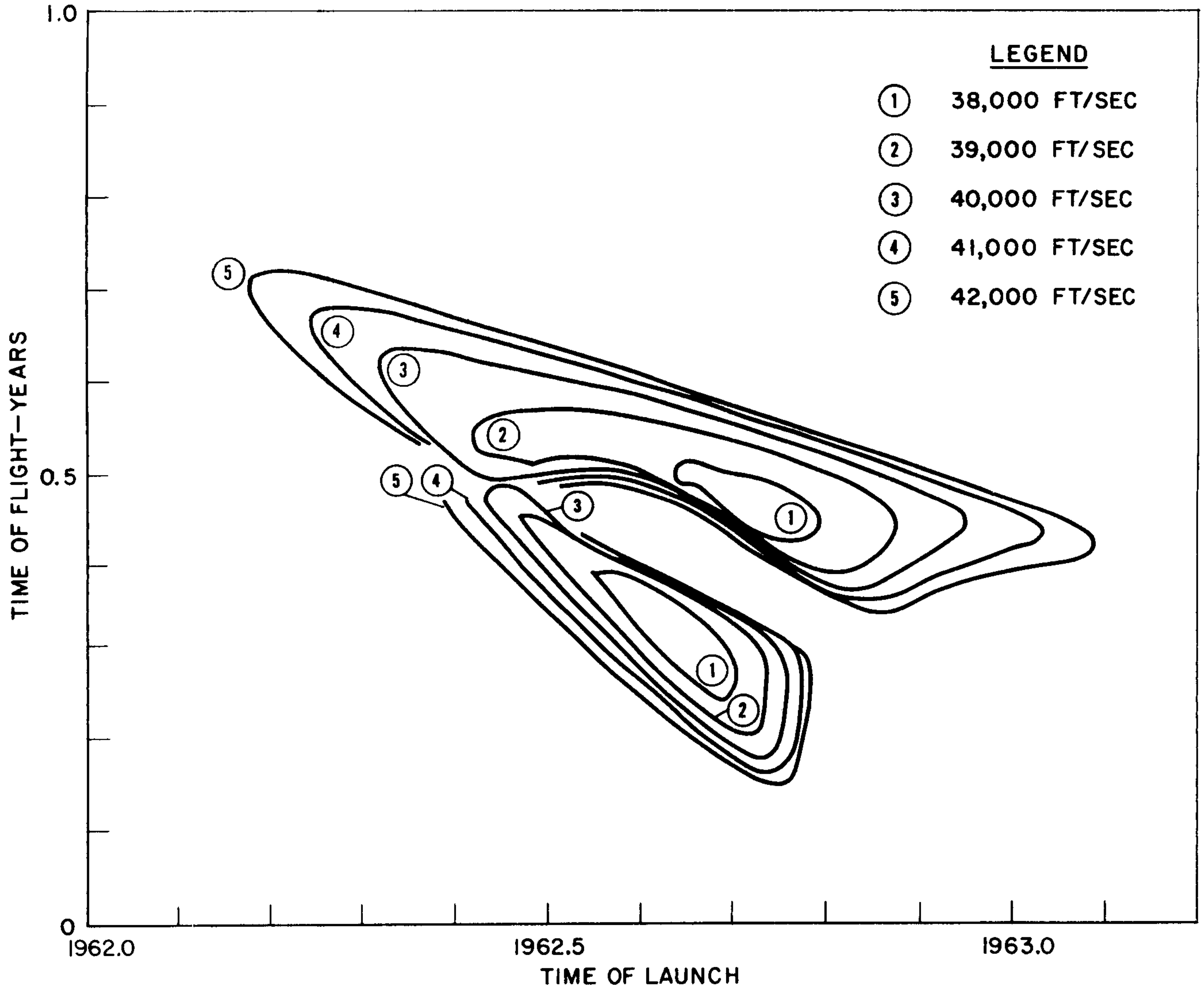

Fig. 2-23 Injection velocity--Venus 45° launch azimuth.

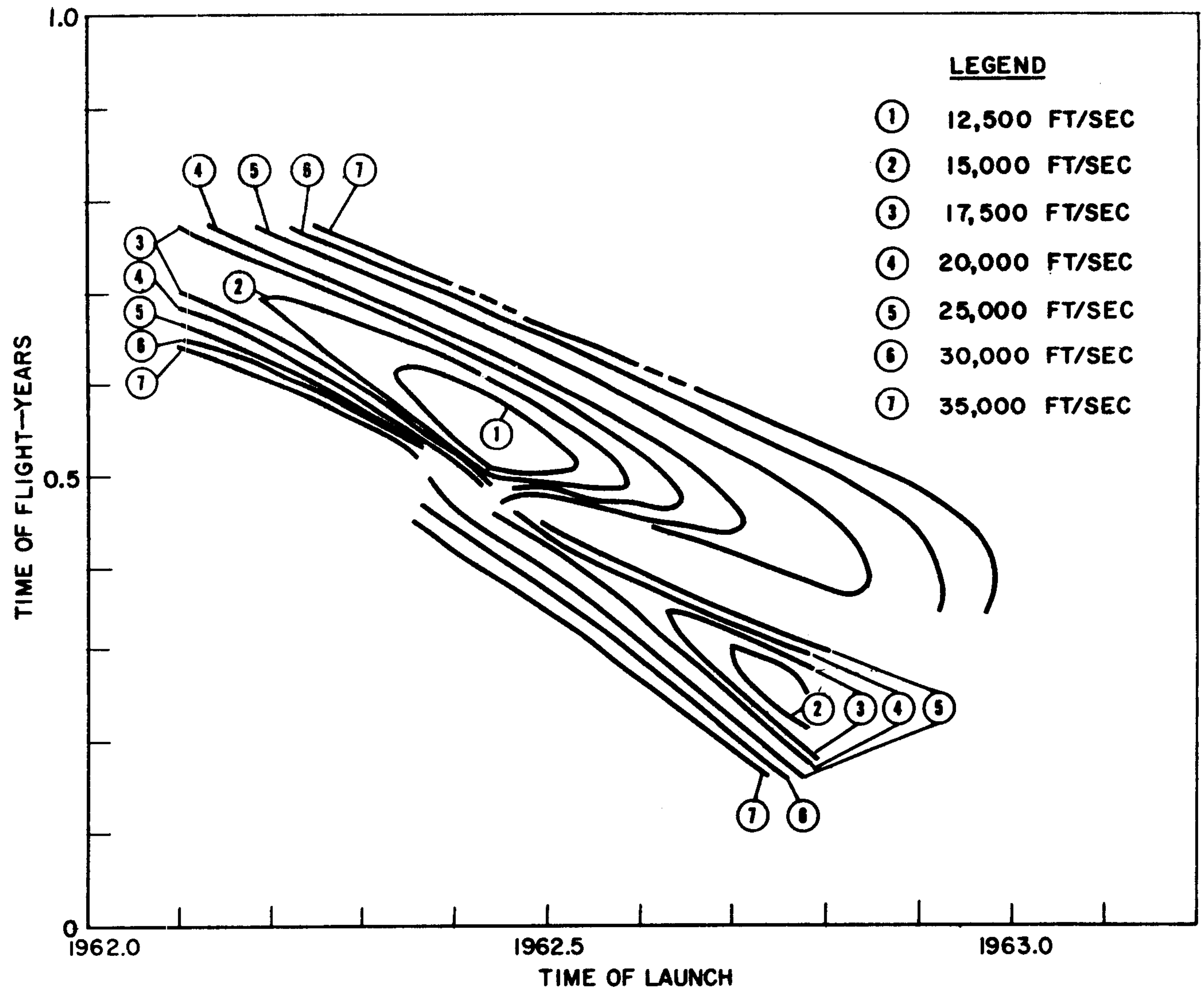

Fig. 2-24 Velocity relative to Venus.

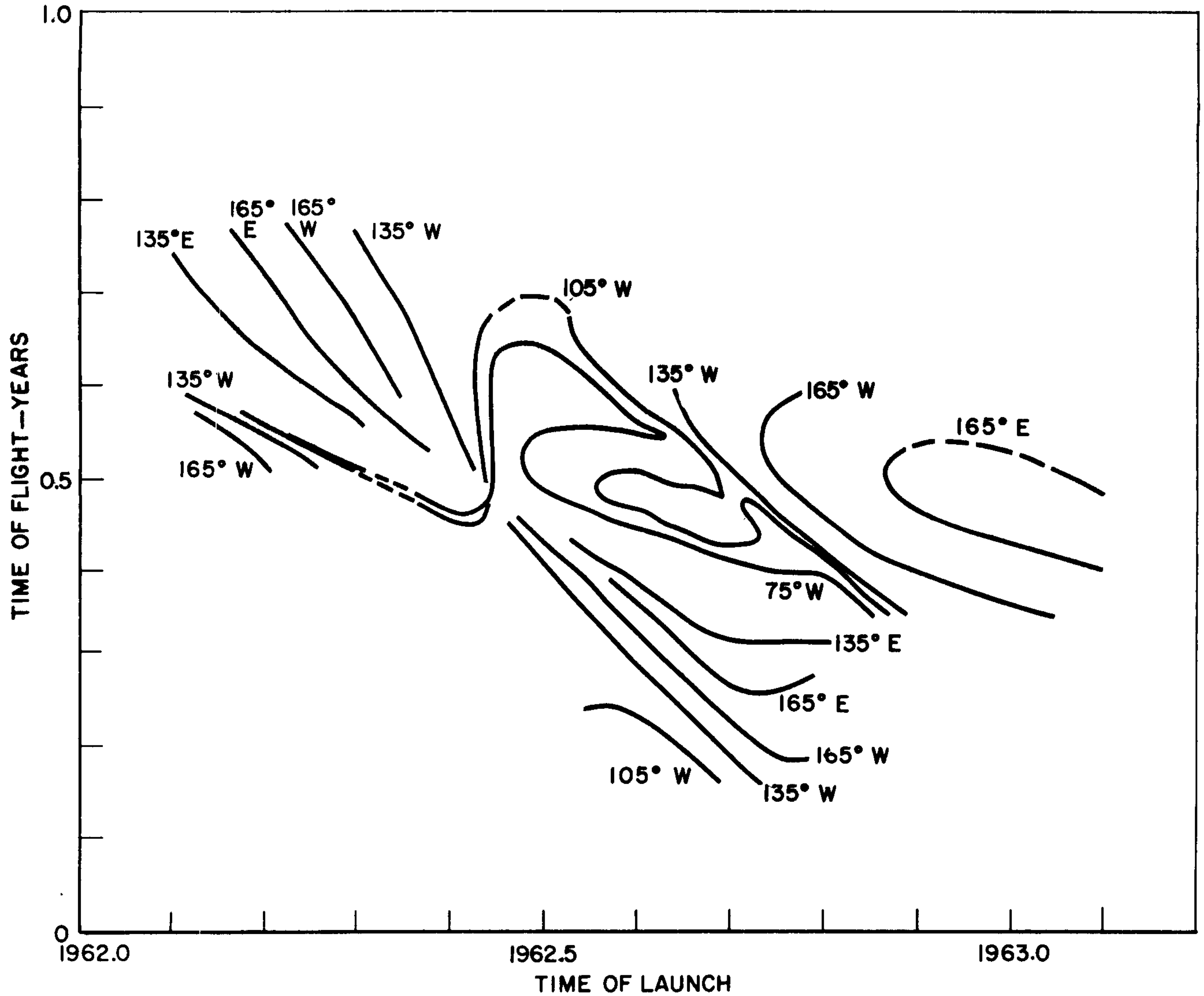

Fig. 2-25 Injection longitude 1--Venus 110° launch azimuth.

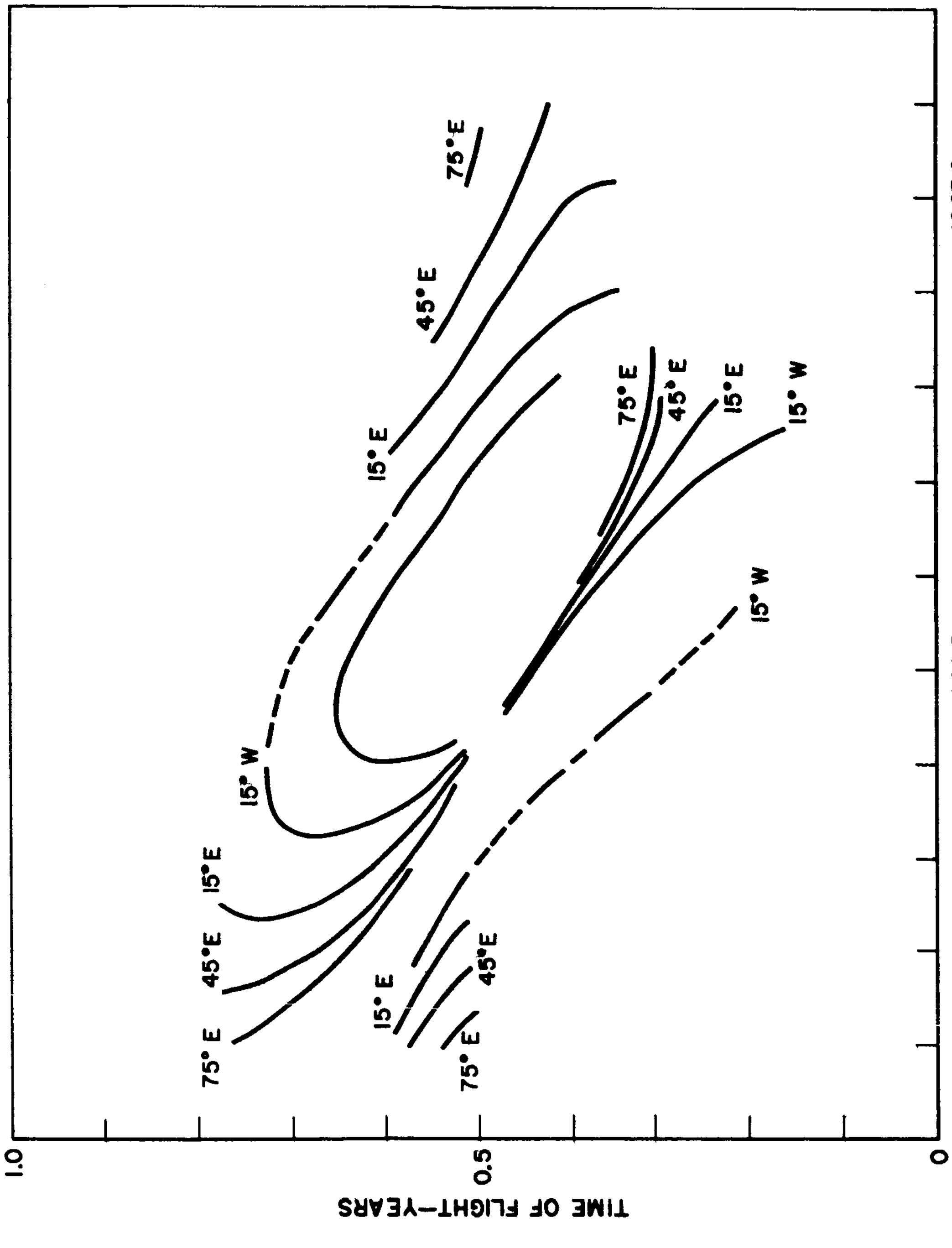

Fig. 2-26 Injection longitude 2--Venus 110° launch azimuth.

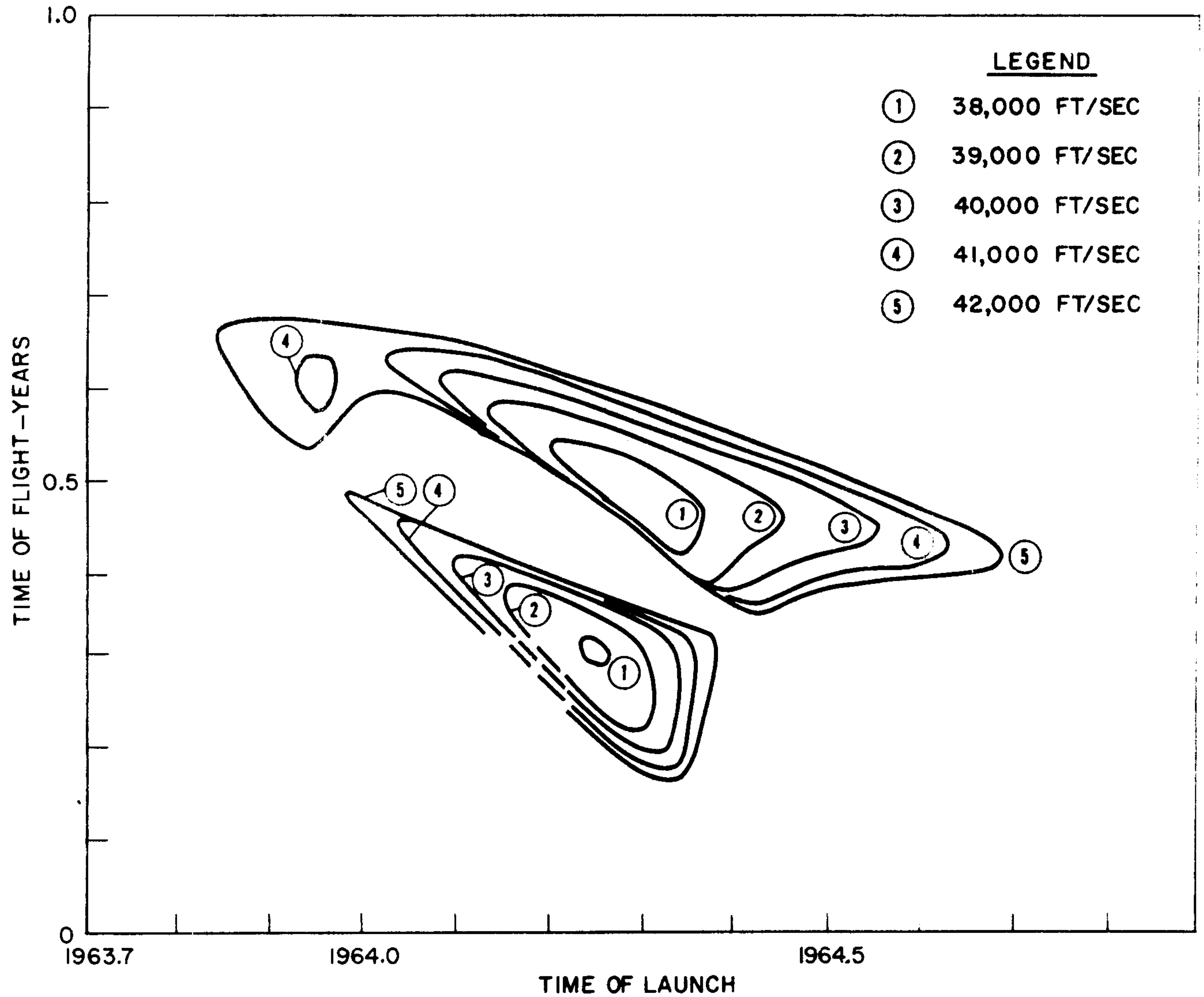

Fig. 2-27 Injection velocity--Venus 110° launch azimuth.

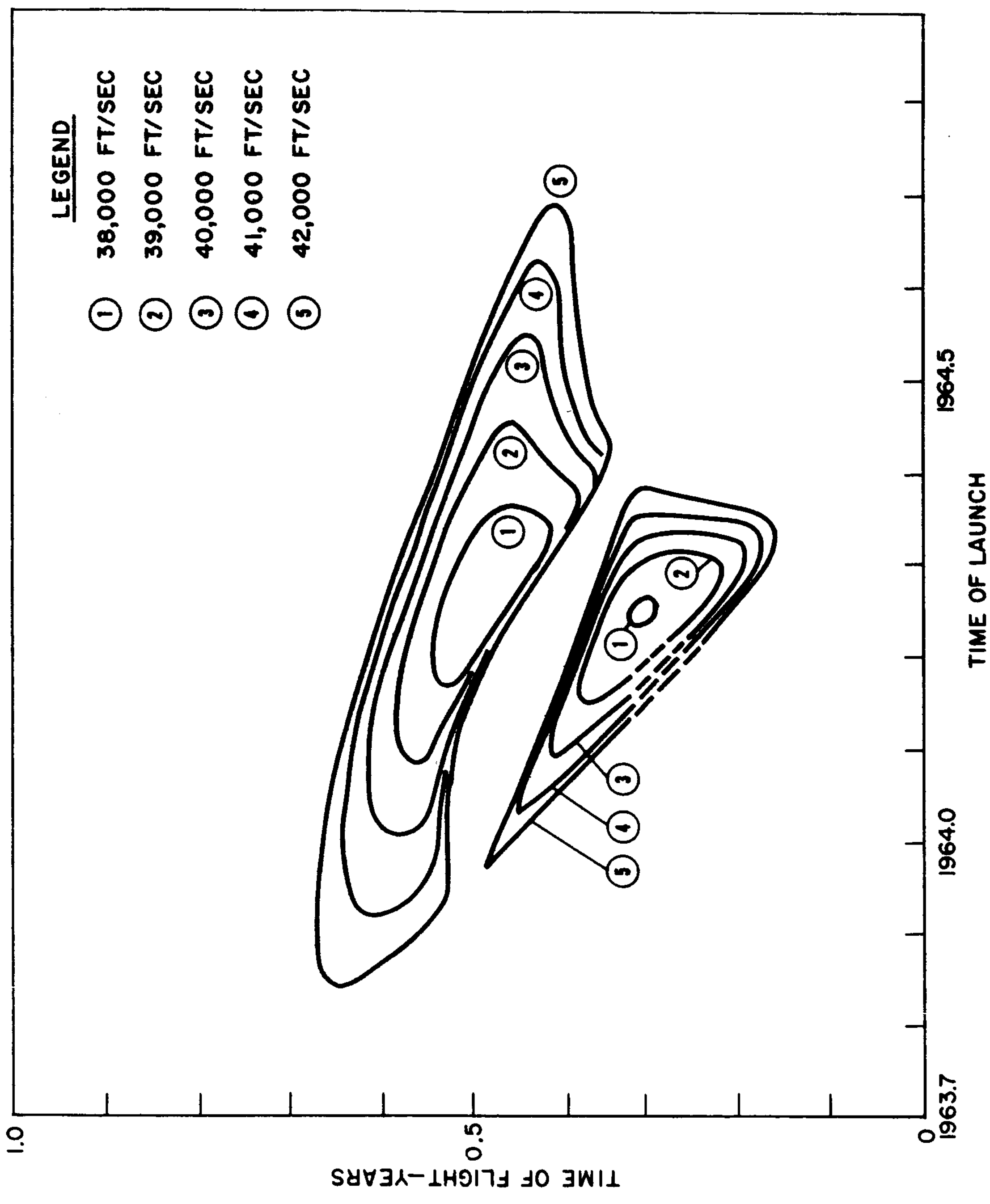

Fig. 2-28 Injection velocity--Venus 45° launch azimuth.

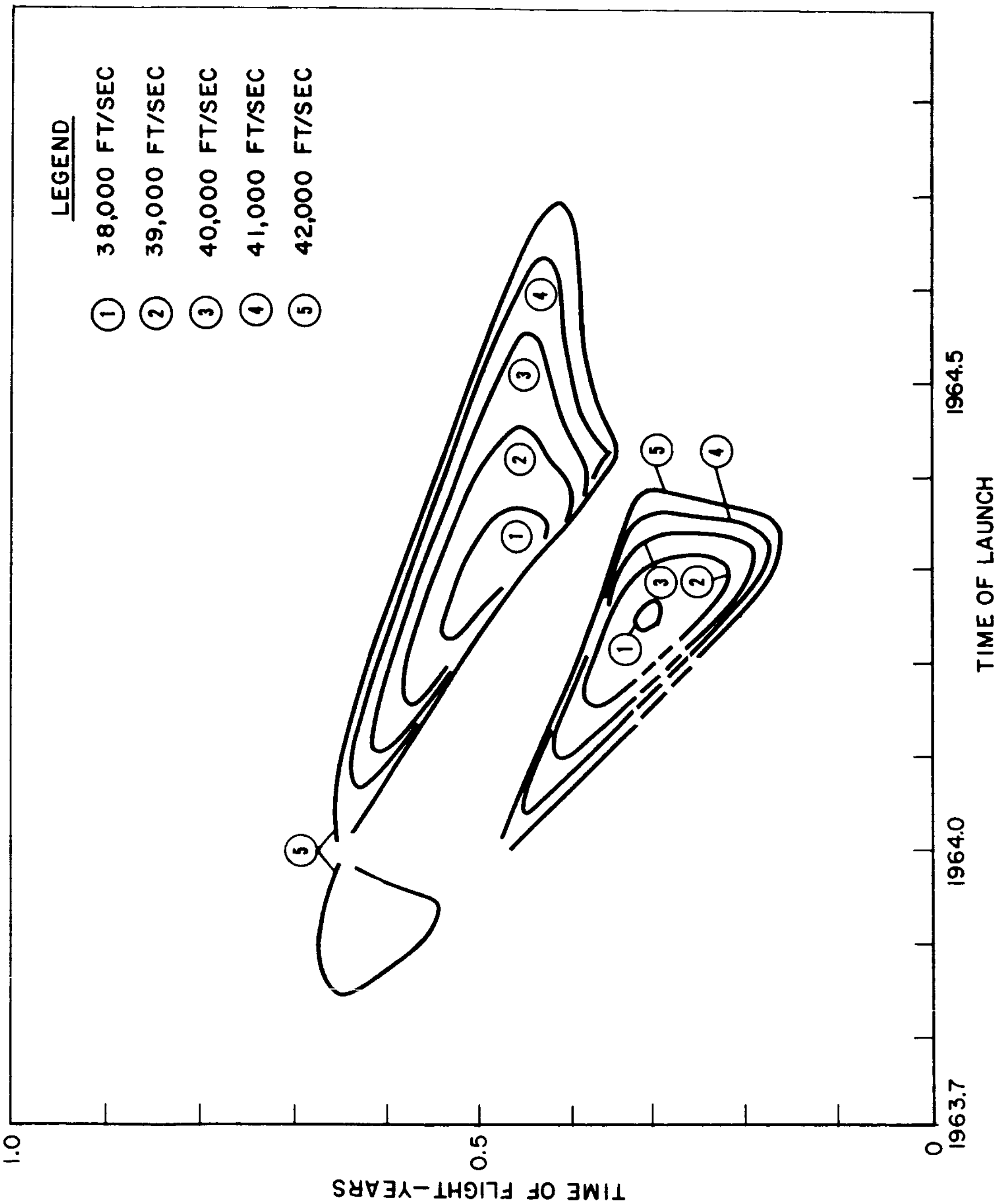

Fig. 2-29 Injection velocity--Venus 100° launch azimuth.

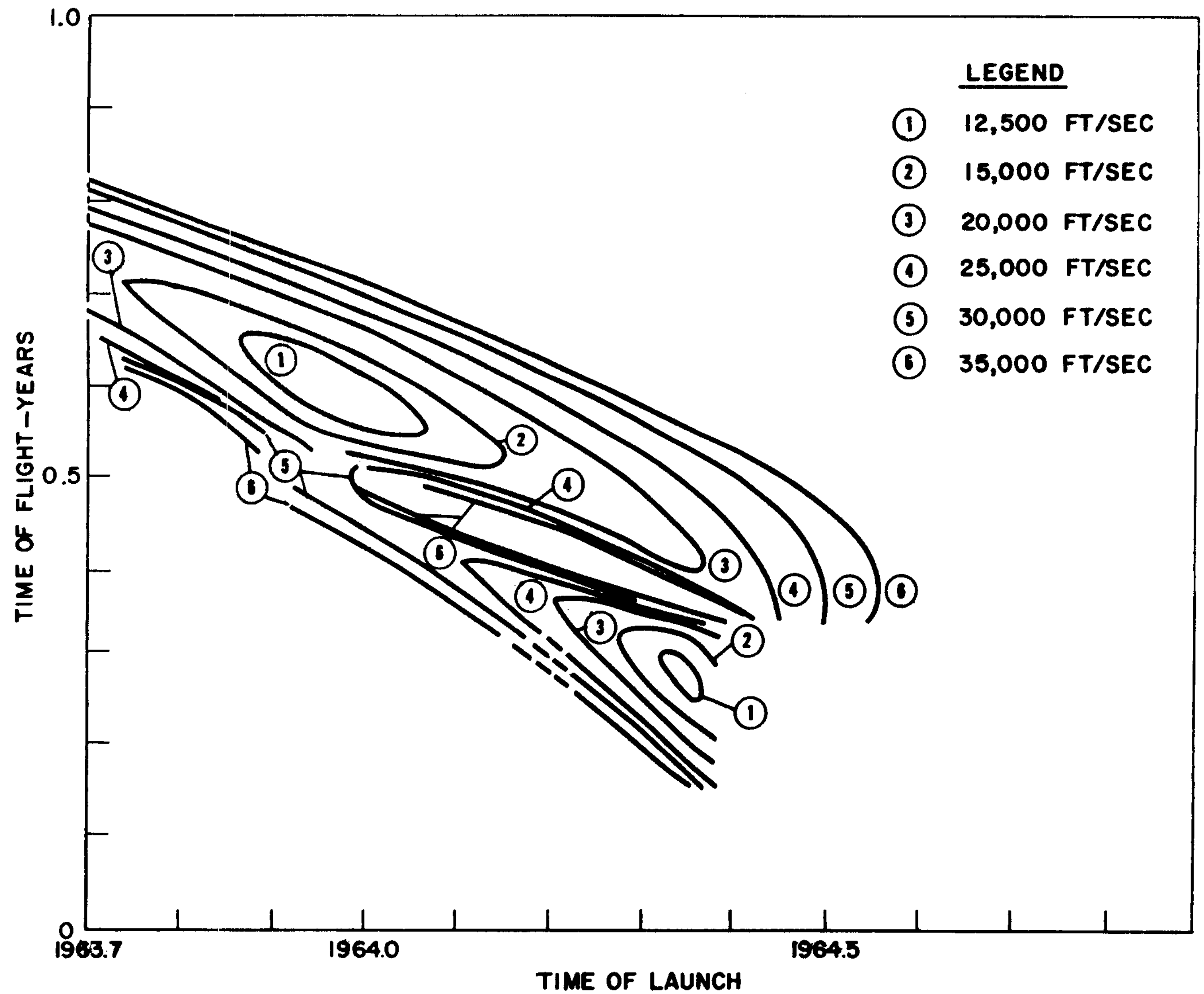

Fig. 2-30 Velocity relative to Venus.

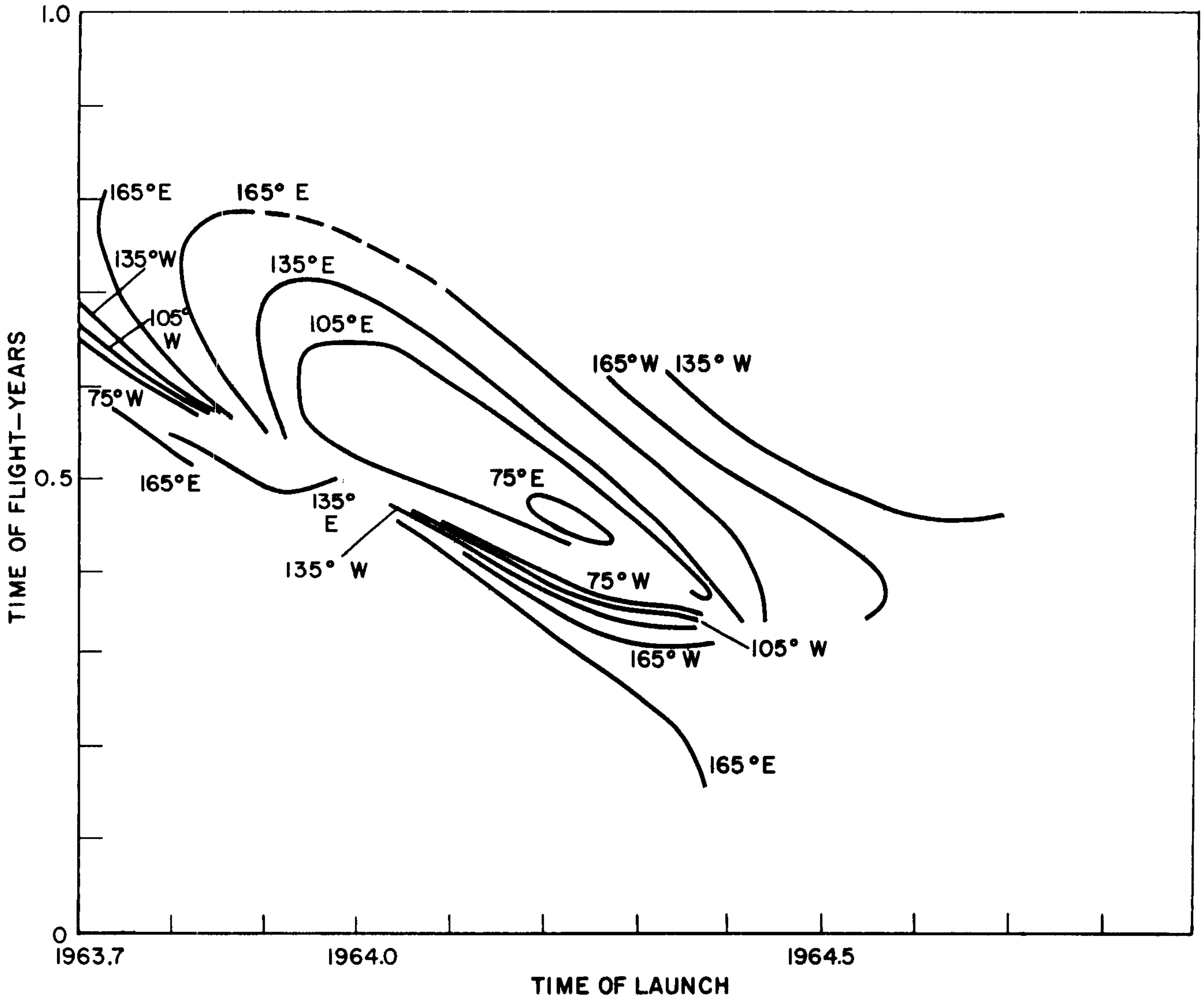

Fig. 2-31 Injection longitude 1--Venus 110° launch azimuth.

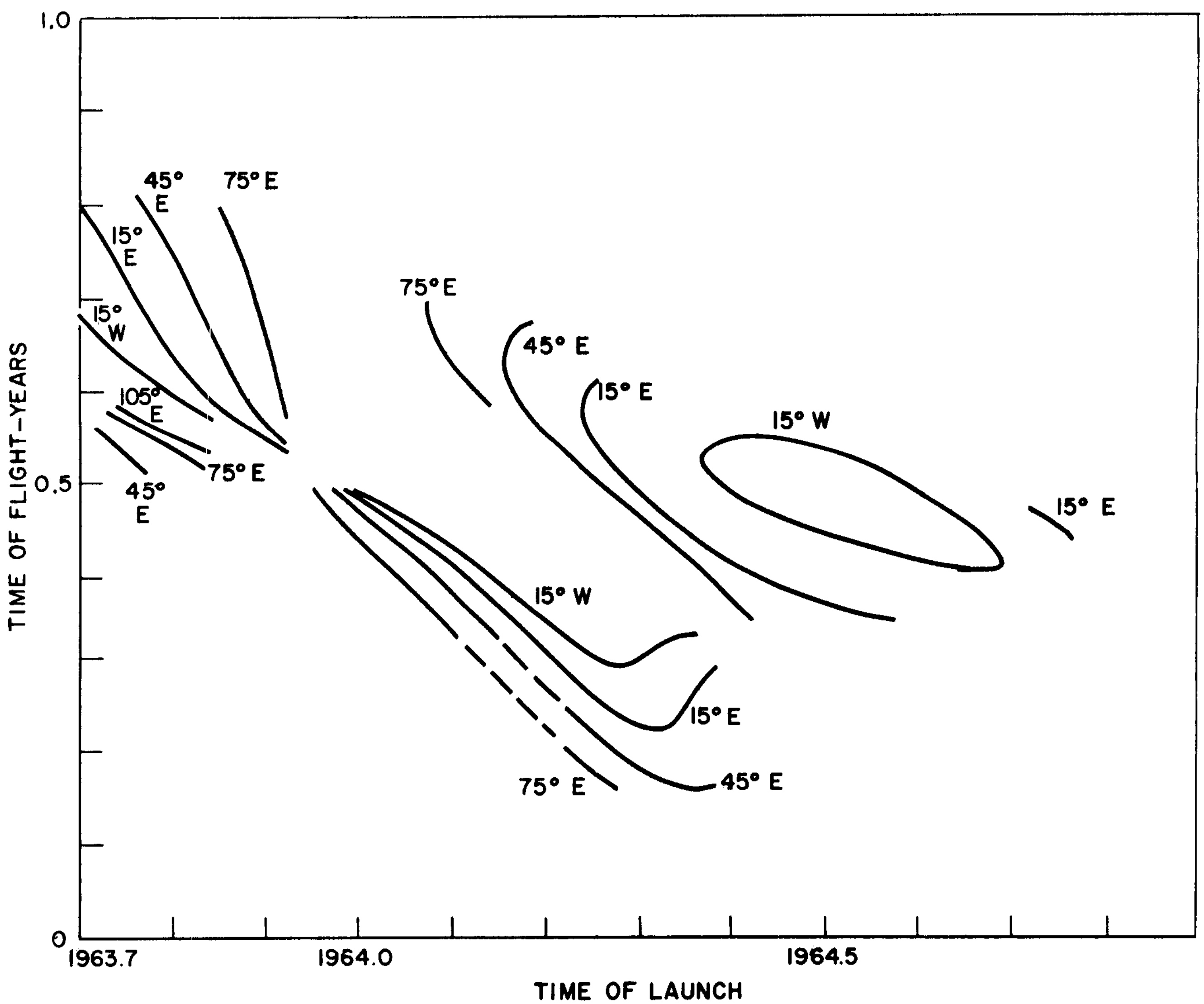

Fig. 2-32 Injection longitude 2--Venus 110° launch azimuth.

[redacted]

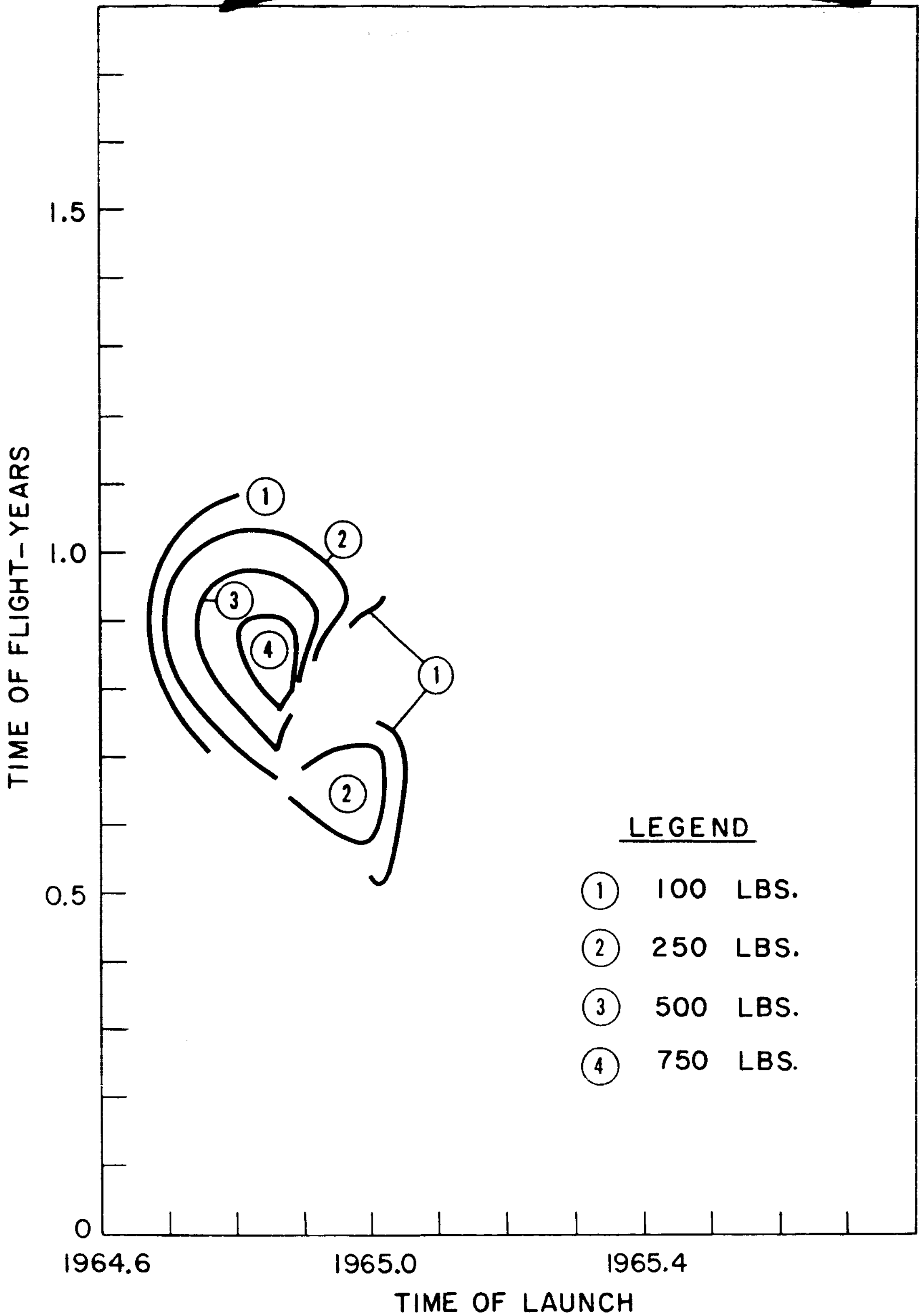

Fig. 2-33 Payload deliverable into orbit--Mars, case A.

[redacted]

SCW RN - 5337

[redacted]

DECLASSIFIED

[redacted]

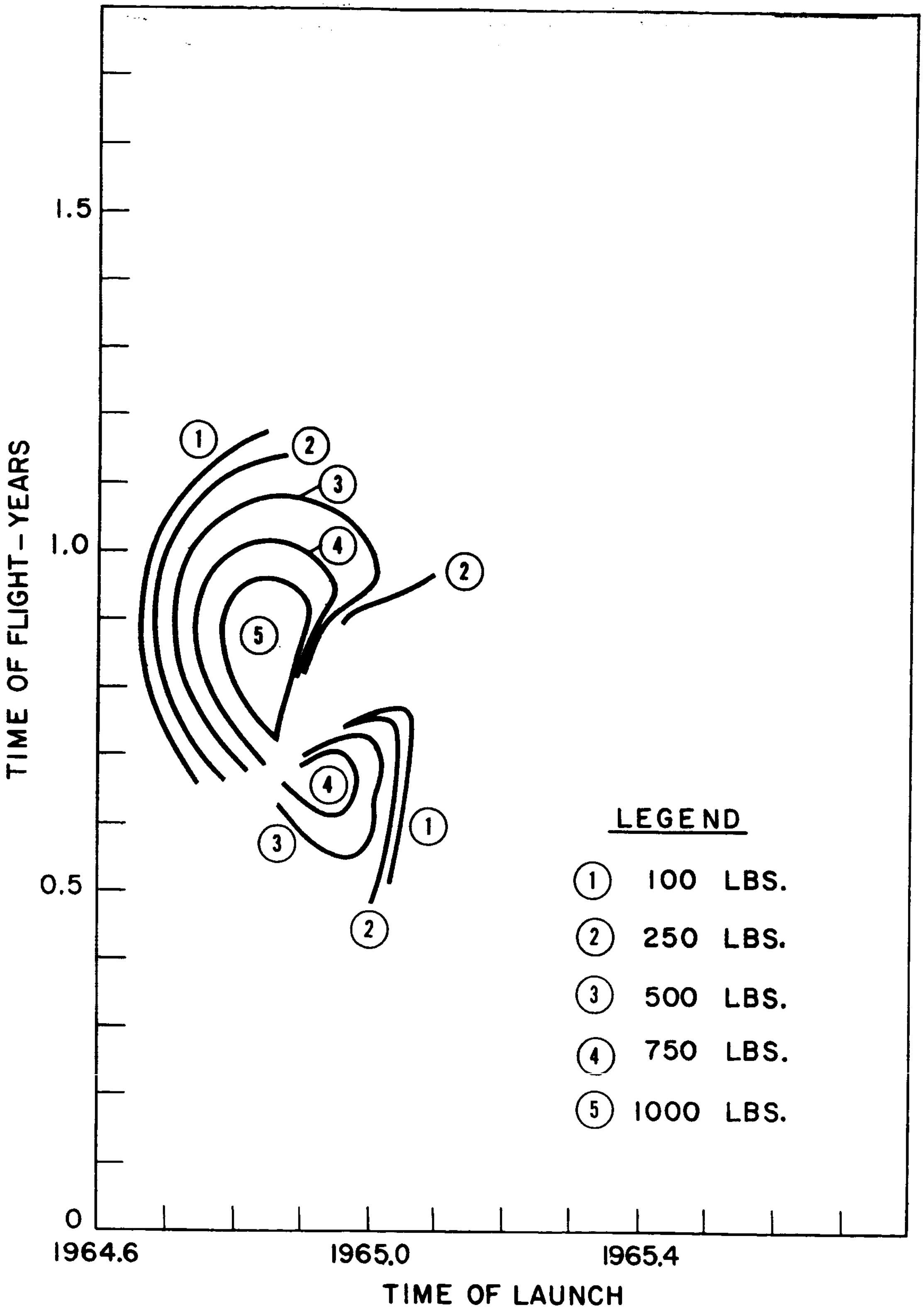

Fig. 2-34 Payload deliverable into orbit--Mars, case B.

[redacted]

[redacted]

DECLASSIFIED

[redacted]

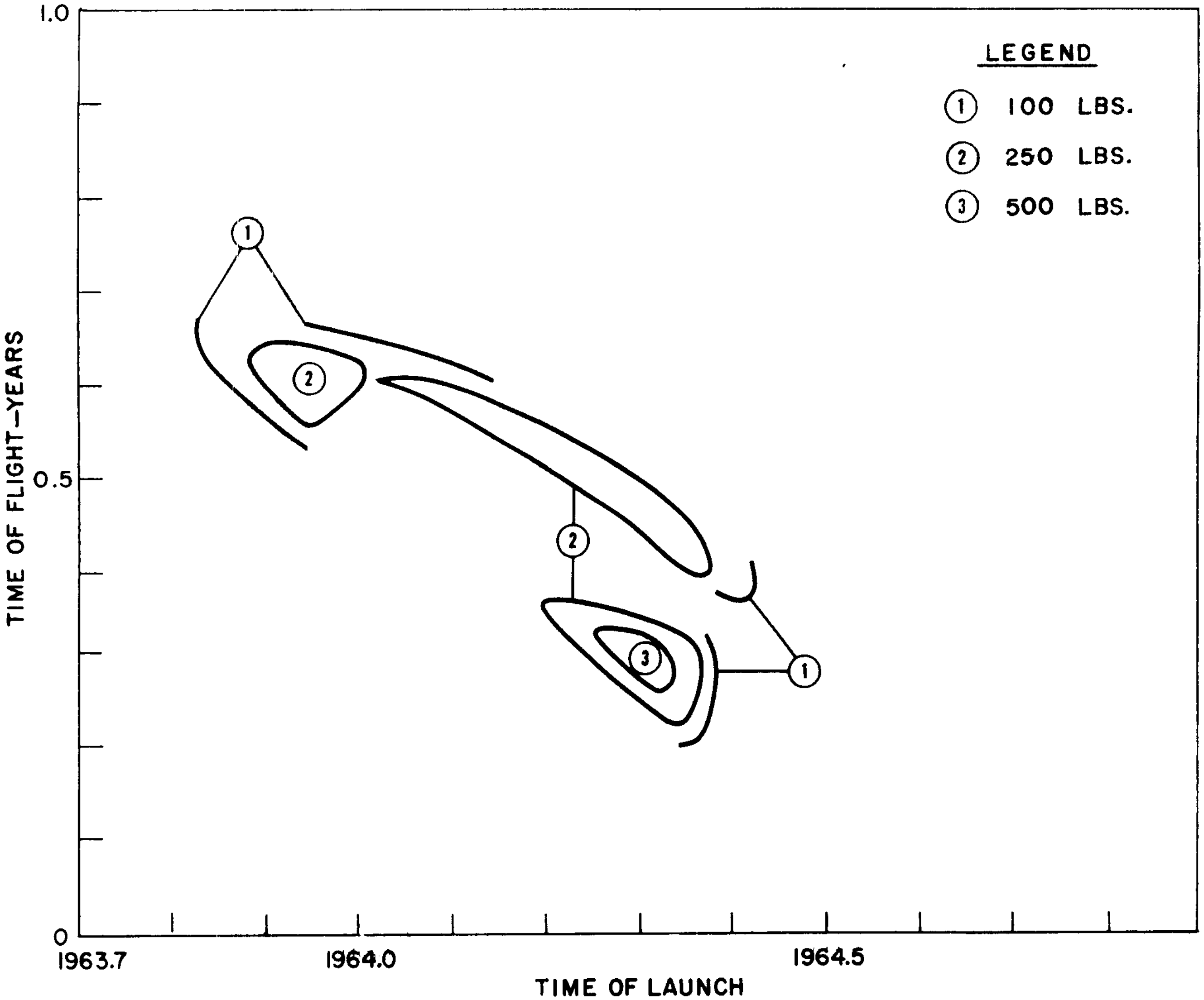

Fig. 2-35 Payload deliverable into orbit--Venus, case A.

[redacted]

60WWRN - 5337

[redacted]

[redacted]

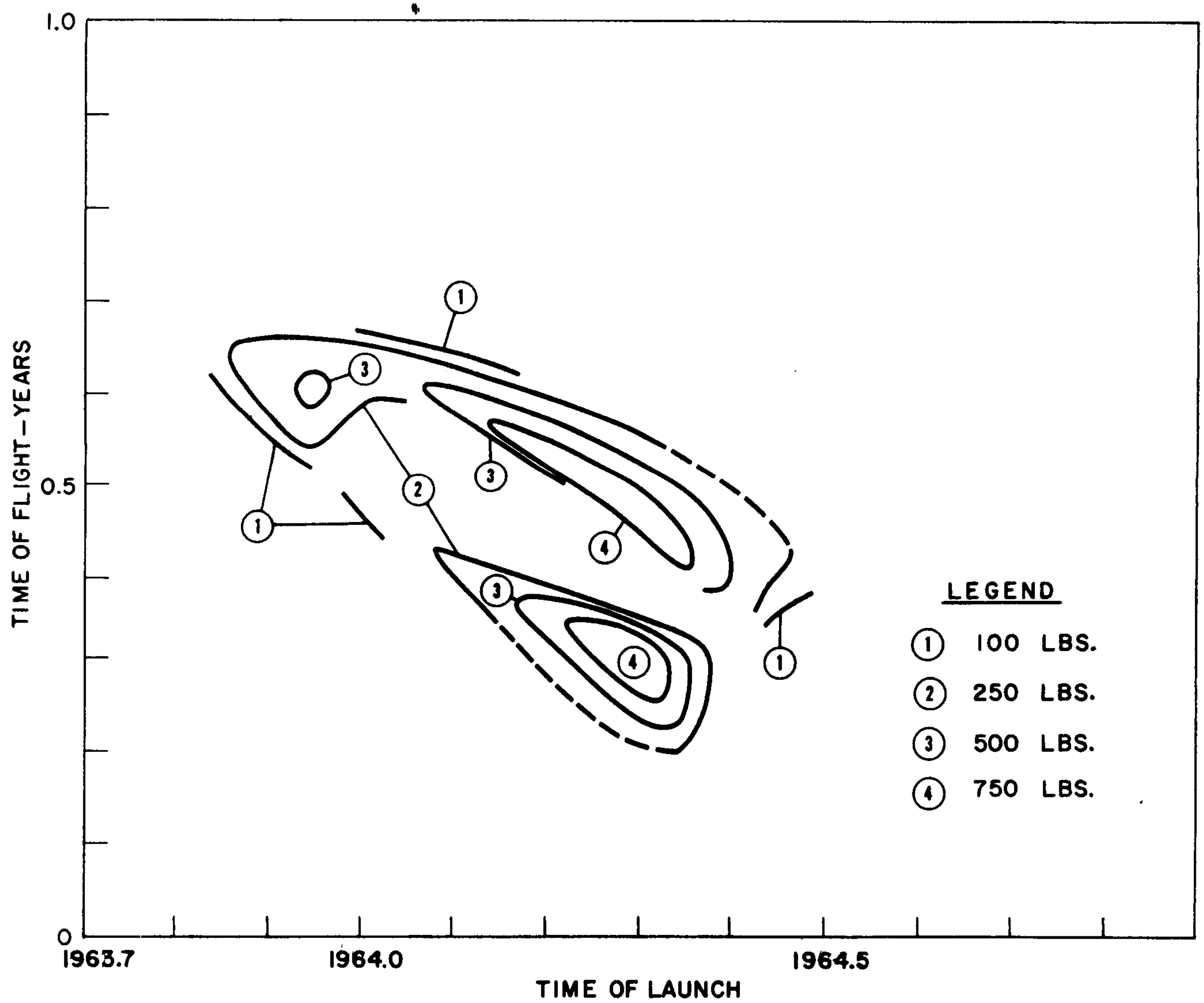

Fig. 2-36 Payload deliverable into orbit--Venus, case B.

[redacted]

60WRN - 5337

[redacted]

CHAPTER 3

NAVIGATION STUDIES

by

R. H. Battin

TABLE OF CONTENTS

CHAPTER 3

NAVIGATION STUDIES

Introduction

A general scheme for self-contained interplanetary navigation has been described in Report R-235. The process involves a sequence of velocity corrections at a number of preselected check-points based on deviations in position from a planned trajectory. Position determination is made by on-board optical measurements of angles between lines of sight to various celestial objects and of the apparent angular diameters of planets. The translation of positional errors into required velocity corrections is made by the spacecraft computer. Then, in turn, the micro-rocket propulsion system alters the velocity of the vehicle under direct control of the computer.

The purpose of this chapter is to describe certain extensions which were made in the implementation of the guidance theory in an effort to improve both the navigational accuracy and the fuel requirements. In our previous studies the specific pattern of celestial sightings had a certain degree of flexibility within an otherwise rigid framework of somewhat arbitrary restrictions. The digital computer program, which was designed to make an initial feasibility study, used the following rules in establishing a positional fix at each check-point.

With P_1 and P_2 used to denote the visible planets which are first and second in order of proximity to the spacecraft, the measured angles were chosen: (1) from the Sun to P_1; (2) from Alpha Centauri to P_1; (3) from that one of Sirius or Arcturus to

P_1, such that the plane of measurement is most nearly orthogonal to the plane of the angle measured in (2); (4) from the Sun to the same star selected in (3); (5) from the Sun to P_2, provided that more than one planet is "visible"; and (6) the angular diameter of P_1, provided that it exceeds one milliradian.

Certain obvious improvements are possible even within the restrictive conditions listed above. First, the Moon may be used as an observed object whenever the spacecraft is near the Earth, which should result in more accurate fixes. Second, a greater variety of stars could be used from which a subset could be selected to improve the accuracy of the measurements. More generally, the rules governing the selection of the observed objects may be changed and the possibility exists of comparing several sets of combinations of measurements, each determined according to some different strategy. This additional generality has been incorporated into our present study. The details and results will be discussed subsequently.

In connection with the problem of applying a velocity correction, two types of guidance were described in Report R-235. The first, fixed-time-of-arrival guidance, is designed to bring the spacecraft to a definite point in space at a fixed time. Our previous study was restricted to this kind of navigation exclusively. The second type, variable-time-of-arrival guidance, has a higher degree of flexibility in that the time of arrival is permitted a variation which is so chosen as to minimize the magnitude of the velocity correction. In either case the form of computation performed by the spacecraft computer is identical. Although variable-time-of-arrival guidance may offer problems in a round-trip mission, there can be little objection to its use on a one-way trip. The variations in arrival time are measured in hours while the savings in fuel can be as high as fifty percent. In our present study the variable-time-of-arrival guidance technique is employed and the results are presented later in the chapter.

I. The Navigational Fix

Three independent and precise angular measurements made at a known instant of time suffice to determine uniquely the position of the vehicle. Because of the presence of instrument errors, additional measurements may be used to reduce the uncertainty of a positional fix. The best choice of measurements at any instant of time depends on the position of the spacecraft within the geometry of the Solar System. In order to demonstrate explicitly the effect of different sets of measurements, we shall derive analytic expressions for the mean-squared errors which result from different combinations of measurements.

Let S_o and P_o be, respectively, the reference position of the spaceship and the position of a planet at time T. Let $\underline{r}$ be the vector from the Sun to S_o and $\underline{z}$ the vector from S_o to P_o. With A denoting the angle between the line of sight to the Sun and the line of sight to the planet, it is shown in Report R-235 that the deviation in position $\delta\underline{r}$ of the spacecraft from the reference position is related to the observed deviation in angular measurement δA by

$$\delta A = \left(\frac{\underline{m} - (\underline{n} \cdot \underline{m})\underline{n}}{r \sin A} + \frac{\underline{n} - (\underline{n} \cdot \underline{m})\underline{m}}{z \sin A} \right) \cdot \delta\underline{r} \tag{3-1}$$

if the observation is made at a known instant of time. Here r and z represent the respective distances of the spacecraft from the Sun and the planet while $\underline{m}$ and $\underline{n}$ are, respectively, the unit vectors from S_o toward the Sun and toward P_o. By letting r or z become infinite, we can include measurements between lines-of-sight to the Sun and a star or a planet and a star. For an angular diameter measurement we have

$$\delta A = \frac{D\underline{m} \cdot \delta\underline{r}}{z^2 \cos(A/2)}, \tag{3-2}$$

where D is the actual diameter of the planet and A is the apparent angular diameter. The two individual vector coefficients of $\delta\underline{r}$ in Eq (3-1) are vectors in the plane of the measurement and normal, respectively, to the lines-of-sight to the Sun and to the planet.

It follows from results derived in Appendix B for three angular measurements made at a known instant of time that the mean squared position error $\overline{\epsilon^2}$ may be computed as*

$$\overline{\epsilon^2} = \mathrm{tr}\,(U_{33}^{-1}\Phi_{33}\,U_{33}^{T-1}) \tag{3-3}$$

where Φ_{33} is the correlation matrix of the measurement errors and U_{33} is a three-dimensional square matrix whose rows are composed of the relevant vector coefficients of $\delta\underline{r}$ for each of the selected measurements. We shall consider three different combinations of measurements and evaluate $\overline{\epsilon^2}$ for each.

A. Planet-Star, Planet-Star, Angular Diameter of Planet Measurement

For convenience choose a coordinate system x, y, z centered in the spaceship with the z axis in the direction of the planet as shown in Fig. 3-1. Let $\underline{n}_1$ and $\underline{n}_2$ be unit vectors in the respective planes of the planet-star measurements and normal to the direction from the spaceship to the planet. These vectors will lie in the x-y plane and we may take $\underline{n}_1$ to be along the positive x-axis. Then, if θ is the angle between $\underline{n}_1$ and $\underline{n}_2$, we have

$$U_{33} = \begin{pmatrix} 1/z & 0 & 0 \\ \cos\theta/z & \sin\theta/z & 0 \\ 0 & 0 & 1/s \end{pmatrix}, \tag{3-4}$$

where

$$s = \frac{z^2}{D}\cos(A/2) = \frac{z}{2D}\sqrt{4z^2 - D^2}\,. \tag{3-5}$$

---

* The superscript T on a matrix is used to denote the matrix transpose and tr indicates the trace of the matrix.

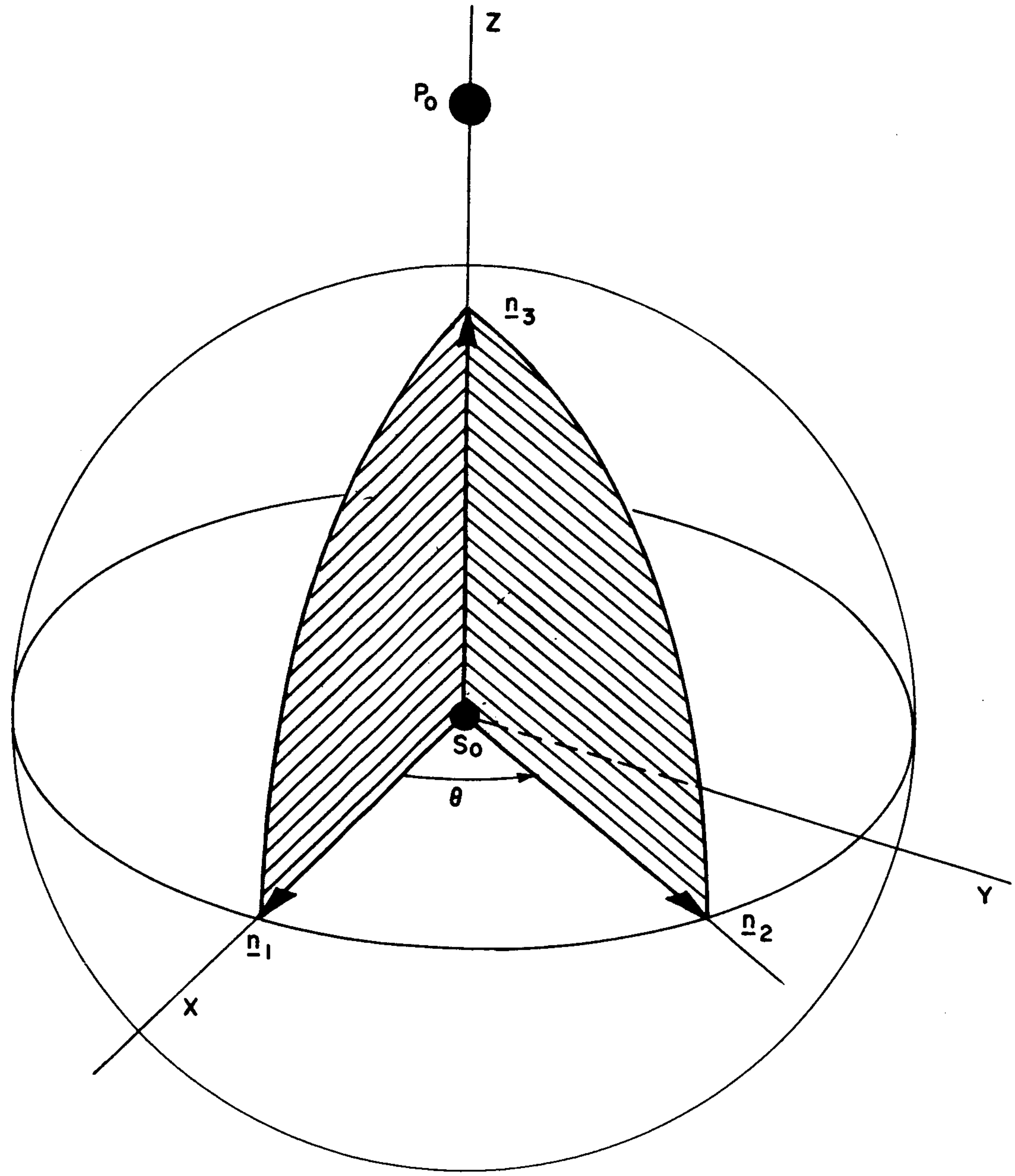

Fig. 3-1 Geometry of the planet-star, planet-star, angular diameter of planet measurement.

The inverse matrix is

$$U_{33}^{-1} = \begin{pmatrix} z & 0 & 0 \\ -z \cot \theta & z \csc \theta & 0 \\ 0 & 0 & s \end{pmatrix} . \tag{3-6}$$

Assuming that the measurement errors are independent random variables with respective standard deviations σ_1, σ_2, and σ_3, we have, according to Eq (3-3),

$$\overline{\epsilon_1^2} = \sigma_1^2 z^2 (1 + \cot^2 \theta) + \sigma_2^2 z^2 \csc^2 \theta + \sigma_3^2 s^2 \tag{3-7}$$

as the mean-squared position error resulting from the three measurements. Clearly, $\overline{\epsilon^2}$ will be a minimum if two stars can be found such that $\underline{n}_1$ and $\underline{n}_2$ are orthogonal. Then we have

$$\text{Min } \overline{\epsilon^2} = z^2 \left[\sigma_1^2 + \sigma_2^2 + \sigma_3^2 \left(\frac{z^2}{D^2} - \frac{1}{4} \right) \right] . \tag{3-8}$$

We further note that the error is reduced as the distance between the spaceship and the planet decreases.

B. Planet-Star, Planet-Star, Sun-Star Measurement

Choose a coordinate system oriented as described above and illustrated in Fig. 3-2. Let $\underline{n}_1$ and $\underline{n}_2$ be unit vectors as previously defined and let $\underline{n}_3$ be a unit vector in the plane of the Sun-star measurement and normal to the direction from the spaceship to the Sun. Then from the figure we have

$$U_{33} = \begin{pmatrix} 1/z & 0 & 0 \\ \cos \theta / z & \sin \theta / z & 0 \\ \cos \gamma \cos \beta / r & \cos \gamma \sin \beta / r & \sin \gamma / r \end{pmatrix} \tag{3-9}$$

and the inverse

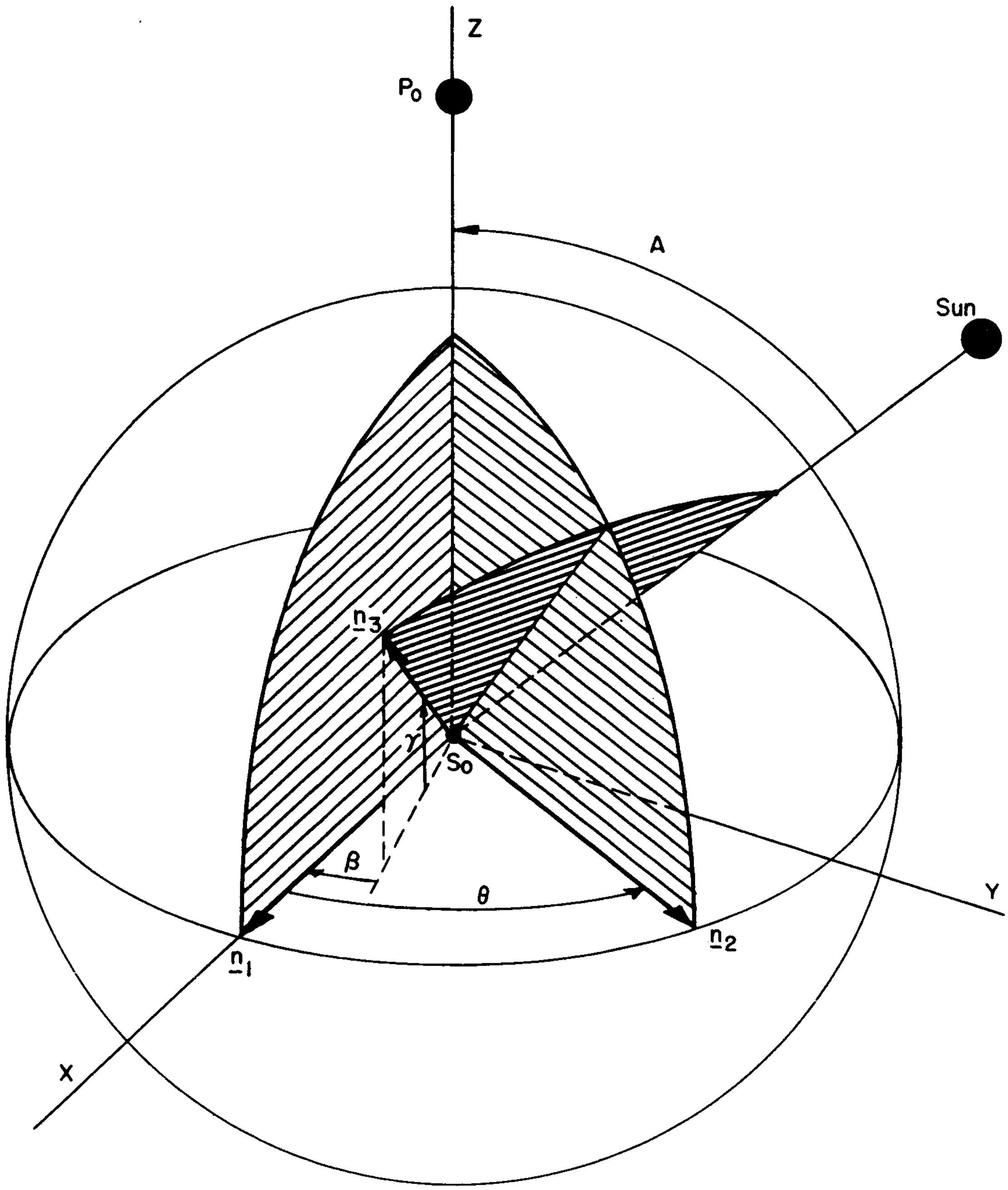

Fig. 3-2 Geometry of the planet-star, planet-star, sun-star measurement.

$$U_{33}^{-1} = \begin{pmatrix} z & 0 & 0 \\ -z\cot\theta & z\csc\theta & 0 \\ z\cot\gamma\csc\theta\sin(\beta-\theta) & -z\cot\gamma\csc\theta\sin\beta & r\csc\gamma \end{pmatrix}. \quad (3\text{-}10)$$

Again assuming independent measurement errors, we have

$$\overline{\epsilon^2} = \sigma_1^2 z^2 \left[1+\cot^2\theta+\cot^2\gamma\csc^2\theta\sin^2(\beta-\theta)\right]$$

$$+\sigma_2^2 z^2(\csc^2\theta+\cot^2\gamma\csc^2\theta\sin^2\beta)+\sigma_3^2 r^2\csc^2\gamma. \quad (3\text{-}11)$$

Clearly, the best star to choose for the Sun-star measurement is one lying in the plane containing the spaceship, Sun, and planet, for then γ will assume its maximum value, i.e., the angle A between the planet and the Sun.

The optimum choice for β to minimize $\overline{\epsilon^2}$ is found by requiring the partial derivative of Eq (3-11) with respect to β to vanish. If $\sigma_1 = \sigma_2$, it follows that β should be just one-half of θ. Therefore, if the star for the Sun-star measurement is optimally selected, the two best stars for the planet-star measurements are those for which the angle between the planes of measurement is bisected by the plane of the Sun-star measurement. The resulting error will be a function of θ only, and from Eq (3-11) we have

$$\text{Min}\,\overline{\epsilon^2}(\theta) = \sigma_1^2 z^2\csc^2\theta\left[2+\cot^2 A\,(1-\cos\theta)\right]+\sigma_3^2 r^2\csc^2 A. \quad (3\text{-}12)$$

The optimum value of θ, denoted by θ_o, is determined as the solution of

$$\cos^2\theta_o - 2(1+2\tan^2 A)\cos\theta_o + 1 = 0. \quad (3\text{-}13)$$

Thus

$$\cos\theta_o = \frac{1-\sin A}{1+\sin A}, \quad (3\text{-}14)$$

and the corresponding mean-squared error $\overline{\epsilon^2}$ is given by

$$\text{Min } \overline{\epsilon^2} = \sigma_1^2 z^2 (1 + \sin A)^2 (1 + \csc A - \sin A)/2 + \sigma_3^2 r^2 \csc^2 A, \qquad (3\text{-}15)$$

Entirely analogous results are obtained if the three basic measurements are Sun-star, Sun-star, and planet-star. We need simply to interchange r and z in our formulas.

C. <u>Planet-Star, Planet-Star, Planet-Sun Measurement</u>

Refer to Fig. 3-3 and let $\underline{n}_1$ and $\underline{n}_2$ be unit vectors defined as before. Let $\underline{n}_3$ and $\underline{n}_4$ be unit vectors in the plane of the planet-Sun measurement normal, respectively, to the lines-of-sight to the planet and to the Sun. Then, according to Eq (B-23) - (B-25) in Appendix B, we have

$$U_{33} = \begin{pmatrix} 1/z & 0 & 0 \\ 0 & 1/z & 0 \\ a/z & b/z & 1/r \end{pmatrix} \begin{pmatrix} 1 & 0 & 0 \\ \cos\theta & \sin\theta & 0 \\ -\cos A \cos\beta & -\cos A \sin\beta & \sin A \end{pmatrix}, \qquad (3\text{-}16)$$

where

$$a = \frac{\sin(\theta - \beta)}{\sin\theta}, \qquad b = \frac{\sin\beta}{\sin\theta}. \qquad (3\text{-}17)$$

The inverse matrix is

$$U_{33}^{-1} = \begin{pmatrix} z & 0 & 0 \\ -z\cot\theta & z\csc\theta & 0 \\ a z \cot A - a r \csc A & b z \cot A - b r \csc A & r \csc A \end{pmatrix}. \qquad (3\text{-}18)$$

If we assume, as before, independent measurement errors with $\sigma_1 = \sigma_2$, we have for the mean-squared error

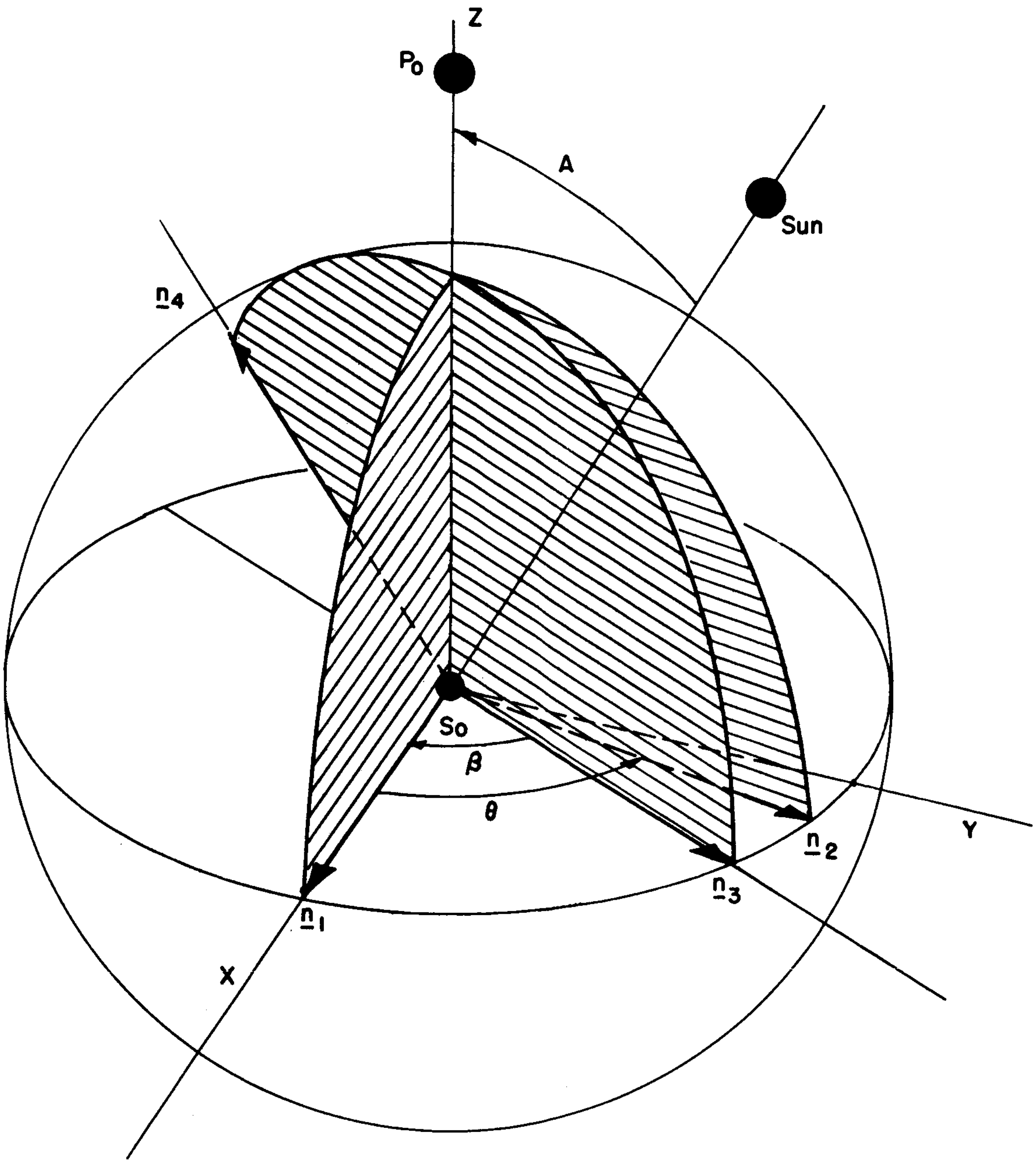

Fig. 3-3 Geometry of the planet-star, planet-star, planet-sun measurement.

$$\overline{\epsilon^2} = \sigma_1^2 \left[2z^2 \csc^2 \theta + (z \cot A - r \csc A)^2 \left(\frac{\sin^2(\theta - \beta) + \sin^2 \beta}{\sin^2 \theta} \right) \right] + \sigma_3^2 r^2 \csc^2 A . \tag{3-19}$$

Again the optimum choice of β is one-half θ, so that the minimum error as a function of θ is obtained from Eq (3-18) as

$$\text{Min } \overline{\epsilon^2}(\theta) = \sigma_1^2 \left[2z^2 \csc^2 \theta + (z \cot A - r \csc A)^2 / (1 + \cos \theta) \right] + \sigma_3^2 r^2 \csc^2 A . \tag{3-20}$$

The optimum $\theta = \theta_o$ is found as the solution of

$$\frac{4z^2 \cos \theta_o}{(1 - \cos \theta_o)^2} = (z \cot A - r \csc A)^2 . \tag{3-21}$$

We have

$$\cos \theta_o = \frac{\sqrt{1 - 2p \cos A + p^2} - \sin A}{\sqrt{1 - 2p \cos A + p^2} + \sin A} , \tag{3-22}$$

where, for convenience, we have defined

$$p = r/z . \tag{3-23}$$

With this value of θ, Eq (3-20) may be written as

$$\text{Min } \overline{\epsilon^2} = \sigma_1^2 z^2 \csc^2 A \left(\sin A + \sqrt{1 - 2p \cos A + p^2}\right)^2 / 2 + \sigma_3^2 r^2 \csc^2 A . \tag{3-24}$$

Here again, by interchanging r and z, we may obtain analogous results for the set of measurements consisting of Sun-star, Sun-star, Sun-planet.

It is important to know under what set of circumstances Measurement (B) or (C) is to be preferred. For this purpose, in

Fig. 3-4 we have plotted in the p, A plane the locus of points for which the measurements produce identical mean-squared errors. This locus is a closed curve which separates the regions in which one set of measurements is better than the other. We note, in particular, that Measurement (B) is always to be preferred when the angle A is greater than 90°.

These results are, to a great extent, of theoretical interest only since it is assumed that stars can be optimally selected. For practical considerations we are restricted to using only bright stars for our measurements. In Report R-235 we restricted our study to three stars and used a single strategy for selecting the angles to be measured. For our present study, in order to increase the attainable accuracy in the determination of spacecraft position, the number of admissible celestial objects was enlarged and the strategies by which pairs of them could be selected were generalized. The Moon was added to the collection of observable objects within the Solar System and the number of available stars was increased to ten. In order of brightness those chosen are as follows:

Star Catalog No.	Name	Magnitude
257	Sirius	-1.58
245	Canopus	-0.86
538	Alpha Centauri	0.06
699	Vega	0.14
193	Capella	0.21
526	Arcturus	0.24
194	Rigel	0.34
291	Procyon	0.48
54	Achernar	0.60
518	Beta Centauri	0.86

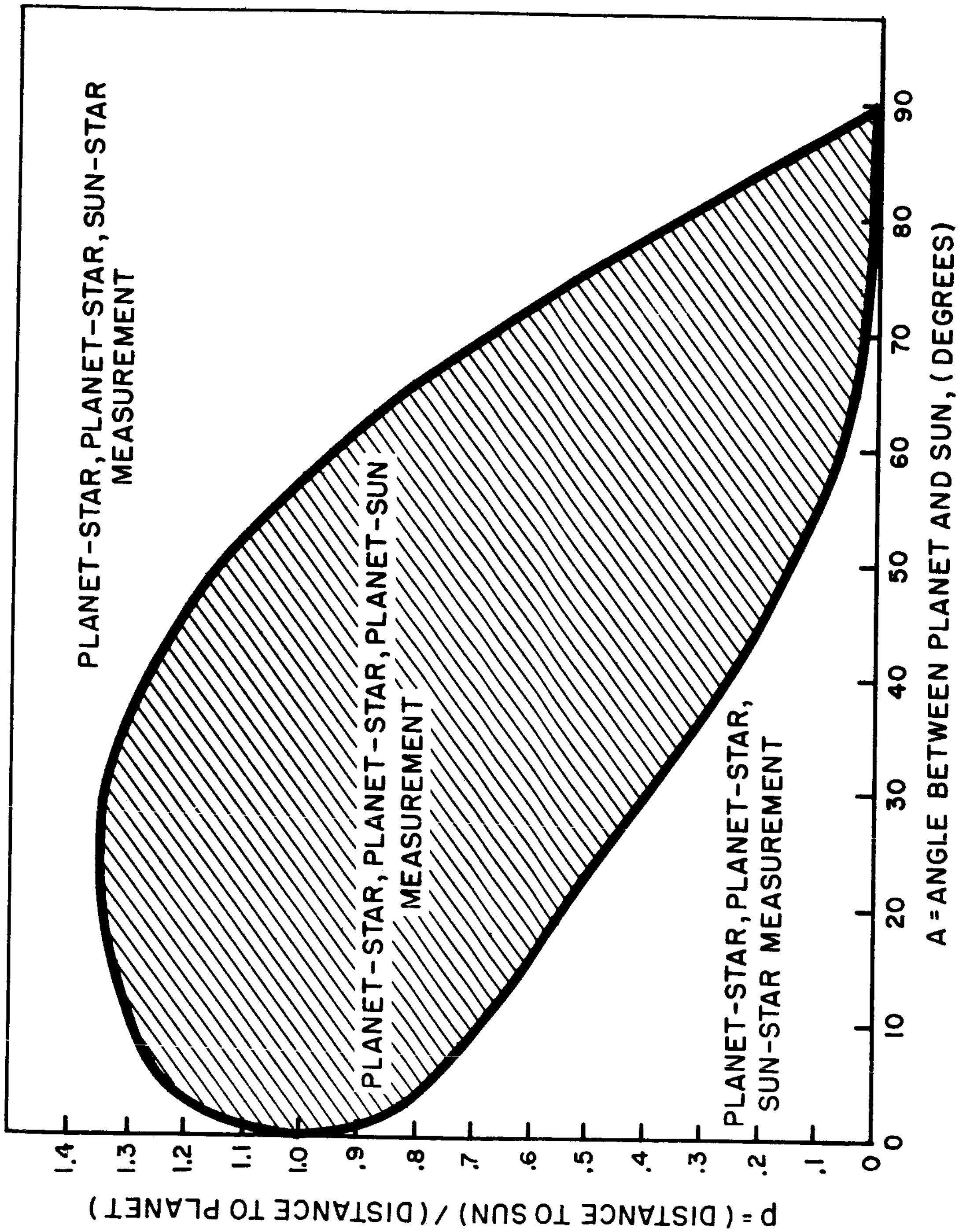

Fig. 3-4 Locus of preferred measurements.

A general purpose digital computer program was prepared which would perform the computations associated with the navigational fix, as described in Appendix B. The input to the program consists of reference trajectory data together with suggested strategies for selecting the appropriate angles to be measured. As many as three different strategies can be analyzed simultaneously, and the computer will produce the best set of measurements, within the imposed restrictions, so that the mean-squared positional error will be a minimum. The following rules were established from which the various strategies may be formulated.

Basic Set of Three Measurements

First Body	Second Body
(1) Body at a finite distance (a) Specific choice of Sun Mercury, Venus, Earth, Mars, or Moon or (b) nearest visible planet or (c) second nearest visible planet	(1) Star (a) Specific choice of a star from among the ten brightest or (b) if unspecified, one of the two best stars, corresponding to the first body, will be selected
(2) Same body as selected for the first measurement	(2) Star (a) Specific choice of a star or (b) the second star of the best pair as mentioned under (1), (b)
(3) Body at a finite distance Same choices available as those listed under (1)	(3) (a) Sun, if first body is the same as that used in the first two measurements

First Body			Second Body
	or	(b)	a specific planet or the nearest or second nearest visible planet if the first body is the sun
	or	(c)	an angular diameter measurement of the first body if that body is a planet
	or	(d)	specific choice of a star
	or	(e)	the best star will be selected in such a way as to minimize the mean-squared error resulting from the first three measurements.

Additional Redundant Measurements

First Body			Second Body
Body at a finite distance Same choices available as those listed under (1)		(a)	A specific planet or the nearest or second nearest visible planet if the first body is the Sun
	or	(b)	an angular diameter measurement of the first body if that body is a planet
	or	(c)	specific choice of a star
	or	(d)	for two redundant measurements, the best pair of stars corresponding to the first body will be selected
	or	(e)	the best star will be selected in such a way as to minimize the mean-squared error resulting from this and all previous measurements

A few remarks are needed to qualify some of the terms used in above rules.

(1) A planet will be said to be visible if the angle between the lines-of-sight to the planet and to the Sun is greater than 15^{o}. The visibility of stars is checked with the same criterion, and only visible stars are selected.

(2) If the Earth is the nearest visible planet, the Moon will be selected as the second nearest planet provided that the angle between the lines-of-sight to the Earth and to the Moon is greater than 3^{o}.

(3) For two measurements involving a body at a finite distance and two stars, the stars referred to as "best" are those for which the two measurement planes are orthogonal. (By "measurement plane" is meant the plane in which the angle is measured.)

(4) An upper limit of six was arbitrarily set on the total number of permissible measurements.

The specific inputs to the digital computer program consist of the following:

(1) Data to determine a specific reference trajectory.

(2) The moment matrix Φ_{mm} of the measurement errors as defined in Appendix B.

(3) A set of times at which celestial fixes are to be made.

(4) As many as three strategies formulated according to the rules described above.

After the computer has evaluated each of the strategies at each of the times specified for a fix, the selected measurements are displayed. The RMS position and time errors are obtained for the basic set of three measurements and again as each redundant measurement is added. In this way the effect of additional measurements is seen explicitly. Finally, the coefficient matrix F_{4m}, defined in Eq (B-32), which relates angular measurement errors to the corresponding position and time errors, is obtained. This matrix is the basic input to the navigation program to be described below.

II. Velocity Correction and Guidance Error Analysis

The fundamental principles of both the fixed and the variable-time-of-arrival navigation techniques are described in detail in Appendix C. Our present study was restricted primarily to an analysis of the variable-time-of-arrival scheme since its advantages, when considering a one-way planetary mission, seem far to overbalance any potential difficulties which could result from an uncertainty in the exact time of rendezvous with the destination planet. To emphasize the advantages of the variable-time-of-arrival scheme, and for comparison purposes, some results for the fixed-time-of-arrival technique are included.

For the most part, the following analysis of the guidance problem is concerned with the fuel requirements of the spacecraft for mid-course velocity corrections and the miss distance at the target planet measured with respect to a point which is fixed relative to the planet. These two quantities are related to the errors, which result from imperfect celestial fixes and imperfect velocity corrections, as shown explicitly in Eq (C-40) and (C-47). Of somewhat lesser importance in the current study is the spacecraft's deviation from the nominal value of velocity at the target planet. This velocity deviation is related to the entire history of applied velocity corrections, as shown in Eq (C-41).

The method of analysis closely parallels the approach taken in R-235 and is entirely statistical in nature. If the moment matrix Φ_{mm} for the measurement errors is postulated, the correlation matrix, E_{44}, of the position and time estimate errors at each check-point may be determined from Eq (B-33). The set of coefficient matrices F_{4m}, one for each check-point, is an output of the celestial fix program. The correlation matrix of the velocity correction errors is calculated by assuming the vector velocity correction error to be isotropic and statistically independent of the corresponding velocity correction but, nonetheless such that its rms value is a predetermined percentage of the rms correction.

A digital computer program was prepared which would perform the statistical analysis of the guidance problem in the manner described above. The program is capable of analyzing both types of navigation techniques.

The specific inputs to the computer program are as follows:

(1) The values of the fundamental matrices, R, R*, V, and V*, for the specific reference trajectory at each of the various fix times.

(2) The coefficient matrices, F_{4m}, at each of the check-points.

(3) The moment matrix, Φ_{mm}, of the measurement errors.

(4) An assumed rms injection velocity error resulting from imperfect injection guidance.

(5) An assumed rms accelerometer error expressed as a percentage of the applied velocity correction at each check-point.

From this input data the computer produces, at each check-point, the rms velocity corrections actually applied together with both the rms deviation in velocity and the rms miss distance at the target planet.

III. Computation Results and Conclusions

From the orbit studies of Chapter 2, four trajectories were selected for use as samples in analyzing the variable-time-of-arrival navigational scheme. These trajectories are illustrated in Figs.3-5 through 3-8 and their basic characteristics are summarized in Table 3-1.

TRAJECTORY DATA

	EARTH TO MARS		EARTH TO VENUS	
	I	II	III	IV
TIME OF DEPARTURE	NOV. 5,1964	NOV.24,1964	APR.19,1964	APR.19,1964
TIME OF FLIGHT (YEARS)	0.85	0.50	0.45	0.30
INJECTION VELOCITY (FT/SEC)	37484	38583	37410	38826
HYPERBOLIC VELOCITY EXCESS AT EARTH (FT/SEC)	9968	13526	9688	14206
COMPONENTS OF HYPERBOLIC VELOCITY EXCESS IN THE ECLIPTIC COORDINATE SYSTEM (FT/SEC)	-8478 4288 3016	-12788 3633 2493	-2582 9324 510	3678 11471 -7529
SEMI-MAJOR AXIS (A.U.)	1.24466	1.40745	0.84580	0.87093
ECCENTRICITY	0.20788	0.30040	0.18806	0.17330
HYPERBOLIC VELOCITY EXCESS AT DESTINATION PLANET (FT/SEC)	9135	25261	18357	13339
DISTANCE FROM EARTH AT TIME OF CONTACT (A.U.)	1.79539	1.07767	0.95173	0.53476
LAUNCH AZIMUTH FROM CAPE CANAVERAL (DEG)	100	110	100	100
LONGITUDE OF INJECTION POINT (DEG)	125 E	144 E	128 E	1 E
LATITUDE OF INJECTION POINT (DEG)	16 S	5 N	15 S	10 S

TABLE 3-1

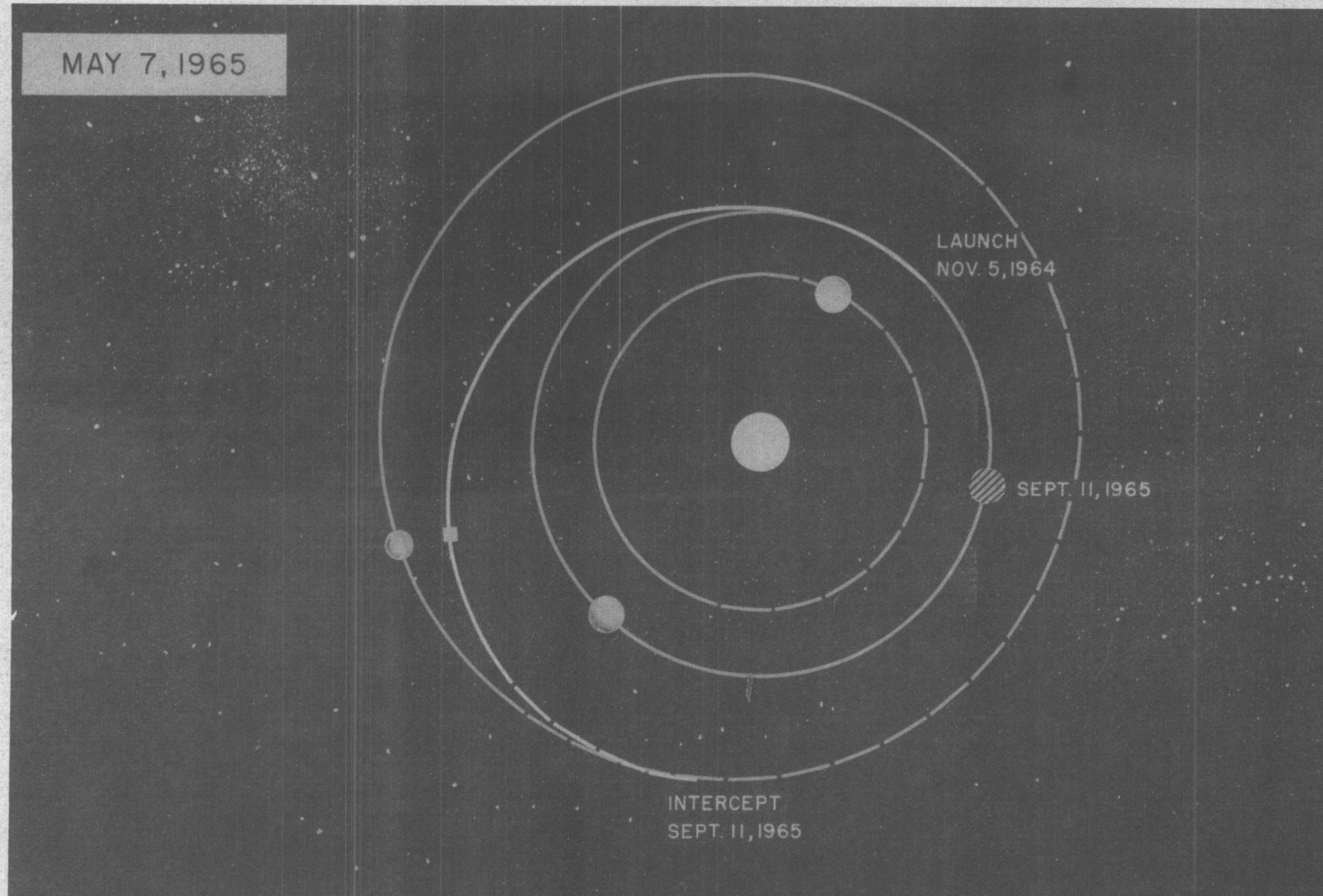

Fig. 3-5 Mars trajectory I.

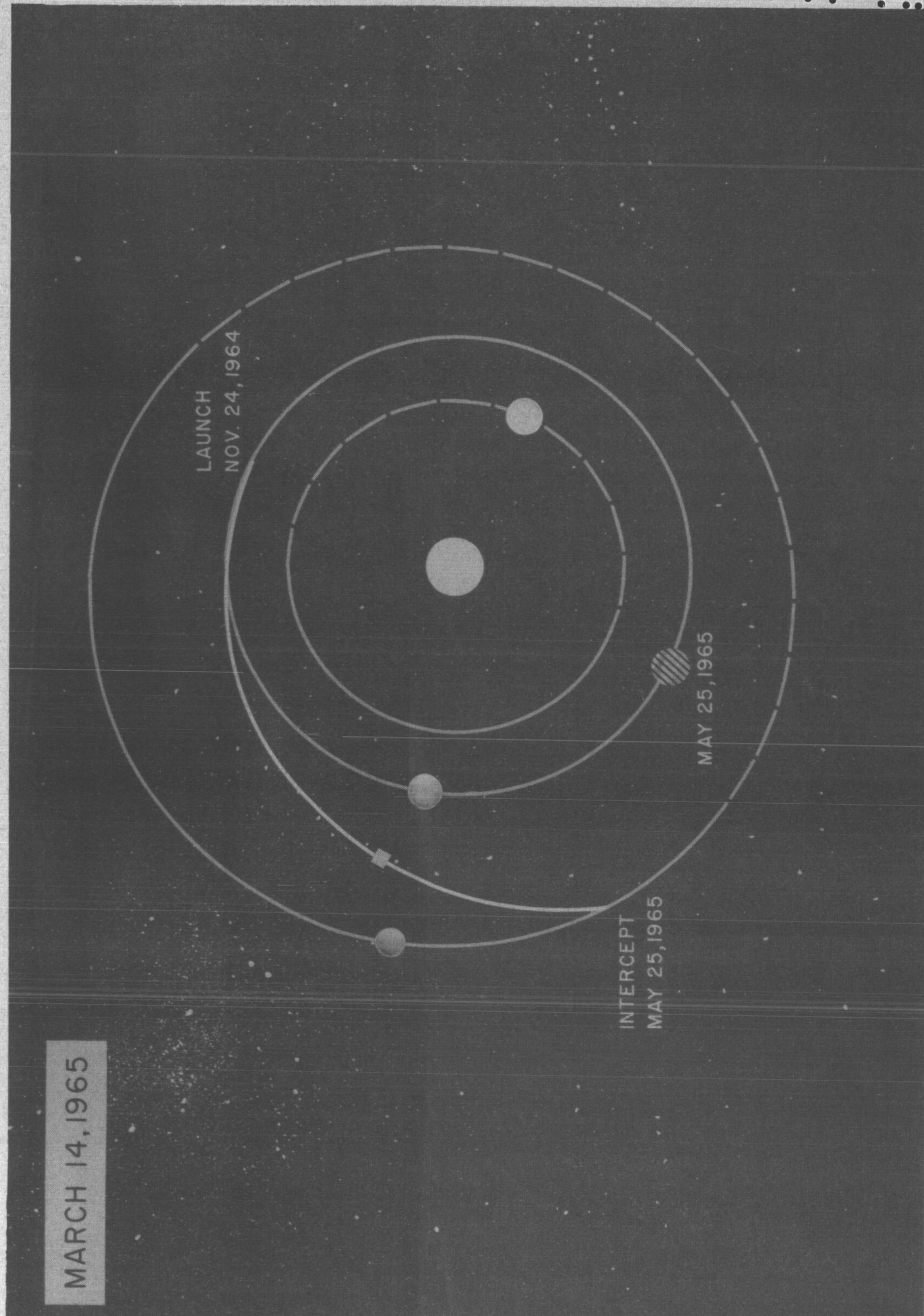

Fig. 3-6 Mars trajectory II.

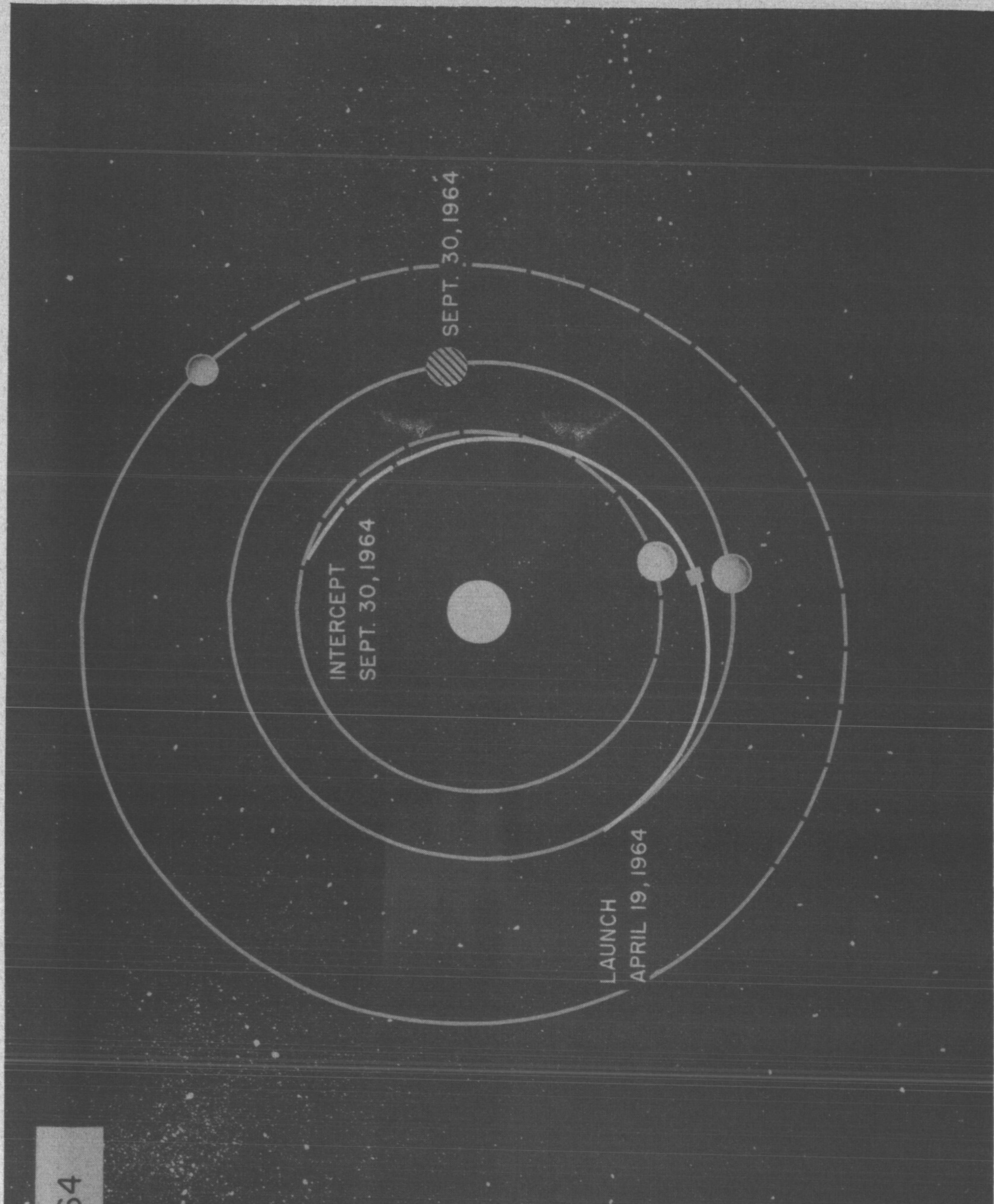

Fig. 3-7 Venus trajectory III.

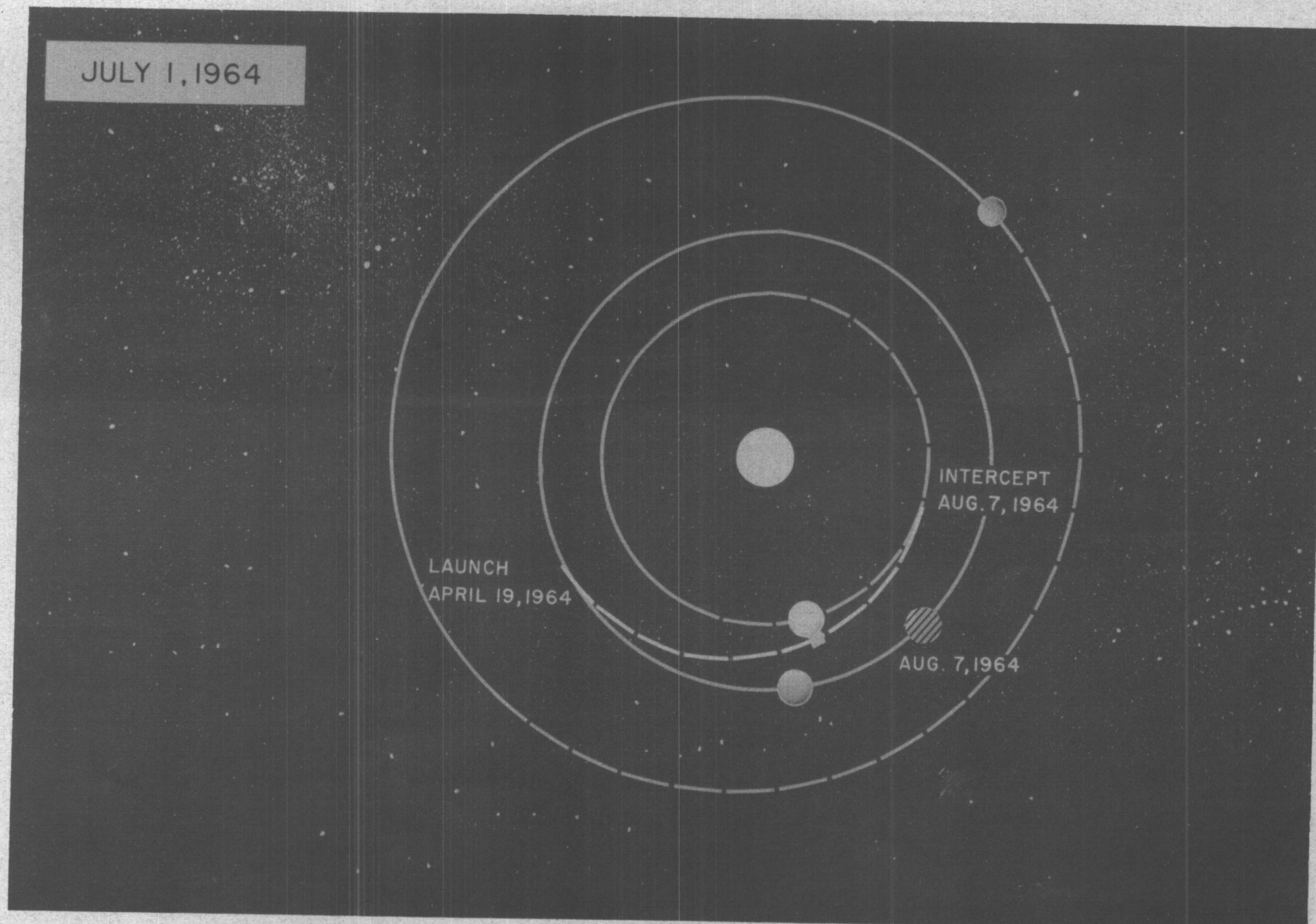

Fig. 3-8 Venus trajectory IV.

The illustrations show the orbits of the spacecraft and the planets Venus, Earth, and Mars. The paths are shown as solid lines when the orbital plane is above the plane of the ecliptic and broken lines when below. The launch and arrival positions are marked with the corresponding dates. The configuration of the spacecraft and the planets is shown for one instant of time during mid-course on the date indicated in the figures. A shaded circle is used to show the position of the Earth at the time of contact with the target planet.

Six different strategies for choosing celestial objects in obtaining a navigation fix were formulated and applied to each of the four selected trajectories. The details of the selection are defined below:

Strategy 1

Basic Measurements

(1) and (2) Nearest visible planet and two best stars

(3) Nearest visible planet and the Sun

Redundant Measurements

(4) and (5) Second nearest visible planet and two best stars

(6) Second nearest visible planet and the Sun or the angular diameter of the nearest visible planet if the planet is close enough to make the measurement significant.

Strategy 2

Basic Measurements

(1) and (2) Nearest visible planet and two best stars

(3) Nearest visible planet and the Sun

Redundant Measurements

(4) and (5) Sun and two best stars

(6) Nearest visible planet and the Sun

or, if a planet is near enough to make an angular diameter measurement significant

(4) Sun and best star to optimize the first four measurements

(5) Sun and second nearest visible planet

(6) The angular diameter of the nearest visible planet.

Strategy 3

Basic Measurements

(1) and (2) Sun and two best stars

(3) Sun and nearest visible planet

Redundant Measurements

(4) and (5) Nearest visible planet and best two stars

(6) Second nearest visible planet and the Sun or the angular diameter of the nearest visible planet if the planet is close enough to make the measurement significant.

Strategy 4

Basic Measurements

(1) and (2) Sun and two best stars

(3) Nearest visible planet and best star to optimize the first three measurements

Redundant Measurements

(4) Nearest visible planet and best star to optimize the first four measurements

(5) Sun and nearest visible planet

(6) Sun and second nearest visible planet or the angular diameter of the nearest visible planet if the planet is close enough to make the measurement significant.

Strategy 5

Basic Measurements

(1) and (2) Sun and two best stars

(3) Sun and nearest visible planet

Redundant Measurements

(4) Nearest visible planet and best star to optimize the first four measurements

(5) Nearest visible planet and best star to optimize the first five measurements

(6) Sun and second nearest visible planet or the angular diameter of the nearest visible planet if the planet is close enough to make the measurement significant.

Strategy 6

Basic Measurements

(1) and (2) Second nearest visible planet and two best stars

(3) Nearest visible planet and best star to optimize the first three measurements

Redundant Measurements

(4) Sun and second nearest visible planet

(5) Nearest visible planet and best star to optimize the first five measurements

(6) Sun and nearest visible planet or the angular diameter of the nearest visible planet if the planet is close enough to make the measurement significant.

In the analysis, the standard deviation of the measurement errors was assumed to be 0.05 milliradians or 10.3 seconds of arc and the clock was assumed to drift at a constant rms rate of one part in 100,000. A comparison of the six celestial fix strategies at various instants of time along the four spacecraft trajectories is shown in Tables 3-2 through 3-5. Several observations are worthy of comment:

(1) The use of the Moon as a navigational aid contributes significantly to a precise positional fix when the spacecraft is in the vicinity of the Earth. A reduction in the positional error by more than a factor of three is seen in some instances.

(2) No single strategy for selecting objects is preferred, i.e., a particular combination of measurements selected according to one set of rules may be best at one instant of time and yet be inferior at some other time.

(3) Although no star was ever explicitly selected, all stars provided in the list were chosen at one time or other. Thus, the added generality provided by a large choice of available stars seems to have importance.

(4) The quantitative effect of redundant measurements on reducing the mean-squared positional error aids considerably in determining which measurements are really worthwile. Before an actual set of measurements could be finalized, it would seem advisable to determine precisely what effect each measurement has on the accuracy of the fix. This can be readily accomplished within the scope of the present computer program.

(5) When the spacecraft is in the vicinity of the Earth at a time when the Moon is visible, the measurement of the apparent diameter of the Earth is almost worthless. Therefore, in preparing data for the navigation program, the Earth's diameter measurement was replaced by the alternate measurement cited under each set of strategy rules.

(6) In Table 3-2, Strategy 1 at time 0.80 years from launch, it is seen that the first redundant measurement apparently causes an increase in the rms position error. If the third and fourth measurements are interchanged, one finds that the measurement of the angle between Earth and Arcturus, together with the first two measurements, results in an rms position error of some 50,000 miles. Therefore, this paradox of an additional measurement resulting in a larger error may be attributed to computational inaccuracies arising from rounding errors.

The data from Tables 3-2 through 3-5 were used to select the most promising strategies to arrive at a single set of "optimum" measurements for each instant of time along the various trajectories. The best obtained rms position and time errors as a function of time from launch are tabulated in Tables 3-6 through 3-9. These data provided the necessary input to the navigation program.

In order to test the concept of variable-time-of-arrival navigation a number of complete runs were made with the navigation program described in Section II. The postulated errors are: (1) an rms injection velocity error of 18 ft per sec as suggested by Centaur booster specifications; (2) an rms error in applying any desired velocity change of 1%; (3) an rms clock drift rate of one part in 100,000; (4) an rms error in angle measurements of 0.05 milliradians.

The injection velocity error corresponds to burn-out of the main propulsion. Therefore, it is necessary to apply a magnification factor of $\left[1 + (v_e / v_R)^2\right]$ to the mean-squared injection velocity error to obtain the mean-squared velocity error after escape. Here v_e and v_R are, respectively, the escape velocity and the excess hyperbolic velocity of the space craft.

For the clock error we assume that between the times of two consecutive fixes the clock is drifting at a constant rate, where the rate is random, and statistically independent of any previous drift.

In each of the navigation runs four fixes and associated velocity corrections were made. The times selected as check points were chosen in the following way for each trajectory.

From the possible times of fix, as listed in Tables 3-6 through 3-9, four subsets of times were picked. Then the fix times for each navigation run were selected, one from each group, by a random choice. The individual groups were made up as follows:

Mars Trajectory I

Group 1:	0.001, 0.002, 0.003, 0.004, 0.005, 0.006
Group 2:	0.300, 0.325, 0.350, 0.375, 0.400, 0.425
Group 3:	0.725, 0.750, 0.775, 0.840
Group 4:	0.843, 0.844, 0.845, 0.846, 0.847, 0.848

Mars Trajectory II

Group 1:	0.001, 0.002, 0.003, 0.004, 0.005
Group 2:	0.025, 0.050, 0.075, 0.100
Group 3:	0.275, 0.300, 0.325, 0.350, 0.400, 0.425
Group 4:	0.493, 0.494, 0.495, 0.496, 0.497, 0.498

Venus Trajectory III

Group 1:	0.001, 0.002, 0.003, 0.004, 0.005, 0.006
Group 2:	0.025, 0.050, 0.200, 0.225
Group 3:	0.250, 0.275, 0.300, 0.325, 0.375, 0.400
Group 4:	0.443, 0.444, 0.445, 0.446, 0.447, 0.448

Venus Trajectory IV

Group 1:	0.001, 0.002, 0.003, 0.004, 0.005, 0.006
Group 2:	0.025, 0.075, 0.100, 0.125, 0.150, 0.175
Group 3:	0.200, 0.225, 0.250
Group 4:	0.293, 0.294, 0.295, 0.296, 0.297, 0.298

Fifty sets of fix times for each trajectory were prepared in this way. The result of each run is represented by a point in the Fig. 3-9 through 3-12 where the final position error in miles has been plotted against total velocity correction in ft per sec. The envelope of these points is shown in the figures and is to be used as the principle criterion in defining a mission. This curve expresses the ultimate precision attainable for the trajectory as far as optimizing the miss distance with respect to total velocity correction. We see that, in general, position accuracy can be increased only at the expense of extra fuel.

Mars trajectory I is superior to II with respect to navigation accuracy. One can perhaps correlate this result with the fact that the velocity relative to Mars at arrival is much less for I than for II. The same thesis is borne out when Venus trajectory III is compared with IV.

The distribution of points in Fig. 3-11 for Venus trajectory III is so widely scattered that it is impossible to recognize any envelope curve from the available data.

The detailed history of each navigation run lying along the envelope curve is presented in Tables 3-10 through 3-13.

Finally, in order to compare the variable-time-of-arrival and the fixed-time-of-arrival navigation schemes, the fifty runs for Mars trajectory I were repeated using the latter guidance technique. The results are presented in Fig. 3-13 and Table 3-14. The conclusion is immediate. The superiority of one over the other is more than two-fold with regard to both position accuracy and total velocity correction required.

[redacted]

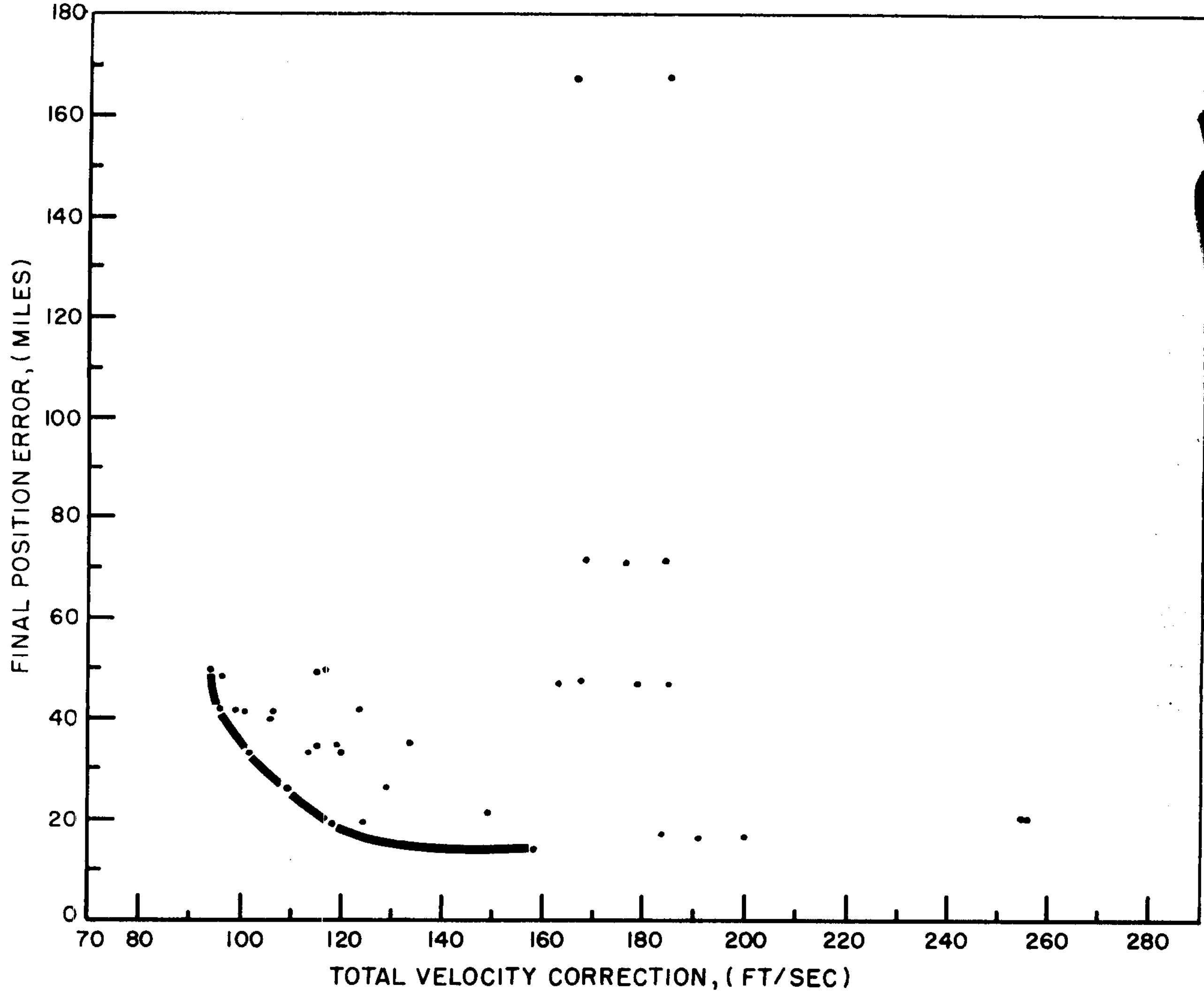

Fig. 3-9 Variable time of arrival--Mars trajectory I.

[redacted]

[redacted]

DECLASSIFIED

[redacted]

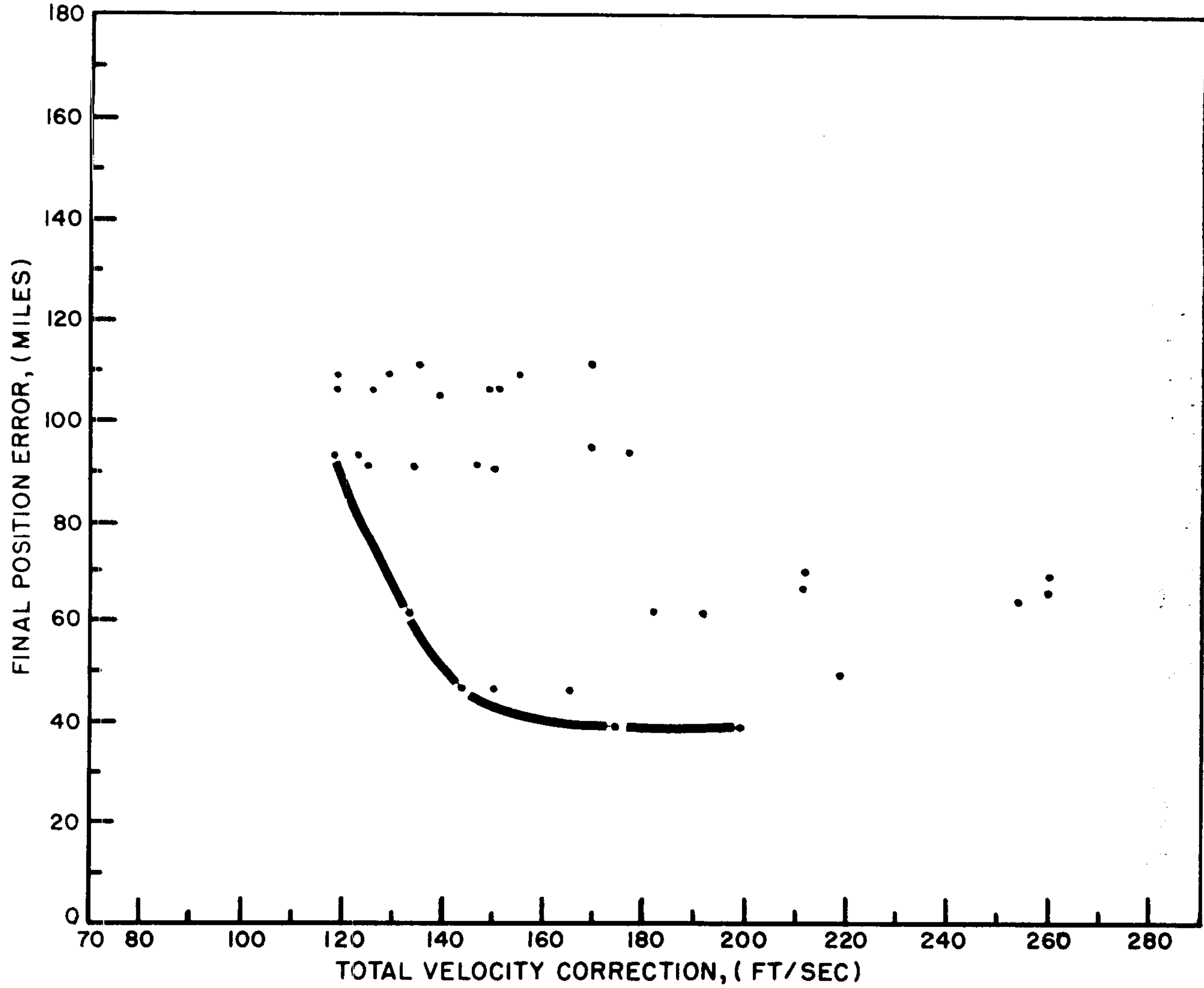

Fig. 3-10 Variable time of arrival--Mars trajectory II.

[redacted]

N - 5337

[redacted]

[redacted] DECLASSIFIED

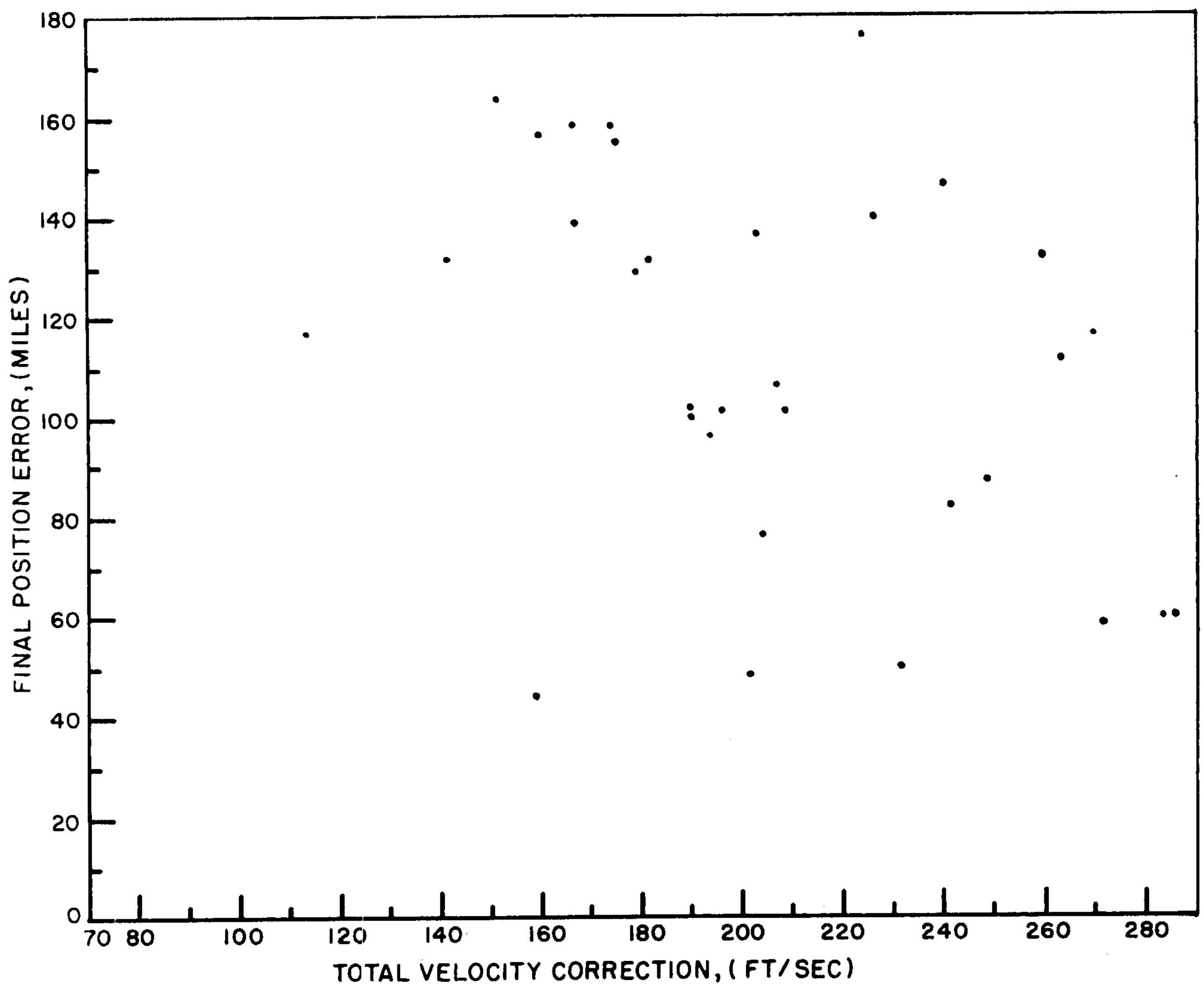

Fig. 3-11 Variable time of arrival--Venus trajectory III.

[redacted]

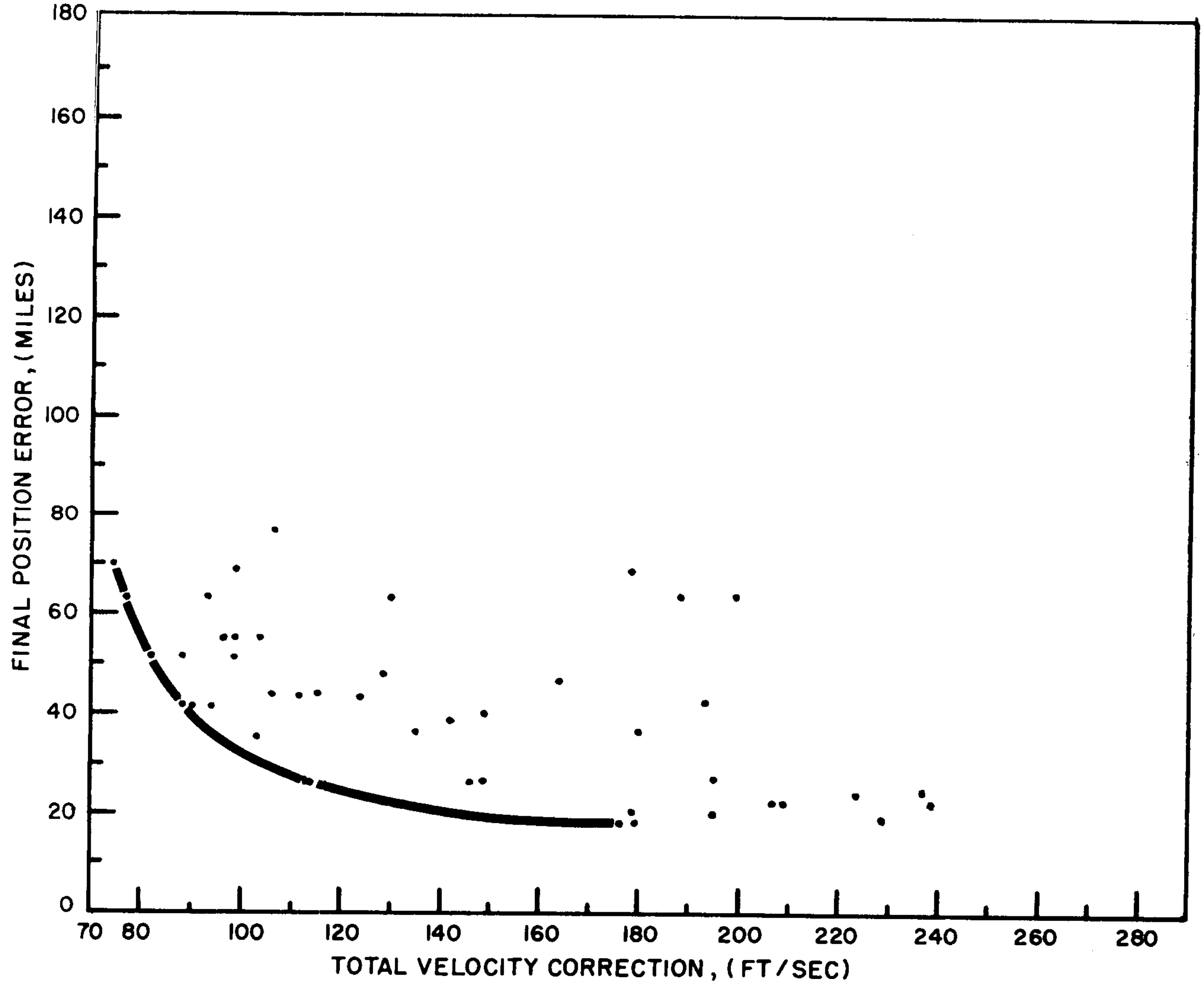

Fig. 3-12 Variable time of arrival--Venus trajectory IV.

[redacted]

[redacted]

[redacted]

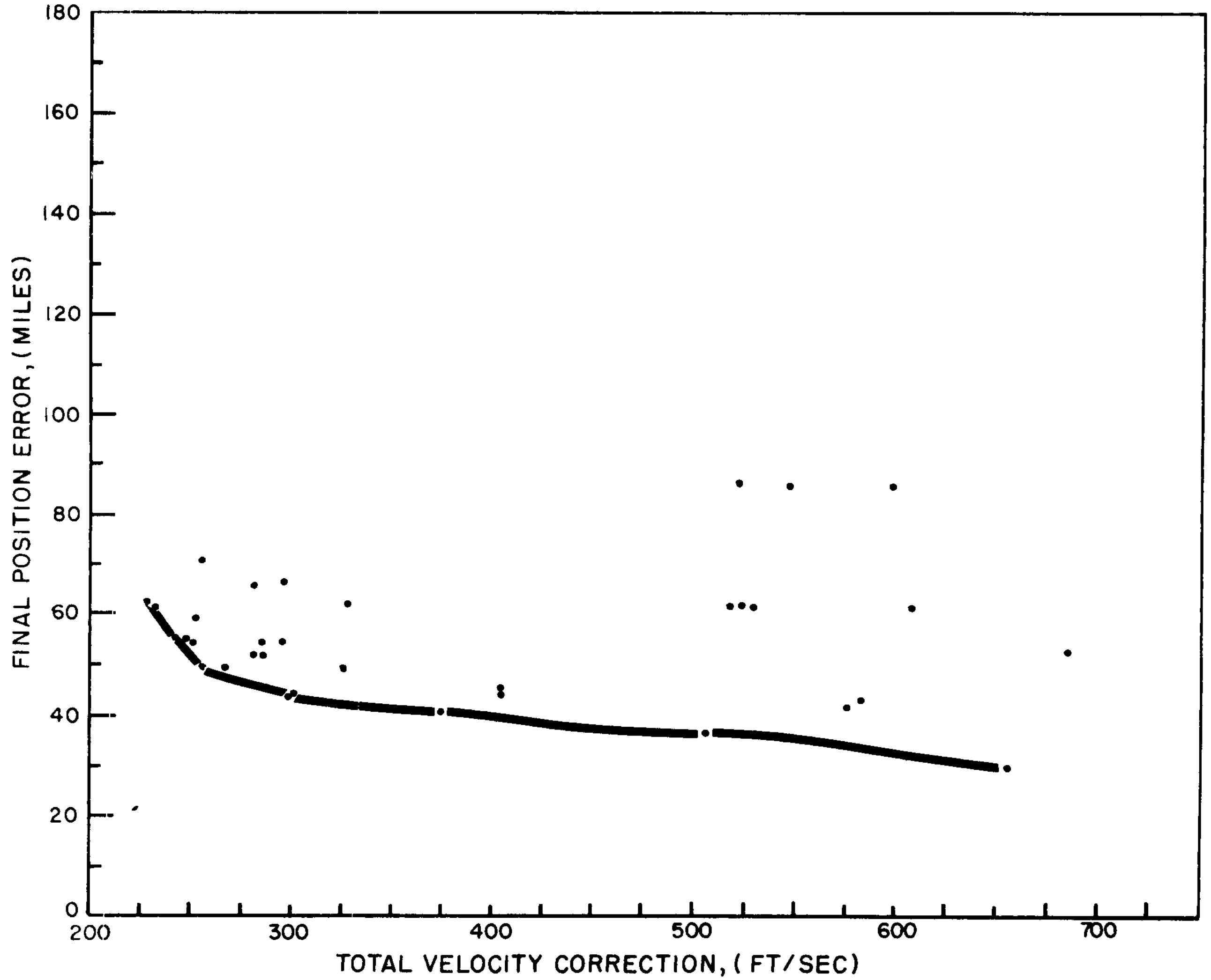

Fig. 3-13 Fixed time of arrival--Mars trajectory I.

[redacted]

[redacted]

[redacted] DECLASSIFIED

C[illegible]ARISON OF CELESTIAL FIX STRATEGIES

MARS TRAJ. NOV.5,1964 V_I = 37484 FT/SEC T_F = 0.85 YEARS V_{RM} = 9135 FT/SEC

TIME IN YEARS	FIRST BODY	SECOND BODY	RMS POSITION ERROR MILES	RMS TIME ERROR HOURS	TIME	FIRST BODY	SECOND BODY	RMS POSITION ERROR MILES	RMS TIME ERROR HOURS
		STRATEGY 1					STRATEGY 4		
0.02	EARTH	VEGA			0.02	SUN	SIRIUS		
	EARTH	CAPELLA				SUN	CAPELLA		
	EARTH	SUN	6572	0.0018		EARTH	CAPELLA	6668	0.0018
	MOON	VEGA	2122	0.0018		EARTH	VEGA	4592	0.0018
	MOON	CAPELLA	2089	0.0018		SUN	EARTH	3768	0.0018
	EARTH	DIAMETER	2035	0.0018		EARTH	DIAMETER	3474	0.0018
		STRATEGY 2					STRATEGY 5		
0.02	EARTH	VEGA			0.02	SUN	SIRIUS		
	EARTH	CAPELLA				SUN	CAPELLA		
	EARTH	SUN	6572	0.0018		SUN	EARTH	6560	0.0018
	SUN	CAPELLA	4014	0.0018		EARTH	PROCYON	4602	0.0018
	SUN	MOON	4014	0.0018		EARTH	CAPELLA	3689	0.0018
	EARTH	DIAMETER	3663	0.0018		EARTH	DIAMETER	3411	0.0018
		STRATEGY 3					STRATEGY 6		
0.02	SUN	SIRIUS			0.02	MOON	VEGA		
	SUN	CAPELLA				MOON	CAPELLA		
	SUN	EARTH	6560	0.0018		EARTH	VEGA	2349	0.0018
	EARTH	VEGA	4602	0.0018		SUN	MOON	2296	0.0018
	EARTH	CAPELLA	3768	0.0018		EARTH	ACHERNAR	2050	0.0018
	EARTH	DIAMETER	3474	0.0018		EARTH	DIAMETER	1998	0.0018

TABLE 3-2

[redacted]

COMPARISON OF CELESTIAL FIX STRATEGIES

MARS TRAJ. NOV.5,1964 V_I = 37484 FT/SEC T_F = 0.85 YEARS V_{RM} = 9135 FT/SEC

TIME IN YEARS	FIRST BODY	SECOND BODY	RMS POSITION ERROR MILES	RMS TIME ERROR HOURS	TIME	FIRST BODY	SECOND BODY	RMS POSITION ERROR MILES	RMS TIME ERROR HOURS
		STRATEGY 1					STRATEGY 4		
0.04	EARTH	VEGA			0.04	SUN	SIRIUS		
	EARTH	CAPELLA				SUN	ARCTURUS		
	EARTH	SUN	6457	0.0035		EARTH	CAPELLA	6653	0.0035
	MOON	SIRIUS	2572	0.0035		EARTH	VEGA	4789	0.0035
	MOON	A CENTAURI	1714	0.0035		SUN	EARTH	3854	0.0035
	EARTH	DIAMETER	1712	0.0035		EARTH	DIAMETER	3831	0.0035
		STRATEGY 2					STRATEGY 5		
0.04	EARTH	VEGA			0.04	SUN	SIRIUS		
	EARTH	CAPELLA				SUN	ARCTURUS		
	EARTH	SUN	6457	0.0035		SUN	EARTH	6530	0.0035
	SUN	ARCTURUS	4054	0.0035		EARTH	A CENTAURI	4791	0.0035
	SUN	MOON	1280	0.0035		EARTH	ARCTURUS	3766	0.0035
	EARTH	DIAMETER	1280	0.0035		EARTH	DIAMETER	3745	0.0035
		STRATEGY 3					STRATEGY 6		
0.04	SUN	SIRIUS			0.04	MOON	SIRIUS		
	SUN	ARCTURUS				MOON	A CENTAURI		
	SUN	EARTH	6530	0.0035		EARTH	CAPELLA	1919	0.0035
	EARTH	VEGA	4801	0.0035		SUN	MOON	1428	0.0035
	EARTH	CAPELLA	3854	0.0035		EARTH	ARCTURUS	1135	0.0035
	EARTH	DIAMETER	3831	0.0035		EARTH	DIAMETER	1134	0.0035

TABLE 3-2

C ARISON OF CELESTIAL FIX STRATEGIES

MARS TRAJ. NOV.5,1964 V_I = 37484 FT/SEC T_F = 0.85 YEARS V_{RM} = 9135 FT/SEC

TIME IN YEARS	FIRST BODY	SECOND BODY	RMS POSITION ERROR MILES	RMS TIME ERROR HOURS	TIME	FIRST BODY	SECOND BODY	RMS POSITION ERROR MILES	RMS TIME ERROR HOURS
		STRATEGY 1					STRATEGY 4		
0.06	EARTH	VEGA			0.06	SUN	SIRIUS		
	EARTH	CAPELLA				SUN	ARCTURUS		
	EARTH	SUN	6468	0.0053		EARTH	CAPELLA	6733	0.0053
	MOON	VEGA	6461	0.0053		EARTH	VEGA	4797	0.0053
	MOON	CAPELLA	3624	0.0053		SUN	EARTH	3862	0.0053
	EARTH	DIAMETER	3620	0.0053		EARTH	DIAMETER	3857	0.0053
		STRATEGY 2					STRATEGY 5		
0.06	EARTH	VEGA			0.06	SUN	SIRIUS		
	EARTH	CAPELLA				SUN	ARCTURUS		
	EARTH	SUN	6468	0.0053		SUN	EARTH	6543	0.0053
	SUN	ARCTURUS	3980	0.0053		EARTH	A CENTAURI	4776	0.0053
	SUN	MOON	3911	0.0052		EARTH	ARCTURUS	3781	0.0053
	EARTH	DIAMETER	3906	0.0052		EARTH	DIAMETER	3777	0.0053
		STRATEGY 3					STRATEGY 6		
0.06	SUN	SIRIUS			0.06	MOON	VEGA		
	SUN	ARCTURUS				MOON	CAPELLA		
	SUN	EARTH	6543	0.0053		EARTH	CAPELLA	8114	0.0053
	EARTH	VEGA	4793	0.0053		SUN	MOON	6036	0.0052
	EARTH	CAPELLA	3862	0.0053		EARTH	B CENTAURI	5738	0.0052
	EARTH	DIAMETER	3857	0.0053		EARTH	DIAMETER	5722	0.0052

TABLE 3-2

DECLASSIFIED

COMPARISON OF CELESTIAL FIX STRATEGIES

MARS TRAJ. NOV.5,1964 V_I = 37484 FT/SEC T_F = 0.85 YEARS V_{RM} = 9135 FT/SEC

TIME IN YEARS	FIRST BODY	SECOND BODY	RMS POSITION ERROR MILES	RMS TIME ERROR HOURS	TIME	FIRST BODY	SECOND BODY	RMS POSITION ERROR MILES	RMS TIME ERROR HOURS
		STRATEGY 1					STRATEGY 4		
0.10	EARTH	VEGA			0.10	SUN	PROCYON		
	EARTH	CAPELLA				SUN	ACHERNAR		
	EARTH	SUN	6915	0.0088		EARTH	ARCTURUS	7074	0.0088
	MARS	SIRIUS	6935	0.0088		EARTH	B CENTAURI	5031	0.0088
	MARS	B CENTAURI	6380	0.0088		SUN	EARTH	4022	0.0088
	SUN	MARS	4568	0.0088		SUN	MARS	3453	0.0088
		STRATEGY 2					STRATEGY 5		
0.10	EARTH	VEGA			0.10	SUN	PROCYON		
	EARTH	CAPELLA				SUN	ACHERNAR		
	EARTH	SUN	6915	0.0088		SUN	EARTH	6758	0.0088
	SUN	PROCYON	5131	0.0088		EARTH	ACHERNAR	4937	0.0088
	SUN	ACHERNAR	4075	0.0088		EARTH	CAPELLA	4123	0.0088
	SUN	MARS	3477	0.0088		SUN	MARS	3504	0.0088
		STRATEGY 3					STRATEGY 6		
0.10	SUN	PROCYON			0.10	MARS	SIRIUS		
	SUN	ACHERNAR				MARS	B CENTAURI		
	SUN	EARTH	6758	0.0088		EARTH	B CENTAURI	16352	0.0088
	EARTH	VEGA	4940	0.0088		SUN	MARS	9330	0.0088
	EARTH	CAPELLA	4075	0.0088		EARTH	RIGEL	6200	0.0088
	SUN	MARS	3477	0.0088		SUN	EARTH	4516	0.0088

TABLE 3-2

C[illegible]RISON OF CELESTIAL FIX STRATEGIES

MARS TRAJ. NOV.5,1964 V_I = 37484 FT/SEC T_F = 0.85 YEARS V_{RM} = 9135 FT/SEC

TIME IN YEARS	FIRST BODY	SECOND BODY	RMS POSITION ERROR MILES	RMS TIME ERROR HOURS	TIME	FIRST BODY	SECOND BODY	RMS POSITION ERROR MILES	RMS TIME ERROR HOURS
		STRATEGY 1					STRATEGY 4		
0.20	EARTH	A CENTAURI			0.20	SUN	RIGEL		
	EARTH	PROCYON				SUN	B CENTAURI		
	EARTH	SUN	16584	0.0175		EARTH	ARCTURUS	13393	0.0175
	MARS	SIRIUS	10257	0.0174		EARTH	B CENTAURI	12453	0.0174
	MARS	A CENTAURI	5609	0.0174		SUN	EARTH	9849	0.0174
	SUN	MARS	5087	0.0170		SUN	MARS	7399	0.0166
		STRATEGY 2					STRATEGY 5		
0.20	EARTH	A CENTAURI			0.20	SUN	RIGEL		
	EARTH	PROCYON				SUN	B CENTAURI		
	EARTH	SUN	16584	0.0175		SUN	EARTH	12341	0.0175
	SUN	RIGEL	9864	0.0175		EARTH	ARCTURUS	11111	0.0175
	SUN	B CENTAURI	9818	0.0174		EARTH	SIRIUS	9750	0.0174
	SUN	MARS	7425	0.0166		SUN	MARS	7632	0.0166
		STRATEGY 3					STRATEGY 6		
0.20	SUN	RIGEL			0.20	MARS	SIRIUS		
	SUN	B CENTAURI				MARS	A CENTAURI		
	SUN	EARTH	12341	0.0175		EARTH	CAPELLA	7140	0.0175
	EARTH	A CENTAURI	11340	0.0174		SUN	MARS	6473	0.0173
	EARTH	PROCYON	9818	0.0174		EARTH	SIRIUS	5213	0.0172
	SUN	MARS	7425	0.0166		SUN	EARTH	5050	0.0170

TABLE 3-2

DECLASSIFIED

COMPARISON OF CELESTIAL FIX STRATEGIES

MARS TRAJ. NOV.5,1964 V_I = 37484 FT/SEC T_F = 0.85 YEARS V_{RM} = 9135 FT/SEC

TIME IN YEARS	FIRST BODY	SECOND BODY	RMS POSITION ERROR MILES	RMS TIME ERROR HOURS	TIME	FIRST BODY	SECOND BODY	RMS POSITION ERROR MILES	RMS TIME ERROR HOURS
		STRATEGY 1					STRATEGY 4		
0.30	EARTH	SIRIUS			0.30	SUN	SIRIUS		
	EARTH	CAPELLA				SUN	A CENTAURI		
	EARTH	SUN	20549	0.0263		EARTH	CAPELLA	17447	0.0263
	MARS	SIRIUS	4734	0.0258		EARTH	PROCYON	16529	0.0262
	MARS	A CENTAURI	3216	0.0257		SUN	EARTH	12548	0.0262
	SUN	MARS	2400	0.0254		SUN	MARS	2984	0.0252
		STRATEGY 2					STRATEGY 5		
0.30	EARTH	SIRIUS			0.30	SUN	SIRIUS		
	EARTH	CAPELLA				SUN	A CENTAURI		
	EARTH	SUN	20549	0.0263		SUN	EARTH	14980	0.0263
	SUN	SIRIUS	18500	0.0262		EARTH	CAPELLA	13823	0.0263
	SUN	A CENTAURI	12561	0.0262		EARTH	ARCTURUS	12511	0.0262
	SUN	MARS	2979	0.0252		SUN	MARS	3149	0.0252
		STRATEGY 3					STRATEGY 6		
0.30	SUN	SIRIUS			0.30	MARS	SIRIUS		
	SUN	A CENTAURI				MARS	A CENTAURI		
	SUN	EARTH	14980	0.0263		EARTH	CAPELLA	4597	0.0263
	EARTH	SIRIUS	13915	0.0262		SUN	MARS	3729	0.0259
	EARTH	CAPELLA	12561	0.0262		EARTH	PROCYON	2563	0.0258
	SUN	MARS	2979	0.0252		SUN	EARTH	2403	0.0253

TABLE 3-2

COMPARISON OF CELESTIAL FIX STRATEGIES

MARS TRAJ. NOV.5,1964 V_I = 37484 FT/SEC T_F = 0.85 YEARS V_{RM} = 9135 FT/SEC

TIME IN YEARS	FIRST BODY	SECOND BODY	RMS POSITION ERROR MILES	RMS TIME ERROR HOURS	TIME	FIRST BODY	SECOND BODY	RMS POSITION ERROR MILES	RMS TIME ERROR HOURS
		STRATEGY 1					STRATEGY 4		
0.40	MARS	RIGEL			0.40	SUN	SIRIUS		
	MARS	B CENTAURI				SUN	B CENTAURI		
	MARS	SUN	34750	0.0351		MARS	PROCYON	24293	0.0351
	EARTH	PROCYON	4489	0.0345		MARS	CAPELLA	23039	0.0351
	EARTH	B CENTAURI	3170	0.0345		SUN	MARS	20109	0.0351
	SUN	EARTH	2633	0.0338		SUN	EARTH	4171	0.0328
		STRATEGY 2					STRATEGY 5		
0.40	MARS	RIGEL			0.40	SUN	SIRIUS		
	MARS	B CENTAURI				SUN	B CENTAURI		
	MARS	SUN	34750	0.0351		SUN	MARS	28760	0.0351
	SUN	SIRIUS	24049	0.0351		MARS	PROCYON	23555	0.0351
	SUN	B CENTAURI	21197	0.0351		MARS	CAPELLA	20109	0.0351
	SUN	EARTH	3541	0.0331		SUN	EARTH	4171	0.0328
		STRATEGY 3					STRATEGY 6		
0.40	SUN	SIRIUS			0.40	EARTH	PROCYON		
	SUN	B CENTAURI				EARTH	B CENTAURI		
	SUN	MARS	28760	0.0351		MARS	PROCYON	4412	0.0351
	MARS	RIGEL	26062	0.0351		SUN	EARTH	3599	0.0343
	MARS	B CENTAURI	21197	0.0351		MARS	A CENTAURI	2896	0.0342
	SUN	EARTH	3541	0.0331		SUN	MARS	2669	0.0337

TABLE 3-2

COMPARISON OF CELESTIAL FIX STRATEGIES

MARS TRAJ. NOV.5,1964 V_I = 37484 FT/SEC T_F = 0.85 YEARS V_{RM} = 9135 FT/SEC

TIME IN YEARS	FIRST BODY	SECOND BODY	RMS POSITION ERROR MILES	RMS TIME ERROR HOURS	TIME	FIRST BODY	SECOND BODY	RMS POSITION ERROR MILES	RMS TIME ERROR HOURS
		STRATEGY 1					STRATEGY 4		
0.50	MARS	SIRIUS			0.50	SUN	PROCYON		
	MARS	A CENTAURI				SUN	ACHERNAR		
	MARS	SUN	64163	0.0438		MARS	CAPELLA	44283	0.0438
	EARTH	SIRIUS	8887	0.0427		MARS	PROCYON	43090	0.0437
	EARTH	A CENTAURI	6363	0.0427		SUN	MARS	36959	0.0437
	SUN	EARTH	4233	0.0419		SUN	EARTH	5660	0.0410
		STRATEGY 2					STRATEGY 5		
0.50	MARS	SIRIUS			0.50	SUN	PROCYON		
	MARS	A CENTAURI				SUN	ACHERNAR		
	MARS	SUN	64163	0.0438		SUN	MARS	49630	0.0438
	SUN	PROCYON	42323	0.0438		MARS	CAPELLA	42450	0.0438
	SUN	ACHERNAR	38466	0.0437		MARS	PROCYON	36959	0.0437
	SUN	EARTH	5450	0.0413		SUN	EARTH	5660	0.0410
		STRATEGY 3					STRATEGY 6		
0.50	SUN	PROCYON			0.50	EARTH	SIRIUS		
	SUN	ACHERNAR				EARTH	A CENTAURI		
	SUN	MARS	49630	0.0438		MARS	PROCYON	7981	0.0438
	MARS	SIRIUS	48953	0.0437		SUN	EARTH	5693	0.0427
	MARS	A CENTAURI	38466	0.0437		MARS	B CENTAURI	4413	0.0426
	SUN	EARTH	5450	0.0413		SUN	MARS	4272	0.0417

TABLE 3-2

COMPARISON OF CELESTIAL FIX STRATEGIES

MARS TRAJ. NOV.5,1964 V_I = 37484 FT/SEC T_F = 0.85 YEARS V_{RM} = 9135 FT/SEC

TIME IN YEARS	FIRST BODY	SECOND BODY	RMS POSITION ERROR MILES	RMS TIME ERROR HOURS	TIME	FIRST BODY	SECOND BODY	RMS POSITION ERROR MILES	RMS TIME ERROR HOURS
		STRATEGY 1					STRATEGY 4		
0.60	MARS	SIRIUS			0.60	SUN	PROCYON		
	MARS	A CENTAURI				SUN	B CENTAURI		
	MARS	SUN	17672	0.0526		MARS	CAPELLA	14654	0.0526
	EARTH	SIRIUS	15172	0.0496		MARS	ARCTURUS	12540	0.0526
	EARTH	B CENTAURI	14757	0.0480		SUN	MARS	10779	0.0526
	SUN	EARTH	7545	0.0480		SUN	EARTH	6796	0.0498
		STRATEGY 2					STRATEGY 5		
0.60	MARS	SIRIUS			0.60	SUN	PROCYON		
	MARS	A CENTAURI				SUN	B CENTAURI		
	MARS	SUN	17672	0.0526		SUN	MARS	14921	0.0526
	SUN	PROCYON	11427	0.0526		MARS	CAPELLA	13253	0.0526
	SUN	B CENTAURI	10885	0.0526		MARS	PROCYON	10494	0.0526
	SUN	EARTH	6814	0.0498		SUN	EARTH	6797	0.0497
		STRATEGY 3					STRATEGY 6		
0.60	SUN	PROCYON			0.60	EARTH	SIRIUS		
	SUN	B CENTAURI				EARTH	B CENTAURI		
	SUN	MARS	14921	0.0526		MARS	PROCYON	36042	0.0526
	MARS	SIRIUS	13436	0.0526		SUN	EARTH	10094	0.0496
	MARS	A CENTAURI	10885	0.0526		MARS	B CENTAURI	8691	0.0492
	SUN	EARTH	6814	0.0498		SUN	MARS	7485	0.0478

TABLE 3-2

COMPARISON OF CELESTIAL FIX STRATEGIES

MARS TRAJ. NOV.5,1964 V_I = 37484 FT/SEC T_F = 0.85 YEARS V_{RM} = 9135 FT/SEC

TIME IN YEARS	FIRST BODY	SECOND BODY	RMS POSITION ERROR MILES	RMS TIME ERROR HOURS	TIME	FIRST BODY	SECOND BODY	RMS POSITION ERROR MILES	RMS TIME ERROR HOURS
		STRATEGY 1					STRATEGY 4		
0.70	MARS	SIRIUS			0.70	SUN	SIRIUS		
	MARS	B CENTAURI				SUN	CAPELLA		
	MARS	SUN	11951	0.0614		MARS	CAPELLA	11319	0.0614
	VENUS	PROCYON	6194	0.0609		MARS	VEGA	8792	0.0613
	VENUS	ACHERNAR	5404	0.0608		SUN	MARS	7543	0.0613
	SUN	VENUS	5090	0.0594		SUN	VENUS	6764	0.0589
		STRATEGY 2					STRATEGY 5		
0.70	MARS	SIRIUS			0.70	SUN	SIRIUS		
	MARS	B CENTAURI				SUN	CAPELLA		
	MARS	SUN	11951	0.0614		SUN	MARS	11077	0.0614
	SUN	SIRIUS	9548	0.0614		MARS	ACHERNAR	9019	0.0613
	SUN	CAPELLA	7576	0.0613		MARS	PROCYON	7666	0.0613
	SUN	VENUS	6788	0.0589		SUN	VENUS	6853	0.0589
		STRATEGY 3					STRATEGY 6		
0.70	SUN	SIRIUS			0.70	VENUS	PROCYON		
	SUN	CAPELLA				VENUS	ACHERNAR		
	SUN	MARS	11077	0.0614		MARS	CAPELLA	8310	0.0614
	MARS	SIRIUS	9033	0.0613		SUN	VENUS	8024	0.0602
	MARS	B CENTAURI	7576	0.0613		MARS	VEGA	5443	0.0601
	SUN	VENUS	6788	0.0589		SUN	MARS	5081	0.0594

TABLE 3-2

DECLASSIFIED

C ARISON OF CELESTIAL FIX STRATEGIES

MARS TRAJ. NOV.5,1964 V_I = 37484 FT/SEC T_F = 0.85 YEARS V_{RM} = 9135 FT/SEC

TIME IN YEARS	FIRST BODY	SECOND BODY	RMS POSITION ERROR MILES	RMS TIME ERROR HOURS	TIME	FIRST BODY	SECOND BODY	RMS POSITION ERROR MILES	RMS TIME ERROR HOURS
		STRATEGY 1					STRATEGY 4		
0.80	MARS	SIRIUS			0.80	SUN	CAPELLA		
	MARS	B CENTAURI				SUN	PROCYON		
	MARS	SUN	10132	0.0701		MARS	CAPELLA	10332	0.0701
	EARTH	ARCTURUS	10285	0.0700		MARS	VEGA	7821	0.0701
	EARTH	PROCYON	9149	0.0680		SUN	MARS	6712	0.0701
	SUN	EARTH	7912	0.0637		SUN	EARTH	6137	0.0670
		STRATEGY 2					STRATEGY 5		
0.80	MARS	SIRIUS			0.80	SUN	CAPELLA		
	MARS	B CENTAURI				SUN	PROCYON		
	MARS	SUN	10132	0.0701		SUN	MARS	9972	0.0701
	SUN	CAPELLA	9009	0.0701		MARS	B CENTAURI	7846	0.0701
	SUN	PROCYON	6737	0.0701		MARS	PROCYON	6631	0.0701
	SUN	EARTH	6157	0.0670		SUN	EARTH	6072	0.0669
		STRATEGY 3					STRATEGY 6		
0.80	SUN	CAPELLA			0.80	EARTH	ARCTURUS		
	SUN	PROCYON				EARTH	PROCYON		
	SUN	MARS	9972	0.0701		MARS	CAPELLA	15056	0.0701
	MARS	SIRIUS	7854	0.0701		SUN	EARTH	13291	0.0647
	MARS	B CENTAURI	6737	0.0701		MARS	VEGA	10602	0.0638
	SUN	EARTH	6157	0.0670		SUN	MARS	7863	0.0637

TABLE 3-2

COMPARISON OF CELESTIAL FIX STRATEGIES

MARS TRAJ. NOV.5,1964 V_I = 37484 FT/SEC T_F = 0.85 YEARS V_{RM} = 9135 FT/SEC

TIME IN YEARS	FIRST BODY	SECOND BODY	RMS POSITION ERROR MILES	RMS TIME ERROR HOURS	TIME	FIRST BODY	SECOND BODY	RMS POSITION ERROR MILES	RMS TIME ERROR HOURS
		STRATEGY 1					STRATEGY 4		
0.80	MARS	SIRIUS			0.80	SUN	CAPELLA		
	MARS	B CENTAURI				SUN	PROCYON		
	MARS	SUN	10132	0.0701		MARS	CAPELLA	10332	0.0701
	EARTH	ARCTURUS	10285	0.0700		MARS	VEGA	7821	0.0701
	EARTH	PROCYON	9149	0.0680		SUN	MARS	6712	0.0701
	MARS	DIAMETER	9096	0.0678		MARS	DIAMETER	6691	0.0700
		STRATEGY 2					STRATEGY 5		
0.80	MARS	SIRIUS			0.80	SUN	CAPELLA		
	MARS	B CENTAURI				SUN	PROCYON		
	MARS	SUN	10132	0.0701		SUN	MARS	9972	0.0701
	SUN	PROCYON	7193	0.0701		MARS	B CENTAURI	7846	0.0701
	SUN	EARTH	6519	0.0670		MARS	PROCYON	6631	0.0701
	MARS	DIAMETER	6500	0.0669		MARS	DIAMETER	6610	0.0700
		STRATEGY 3					STRATEGY 6		
0.80	SUN	CAPELLA			0.80	EARTH	ARCTURUS		
	SUN	PROCYON				EARTH	PROCYON		
	SUN	MARS	9972	0.0701		MARS	CAPELLA	15056	0.0701
	MARS	SIRIUS	7854	0.0701		SUN	EARTH	13291	0.0647
	MARS	B CENTAURI	6737	0.0701		MARS	VEGA	10602	0.0638
	MARS	DIAMETER	6715	0.0700		MARS	DIAMETER	10521	0.0637

TABLE 3-2

C RISON OF CELESTIAL FIX STRATEGIES

MARS TRAJ. NOV.5,1964 V_I = 37484 FT/SEC T_F = 0.85 YEARS V_{RM} = 9135 FT/SEC

TIME IN YEARS	FIRST BODY	SECOND BODY	RMS POSITION ERROR MILES	RMS TIME ERROR HOURS	TIME	FIRST BODY	SECOND BODY	RMS POSITION ERROR MILES	RMS TIME ERROR HOURS
		STRATEGY 1					STRATEGY 4		
0.82	MARS	SIRIUS			0.82	SUN	PROCYON		
	MARS	B CENTAURI				SUN	ACHERNAR		
	MARS	SUN	9957	0.0719		MARS	CAPELLA	10301	0.0719
	EARTH	PROCYON	9158	0.0697		MARS	VEGA	7553	0.0719
	EARTH	B CENTAURI	8980	0.0697		SUN	MARS	6558	0.0719
	MARS	DIAMETER	8611	0.0688		MARS	DIAMETER	6407	0.0713
		STRATEGY 2					STRATEGY 5		
0.82	MARS	SIRIUS			0.82	SUN	PROCYON		
	MARS	B CENTAURI				SUN	ACHERNAR		
	MARS	SUN	9957	0.0719		SUN	MARS	9907	0.0719
	SUN	PROCYON	7179	0.0719		MARS	CAPELLA	7560	0.0719
	SUN	EARTH	6546	0.0686		MARS	PROCYON	6392	0.0719
	MARS	DIAMETER	6398	0.0682		MARS	DIAMETER	6252	0.0713
		STRATEGY 3					STRATEGY 6		
0.82	SUN	PROCYON			0.82	EARTH	PROCYON		
	SUN	ACHERNAR				EARTH	B CENTAURI		
	SUN	MARS	9907	0.0719		MARS	CAPELLA	14702	0.0719
	MARS	SIRIUS	7569	0.0719		SUN	EARTH	13335	0.0664
	MARS	B CENTAURI	6580	0.0719		MARS	VEGA	10517	0.0655
	MARS	DIAMETER	6428	0.0713		MARS	DIAMETER	9949	0.0649

TABLE 3-2

DECLASSIFIED

COMPARISON OF CELESTIAL FIX STRATEGIES

MARS TRAJ. NOV.24,1964 V_I = 38583 FT/SEC T_F = 0.5 YEARS V_{RM} = 25261 FT/SEC

TIME IN YEARS	FIRST BODY	SECOND BODY	RMS POSITION ERROR MILES	RMS TIME ERROR HOURS	TIME	FIRST BODY	SECOND BODY	RMS POSITION ERROR MILES	RMS TIME ERROR HOURS
		STRATEGY 1					STRATEGY 4		
0.02	EARTH	SIRIUS			0.02	SUN	CAPELLA		
	EARTH	A CENTAURI				SUN	PROCYON		
	EARTH	SUN	6508	0.0018		EARTH	CAPELLA	6714	0.0018
	MOON	VEGA	1947	0.0018		EARTH	VEGA	4555	0.0018
	MOON	CAPELLA	632	0.0018		SUN	EARTH	3722	0.0018
	EARTH	DIAMETER	631	0.0018		EARTH	DIAMETER	3631	0.0018
		STRATEGY 2					STRATEGY 5		
0.02	EARTH	SIRIUS			0.02	SUN	CAPELLA		
	EARTH	A CENTAURI				SUN	PROCYON		
	EARTH	SUN	6508	0.0018		SUN	EARTH	6486	0.0018
	SUN	ARCTURUS	4076	0.0018		EARTH	ACHERNAR	4560	0.0018
	SUN	MOON	707	0.0018		EARTH	CAPELLA	3813	0.0018
	EARTH	DIAMETER	706	0.0018		EARTH	DIAMETER	3715	0.0018
		STRATEGY 3					STRATEGY 6		
0.02	SUN	CAPELLA			0.02	MOON	VEGA		
	SUN	PROCYON				MOON	CAPELLA		
	SUN	EARTH	6486	0.0018		EARTH	CAPELLA	846	0.0018
	EARTH	SIRIUS	4562	0.0018		SUN	MOON	788	0.0018
	EARTH	A CENTAURI	3734	0.0018		EARTH	PROCYON	627	0.0018
	EARTH	DIAMETER	3642	0.0018		EARTH	DIAMETER	626	0.0018

TABLE 3-3

COMPARISON OF CELESTIAL FIX STRATEGIES

MARS TRAJ. NOV.24,1964 V_I = 38583 FT/SEC T_F = 0.5 YEARS V_{RM} = 25261 FT/SEC

TIME IN YEARS	FIRST BODY	SECOND BODY	RMS POSITION ERROR MILES	RMS TIME ERROR HOURS	TIME	FIRST BODY	SECOND BODY	RMS POSITION ERROR MILES	RMS TIME ERROR HOURS
		STRATEGY 1					STRATEGY 4		
0.04	EARTH	SIRIUS			0.04	SUN	PROCYON		
	EARTH	A CENTAURI				SUN	ACHERNAR		
	EARTH	SUN	6527	0.0035		EARTH	CAPELLA	6806	0.0035
	MOON	SIRIUS	3845	0.0035		EARTH	VEGA	4467	0.0035
	MOON	A CENTAURI	3016	0.0035		SUN	EARTH	3677	0.0035
	EARTH	DIAMETER	3012	0.0035		EARTH	DIAMETER	3671	0.0035
		STRATEGY 2					STRATEGY 5		
0.04	EARTH	SIRIUS			0.04	SUN	PROCYON		
	EARTH	A CENTAURI				SUN	ACHERNAR		
	EARTH	SUN	6527	0.0035		SUN	EARTH	6514	0.0035
	SUN	ARCTURUS	4027	0.0035		EARTH	ACHERNAR	4456	0.0035
	SUN	MOON	3656	0.0035		EARTH	CAPELLA	3767	0.0035
	EARTH	DIAMETER	3650	0.0035		EARTH	DIAMETER	3761	0.0035
		STRATEGY 3					STRATEGY 6		
0.04	SUN	PROCYON			0.04	MOON	SIRIUS		
	SUN	ACHERNAR				MOON	A CENTAURI		
	SUN	EARTH	6514	0.0035		EARTH	PROCYON	5726	0.0035
	EARTH	SIRIUS	4464	0.0035		SUN	MOON	5197	0.0035
	EARTH	A CENTAURI	3689	0.0035		EARTH	CAPELLA	4782	0.0035
	EARTH	DIAMETER	3683	0.0035		EARTH	DIAMETER	4769	0.0035

TABLE 3-3

C[illegible]RISON OF CELESTIAL FIX STRATEGIES

MARS TRAJ. NOV.24,1964 V_I = 38583 FT/SEC T_F = 0.5 YEARS V_{RM} = 25261 FT/SEC

TIME IN YEARS	FIRST BODY	SECOND BODY	RMS POSITION ERROR MILES	RMS TIME ERROR HOURS	TIME	FIRST BODY	SECOND BODY	RMS POSITION ERROR MILES	RMS TIME ERROR HOURS
		STRATEGY 1					STRATEGY 4		
0.06	EARTH	SIRIUS			0.06	SUN	PROCYON		
	EARTH	A CENTAURI				SUN	ACHERNAR		
	EARTH	SUN	6706	0.0053		EARTH	CAPELLA	6945	0.0053
	MARS	SIRIUS	6699	0.0053		EARTH	VEGA	4881	0.0053
	MARS	B CENTAURI	6595	0.0053		SUN	EARTH	3933	0.0053
	EARTH	DIAMETER	6588	0.0053		EARTH	DIAMETER	3932	0.0053
		STRATEGY 2					STRATEGY 5		
0.06	EARTH	SIRIUS			0.06	SUN	PROCYON		
	EARTH	A CENTAURI				SUN	ACHERNAR		
	EARTH	SUN	6706	0.0053		SUN	EARTH	6607	0.0053
	SUN	ARCTURUS	4102	0.0053		EARTH	ACHERNAR	4831	0.0053
	SUN	MARS	3198	0.0053		EARTH	CAPELLA	4039	0.0053
	EARTH	DIAMETER	3197	0.0053		EARTH	DIAMETER	4037	0.0053
		STRATEGY 3					STRATEGY 6		
0.06	SUN	PROCYON			0.06	MARS	SIRIUS		
	SUN	ACHERNAR				MARS	B CENTAURI		
	SUN	EARTH	6607	0.0053		EARTH	B CENTAURI	33947	0.0053
	EARTH	SIRIUS	4842	0.0053		SUN	MARS	8827	0.0053
	EARTH	A CENTAURI	3947	0.0053		EARTH	RIGEL	5135	0.0053
	EARTH	DIAMETER	3946	0.0053		EARTH	DIAMETER	5132	0.0053

TABLE 3-3

COMPARISON OF CELESTIAL FIX STRATEGIES

MARS TRAJ. NOV.24,1964 V_I = 38583 FT/SEC T_F = 0.5 YEARS V_{RM} = 25261 FT/SEC

TIME IN YEARS	FIRST BODY	SECOND BODY	RMS POSITION ERROR MILES	RMS TIME ERROR HOURS	TIME	FIRST BODY	SECOND BODY	RMS POSITION ERROR MILES	RMS TIME ERROR HOURS
		STRATEGY 1					STRATEGY 4		
0.10	EARTH	SIRIUS			0.10	SUN	ARCTURUS		
	EARTH	A CENTAURI				SUN	PROCYON		
	EARTH	SUN	7707	0.0088		EARTH	PROCYON	7727	0.0088
	MERCURY	PROCYON	4312	0.0087		EARTH	B CENTAURI	5528	0.0088
	MERCURY	ACHERNAR	3545	0.0087		SUN	EARTH	4419	0.0088
	SUN	MERCURY	3459	0.0087		SUN	MERCURY	4246	0.0087
		STRATEGY 2					STRATEGY 5		
0.10	EARTH	SIRIUS			0.10	SUN	ARCTURUS		
	EARTH	A CENTAURI				SUN	PROCYON		
	EARTH	SUN	7707	0.0088		SUN	EARTH	7145	0.0088
	SUN	ARCTURUS	4682	0.0088		EARTH	CANOPUS	5321	0.0088
	SUN	PROCYON	4473	0.0088		EARTH	CAPELLA	4511	0.0088
	SUN	MERCURY	4295	0.0087		SUN	MERCURY	4329	0.0087
		STRATEGY 3					STRATEGY 6		
0.10	SUN	ARCTURUS			0.10	MERCURY	PROCYON		
	SUN	PROCYON				MERCURY	ACHERNAR		
	SUN	EARTH	7145	0.0088		EARTH	PROCYON	6071	0.0088
	EARTH	SIRIUS	5342	0.0088		SUN	MERCURY	5940	0.0087
	EARTH	A CENTAURI	4473	0.0088		EARTH	B CENTAURI	3875	0.0087
	SUN	MERCURY	4295	0.0087		SUN	EARTH	3434	0.0087

TABLE 3-3

ARISON OF CELESTIAL FIX STRATEGIES

MARS TRAJ. NOV.24,1964 V_I = 38583 FT/SEC T_F = 0.5 YEARS V_{RM} = 25261 FT/SEC

TIME IN YEARS	FIRST BODY	SECOND BODY	RMS POSITION ERROR MILES	RMS TIME ERROR HOURS	TIME	FIRST BODY	SECOND BODY	RMS POSITION ERROR MILES	RMS TIME ERROR HOURS
		STRATEGY 1					STRATEGY 4		
0.20	MARS	SIRIUS			0.20	SUN	PROCYON		
	MARS	A CENTAURI				SUN	B CENTAURI		
	MARS	SUN	13434	0.0175		MARS	PROCYON	10440	0.0175
	VENUS	RIGEL	10391	0.0175		MARS	B CENTAURI	8669	0.0175
	VENUS	B CENTAURI	9125	0.0175		SUN	MARS	8146	0.0175
	SUN	VENUS	9059	0.0173		SUN	VENUS	8110	0.0174
		STRATEGY 2					STRATEGY 5		
0.20	MARS	SIRIUS			0.20	SUN	PROCYON		
	MARS	A CENTAURI				SUN	B CENTAURI		
	MARS	SUN	13434	0.0175		SUN	MARS	12406	0.0175
	SUN	PROCYON	9714	0.0175		MARS	PROCYON	10026	0.0175
	SUN	B CENTAURI	8273	0.0175		MARS	A CENTAURI	8133	0.0175
	SUN	VENUS	8239	0.0174		SUN	VENUS	8096	0.0174
		STRATEGY 3					STRATEGY 6		
0.20	SUN	PROCYON			0.20	VENUS	RIGEL		
	SUN	B CENTAURI				VENUS	B CENTAURI		
	SUN	MARS	12406	0.0175		MARS	PROCYON	13496	0.0175
	MARS	SIRIUS	10715	0.0175		SUN	VENUS	13406	0.0174
	MARS	A CENTAURI	8273	0.0175		MARS	B CENTAURI	10255	0.0174
	SUN	VENUS	8239	0.0174		SUN	MARS	8954	0.0173

TABLE 3-3

COMPARISON OF CELESTIAL FIX STRATEGIES

MARS TRAJ. NOV.24,1964 V_I = 38583 FT/SEC T_F = 0.5 YEARS V_{RM} = 25261 FT/SEC

TIME IN YEARS	FIRST BODY	SECOND BODY	RMS POSITION ERROR MILES	RMS TIME ERROR HOURS	TIME	FIRST BODY	SECOND BODY	RMS POSITION ERROR MILES	RMS TIME ERROR HOURS
		STRATEGY 1					STRATEGY 4		
0.30	EARTH	VEGA			0.30	SUN	SIRIUS		
	EARTH	CAPELLA				SUN	B CENTAURI		
	EARTH	SUN	20453	0.0263		EARTH	CAPELLA	18458	0.0263
	MARS	CAPELLA	3476	0.0259		EARTH	ARCTURUS	16806	0.0263
	MARS	ARCTURUS	3122	0.0259		SUN	EARTH	12395	0.0263
	SUN	MARS	2700	0.0256		SUN	MARS	3523	0.0253
		STRATEGY 2					STRATEGY 5		
0.30	EARTH	VEGA			0.30	SUN	SIRIUS		
	EARTH	CAPELLA				SUN	B CENTAURI		
	EARTH	SUN	20453	0.0263		SUN	EARTH	14636	0.0263
	SUN	SIRIUS	15878	0.0263		EARTH	VEGA	13350	0.0263
	SUN	B CENTAURI	12416	0.0263		EARTH	CAPELLA	12416	0.0263
	SUN	MARS	3262	0.0254		SUN	MARS	3262	0.0254
		STRATEGY 3					STRATEGY 6		
0.30	SUN	SIRIUS			0.30	MARS	CAPELLA		
	SUN	B CENTAURI				MARS	ARCTURUS		
	SUN	EARTH	14636	0.0263		EARTH	CAPELLA	4269	0.0263
	EARTH	VEGA	13350	0.0263		SUN	MARS	3675	0.0260
	EARTH	CAPELLA	12416	0.0263		EARTH	ARCTURUS	2877	0.0260
	SUN	MARS	3262	0.0254		SUN	EARTH	2634	0.0255

TABLE 3-3

COMPARISON OF CELESTIAL FIX STRATEGIES

MARS TRAJ. NOV.24,1964 V_I = 38583 FT/SEC T_F = 0.5 YEARS V_{RM} = 25261 FT/SEC

TIME IN YEARS	FIRST BODY	SECOND BODY	RMS POSITION ERROR MILES	RMS TIME ERROR HOURS	TIME	FIRST BODY	SECOND BODY	RMS POSITION ERROR MILES	RMS TIME ERROR HOURS
		STRATEGY 1					STRATEGY 4		
0.40	MARS	RIGEL			0.40	SUN	SIRIUS		
	MARS	B CENTAURI				SUN	A CENTAURI		
	MARS	SUN	138200	0.0351		MARS	RIGEL	94916	0.0351
	EARTH	SIRIUS	7530	0.0347		MARS	PROCYON	94076	0.0349
	EARTH	A CENTAURI	5224	0.0346		SUN	MARS	76953	0.0349
	SUN	EARTH	3773	0.0341		SUN	EARTH	6385	0.0334
		STRATEGY 2					STRATEGY 5		
0.40	MARS	RIGEL			0.40	SUN	SIRIUS		
	MARS	B CENTAURI				SUN	A CENTAURI		
	MARS	SUN	138200	0.0351		SUN	MARS	104453	0.0351
	SUN	SIRIUS	83215	0.0351		MARS	RIGEL	88681	0.0350
	SUN	A CENTAURI	81913	0.0348		MARS	PROCYON	76593	0.0349
	SUN	EARTH	5302	0.0336		SUN	EARTH	6385	0.0334
		STRATEGY 3					STRATEGY 6		
0.40	SUN	SIRIUS			0.40	EARTH	SIRIUS		
	SUN	A CENTAURI				EARTH	A CENTAURI		
	SUN	MARS	104453	0.0351		MARS	PROCYON	6453	0.0351
	MARS	RIGEL	88681	0.0350		SUN	EARTH	5048	0.0345
	MARS	B CENTAURI	81914	0.0348		MARS	B CENTAURI	3835	0.0345
	SUN	EARTH	5302	0.0336		SUN	MARS	3770	0.0341

TABLE 3-3

DECLASSIFIED

COMPARISON OF CELESTIAL FIX STRATEGIES

MARS TRAJ. NOV.24,1964 V_I = 38583 FT/SEC T_F = 0.5 YEARS V_{RM} = 25261 FT/SEC

TIME IN YEARS	FIRST BODY	SECOND BODY	RMS POSITION ERROR MILES	RMS TIME ERROR HOURS	TIME	FIRST BODY	SECOND BODY	RMS POSITION ERROR MILES	RMS TIME ERROR HOURS
		STRATEGY 1					STRATEGY 4		
0.46	MARS	SIRIUS			0.46	SUN	A CENTAURI		
	MARS	A CENTAURI				SUN	RIGEL		
	MARS	SUN	85679	0.0403		MARS	CAPELLA	60596	0.0403
	EARTH	VEGA	17860	0.0396		MARS	PROCYON	59568	0.0402
	EARTH	CAPELLA	8287	0.0395		SUN	MARS	49200	0.0402
	MARS	DIAMETER	8285	0.0395		MARS	DIAMETER	48889	0.0402
		STRATEGY 2					STRATEGY 5		
0.46	MARS	SIRIUS			0.46	SUN	A CENTAURI		
	MARS	A CENTAURI				SUN	RIGEL		
	MARS	SUN	85679	0.0403		SUN	MARS	62444	0.0403
	SUN	CAPELLA	50962	0.0403		MARS	CAPELLA	59647	0.0402
	SUN	EARTH	7168	0.0387		MARS	PROCYON	49200	0.0402
	MARS	DIAMETER	7167	0.0387		MARS	DIAMETER	48889	0.0402
		STRATEGY 3					STRATEGY 6		
0.46	SUN	A CENTAURI			0.46	EARTH	VEGA		
	SUN	RIGEL				EARTH	CAPELLA		
	SUN	MARS	62444	0.0403		MARS	PROCYON	9811	0.0403
	MARS	SIRIUS	61900	0.0402		SUN	EARTH	7121	0.0396
	MARS	A CENTAURI	50532	0.0402		MARS	ACHERNAR	5485	0.0395
	MARS	DIAMETER	50195	0.0402		MARS	DIAMETER	5484	0.0395

TABLE 3-3

C[illegible]RISON OF CELESTIAL FIX STRATEGIES

MARS TRAJ. NOV.24.1964 V_I = 38583 FT/SEC T_F = 0.5 YEARS V_{RM} = 25261 FT/SEC

TIME IN YEARS	FIRST BODY	SECOND BODY	RMS POSITION ERROR MILES	RMS TIME ERROR HOURS	TIME	FIRST BODY	SECOND BODY	RMS POSITION ERROR MILES	RMS TIME ERROR HOURS
		STRATEGY 1					STRATEGY 4		
0.48	MARS	SIRIUS			0.48	SUN	VEGA		
	MARS	A CENTAURI				SUN	CAPELLA		
	MARS	SUN	59889	0.0421		MARS	CAPELLA	43980	0.0421
	EARTH	SIRIUS	12708	0.0411		MARS	PROCYON	42008	0.0420
	EARTH	B CENTAURI	9912	0.0410		SUN	MARS	34106	0.0420
	MARS	DIAMETER	9872	0.0410		MARS	DIAMETER	32521	0.0418
		STRATEGY 2					STRATEGY 5		
0.48	MARS	SIRIUS			0.48	SUN	VEGA		
	MARS	A CENTAURI				SUN	CAPELLA		
	MARS	SUN	59889	0.0421		SUN	MARS	43549	0.0421
	SUN	CAPELLA	36083	0.0421		MARS	CAPELLA	42720	0.0420
	SUN	EARTH	7779	0.0404		MARS	PROCYON	34106	0.0420
	MARS	DIAMETER	7759	0.0404		MARS	DIAMETER	32521	0.0418
		STRATEGY 3					STRATEGY 6		
0.48	SUN	VEGA			0.48	EARTH	SIRIUS		
	SUN	CAPELLA				EARTH	B CENTAURI		
	SUN	MARS	43549	0.0421		MARS	PROCYON	11574	0.0421
	MARS	SIRIUS	42786	0.0420		SUN	EARTH	7962	0.0412
	MARS	A CENTAURI	35352	0.0420		MARS	ACHERNAR	6269	0.0412
	MARS	DIAMETER	33596	0.0418		MARS	DIAMETER	6259	0.0412

TABLE 3-3

COMPARISON OF CELESTIAL FIX STRATEGIES

VENUS TRAJ. APRIL 19,1964 V_I = 37410 FT/SEC T_F = 0.45 YEARS V_{RV} = 18357 FT/SEC

TIME IN YEARS	FIRST BODY	SECOND BODY	RMS POSITION ERROR MILES	RMS TIME ERROR HOURS	TIME	FIRST BODY	SECOND BODY	RMS POSITION ERROR MILES	RMS TIME ERROR HOURS
		STRATEGY 1					STRATEGY 4		
0.02	EARTH	ARCTURUS			0.02	SUN	PROCYON		
	EARTH	PROCYON				SUN	B CENTAURI		
	EARTH	SUN	7176	0.0018		EARTH	ARCTURUS	7399	0.0018
	MOON	A CENTAURI	966	0.0018		EARTH	PROCYON	4950	0.0018
	MOON	ARCTURUS	406	0.0018		SUN	EARTH	4082	0.0018
	EARTH	DIAMETER	405	0.0018		EARTH	DIAMETER	3678	0.0018
		STRATEGY 2					STRATEGY 5		
0.02	EARTH	ARCTURUS			0.02	SUN	PROCYON		
	EARTH	PROCYON				SUN	B CENTAURI		
	EARTH	SUN	7176	0.0018		SUN	EARTH	6827	0.0018
	SUN	PROCYON	4251	0.0018		EARTH	ACHERNAR	4972	0.0018
	SUN	MOON	384	0.0018		EARTH	CAPELLA	4159	0.0018
	EARTH	DIAMETER	384	0.0018		EARTH	DIAMETER	3734	0.0018
		STRATEGY 3					STRATEGY 6		
0.02	SUN	PROCYON			0.02	MOON	A CENTAURI		
	SUN	B CENTAURI				MOON	ARCTURUS		
	SUN	EARTH	6827	0.0018		EARTH	ARCTURUS	514	0.0018
	EARTH	ARCTURUS	4973	0.0018		SUN	MOON	434	0.0018
	EARTH	PROCYON	4082	0.0018		EARTH	CAPELLA	347	0.0018
	EARTH	DIAMETER	3678	0.0018		EARTH	DIAMETER	347	0.0018

TABLE 3-4

OMPARISON OF CELESTIAL FIX STRATEGIES

VENUS TRAJ. APRIL 19,1964 V_I = 37410 FT/SEC T_F = 0.45 YEARS V_{RV} = 18357 FT/SEC

TIME IN YEARS	FIRST BODY	SECOND BODY	RMS POSITION ERROR MILES	RMS TIME ERROR HOURS	TIME	FIRST BODY	SECOND BODY	RMS POSITION ERROR MILES	RMS TIME ERROR HOURS
		STRATEGY 1					STRATEGY 4		
0.04	EARTH	ARCTURUS			0.04	SUN	A CENTAURI		
	EARTH	PROCYON				SUN	PROCYON		
	EARTH	SUN	7527	0.0035		EARTH	ARCTURUS	7588	0.0035
	MOON	CAPELLA	4721	0.0035		EARTH	A CENTAURI	5208	0.0035
	MOON	RIGEL	3835	0.0035		SUN	EARTH	4241	0.0035
	EARTH	DIAMETER	3810	0.0035		EARTH	DIAMETER	4208	0.0035
		STRATEGY 2					STRATEGY 5		
0.04	EARTH	ARCTURUS			0.04	SUN	A CENTAURI		
	EARTH	PROCYON				SUN	PROCYON		
	EARTH	SUN	7527	0.0035		SUN	EARTH	7022	0.0035
	SUN	PROCYON	4488	0.0035		EARTH	SIRIUS	5269	0.0035
	SUN	MOON	4282	0.0035		EARTH	ARCTURUS	4504	0.0035
	EARTH	DIAMETER	4247	0.0035		EARTH	DIAMETER	4464	0.0035
		STRATEGY 3					STRATEGY 6		
0.04	SUN	A CENTAURI			0.04	MOON	CAPELLA		
	SUN	PROCYON				MOON	RIGEL		
	SUN	EARTH	7022	0.0035		EARTH	ARCTURUS	8798	0.0035
	EARTH	ARCTURUS	5274	0.0035		SUN	MOON	6871	0.0035
	EARTH	PROCYON	4304	0.0035		EARTH	CAPELLA	6424	0.0035
	EARTH	DIAMETER	4269	0.0035		EARTH	DIAMETER	6309	0.0035

TABLE 3-4

DECLASSIFIED

COMPARISON OF CELESTIAL FIX STRATEGIES

VENUS TRAJ. APRIL 19,1964 V_I = 37410 FT/SEC T_F = 0.45 YEARS V_{RV} = 18357 FT/SEC

TIME IN YEARS	FIRST BODY	SECOND BODY	RMS POSITION ERROR MILES	RMS TIME ERROR HOURS
		STRATEGY 1		
0.06	EARTH	ARCTURUS		
	EARTH	PROCYON		
	EARTH	SUN	8056	0.0053
	MOON	CAPELLA	3624	0.0053
	MOON	RIGEL	2568	0.0053
	EARTH	DIAMETER	2566	0.0053
		STRATEGY 2		
0.06	EARTH	ARCTURUS		
	EARTH	PROCYON		
	EARTH	SUN	8056	0.0053
	SUN	PROCYON	4856	0.0053
	SUN	MOON	3255	0.0052
	EARTH	DIAMETER	3252	0.0052
		STRATEGY 3		
0.06	SUN	CAPELLA		
	SUN	RIGEL		
	SUN	EARTH	7360	0.0053
	EARTH	ARCTURUS	5800	0.0053
	EARTH	PROCYON	4680	0.0053
	EARTH	DIAMETER	4671	0.0053

TIME	FIRST BODY	SECOND BODY	RMS POSITION ERROR MILES	RMS TIME ERROR HOURS
		STRATEGY 4		
0.06	SUN	CAPELLA		
	SUN	RIGEL		
	EARTH	ARCTURUS	7897	0.0053
	EARTH	A CENTAURI	5670	0.0053
	SUN	EARTH	4625	0.0053
	EARTH	DIAMETER	4616	0.0053
		STRATEGY 5		
0.06	SUN	CAPELLA		
	SUN	RIGEL		
	SUN	EARTH	7360	0.0053
	EARTH	SIRIUS	5793	0.0053
	EARTH	ARCTURUS	4908	0.0053
	EARTH	DIAMETER	4898	0.0053
		STRATEGY 6		
0.06	MOON	CAPELLA		
	MOON	RIGEL		
	EARTH	ARCTURUS	4371	0.0053
	SUN	MOON	4311	0.0052
	EARTH	CAPELLA	3738	0.0052
	EARTH	DIAMETER	3734	0.0052

TABLE 3-4

MPARISON OF CELESTIAL FIX STRATEGIES

VENUS TRAJ. APRIL 19,1964 V_I = 37410 FT/SEC T_F = 0.45 YEARS V_{RV} = 18357 FT/SEC

TIME IN YEARS	FIRST BODY	SECOND BODY	RMS POSITION ERROR MILES	RMS TIME ERROR HOURS	TIME	FIRST BODY	SECOND BODY	RMS POSITION ERROR MILES	RMS TIME ERROR HOURS
		STRATEGY 1					STRATEGY 4		
0.10	EARTH	ARCTURUS			0.10	SUN	SIRIUS		
	EARTH	PROCYON				SUN	ARCTURUS		
	EARTH	SUN	10325	0.0088		EARTH	ARCTURUS	9443	0.0088
	VENUS	CAPELLA	9773	0.0088		EARTH	CAPELLA	7611	0.0088
	VENUS	ARCTURUS	9185	0.0088		SUN	EARTH	6215	0.0088
	SUN	VENUS	7239	0.0088		SUN	VENUS	5527	0.0088
		STRATEGY 2					STRATEGY 5		
0.10	EARTH	ARCTURUS			0.10	SUN	SIRIUS		
	EARTH	PROCYON				SUN	ARCTURUS		
	EARTH	SUN	10325	0.0088		SUN	EARTH	9069	0.0088
	SUN	SIRIUS	8181	0.0088		EARTH	ARCTURUS	7951	0.0088
	SUN	ARCTURUS	6254	0.0088		EARTH	CAPELLA	6215	0.0088
	SUN	VENUS	5550	0.0088		SUN	VENUS	5527	0.0088
		STRATEGY 3					STRATEGY 6		
0.10	SUN	SIRIUS			0.10	VENUS	CAPELLA		
	SUN	ARCTURUS				VENUS	ARCTURUS		
	SUN	EARTH	9069	0.0088		EARTH	ARCTURUS	20611	0.0088
	EARTH	ARCTURUS	7951	0.0088		SUN	VENUS	10275	0.0088
	EARTH	PROCYON	6254	0.0088		EARTH	PROCYON	10103	0.0088
	SUN	VENUS	5550	0.0088		SUN	EARTH	7239	0.0088

TABLE 3-4

COMPARISON OF CELESTIAL FIX STRATEGIES

VENUS TRAJ. APRIL 19,1964 V_I = 37410 FT/SEC T_F = 0.45 YEARS V_{RV} = 18357 FT/SEC

TIME IN YEARS	FIRST BODY	SECOND BODY	RMS POSITION ERROR MILES	RMS TIME ERROR HOURS	TIME	FIRST BODY	SECOND BODY	RMS POSITION ERROR MILES	RMS TIME ERROR HOURS
		STRATEGY 1					STRATEGY 4		
0.20	VENUS	CAPELLA			0.20	SUN	A CENTAURI		
	VENUS	PROCYON				SUN	ARCTURUS		
	VENUS	SUN	11118	0.0175		VENUS	ARCTURUS	9813	0.0175
	EARTH	ARCTURUS	2699	0.0173		VENUS	SIRIUS	8715	0.0175
	EARTH	B CENTAURI	2654	0.0172		SUN	VENUS	6833	0.0175
	SUN	EARTH	2371	0.0170		SUN	EARTH	3176	0.0171
		STRATEGY 2					STRATEGY 5		
0.20	VENUS	CAPELLA			0.20	SUN	A CENTAURI		
	VENUS	PROCYON				SUN	ARCTURUS		
	VENUS	SUN	11118	0.0175		SUN	VENUS	8439	0.0175
	SUN	A CENTAURI	10593	0.0175		VENUS	CAPELLA	7562	0.0175
	SUN	ARCTURUS	6844	0.0175		VENUS	PROCYON	6844	0.0175
	SUN	EARTH	3181	0.0171		SUN	EARTH	3181	0.0171
		STRATEGY 3					STRATEGY 6		
0.20	SUN	A CENTAURI			0.20	EARTH	ARCTURUS		
	SUN	ARCTURUS				EARTH	B CENTAURI		
	SUN	VENUS	8439	0.0175		VENUS	ARCTURUS	3383	0.0175
	VENUS	CAPELLA	7562	0.0175		SUN	EARTH	2904	0.0173
	VENUS	PROCYON	6844	0.0175		VENUS	ARCTURUS	2504	0.0173
	SUN	EARTH	3181	0.0171		SUN	VENUS	2277	0.0170

TABLE 3-4

COMPARISON OF CELESTIAL FIX STRATEGIES

VENUS TRAJ. APRIL 19,1964 V_I = 37410 FT/SEC T_F = 0.45 YEARS V_{RV} = 18357 FT/SEC

TIME IN YEARS	FIRST BODY	SECOND BODY	RMS POSITION ERROR MILES	RMS TIME ERROR HOURS	TIME	FIRST BODY	SECOND BODY	RMS POSITION ERROR MILES	RMS TIME ERROR HOURS
		STRATEGY 1					STRATEGY 4		
0.30	VENUS	VEGA			0.30	SUN	SIRIUS		
	VENUS	ARCTURUS				SUN	A CENTAURI		
	VENUS	SUN	5073	0.0263		VENUS	PROCYON	4942	0.0263
	EARTH	A CENTAURI	5354	0.0260		VENUS	CAPELLA	4145	0.0259
	EARTH	ARCTURUS	2815	0.0241		SUN	VENUS	3569	0.0259
	SUN	EARTH	1865	0.0238		SUN	EARTH	2109	0.0243
		STRATEGY 2					STRATEGY 5		
0.30	VENUS	VEGA			0.30	SUN	SIRIUS		
	VENUS	ARCTURUS				SUN	A CENTAURI		
	VENUS	SUN	5073	0.0263		SUN	VENUS	4896	0.0263
	SUN	SIRIUS	3727	0.0263		VENUS	B CENTAURI	4106	0.0259
	SUN	A CENTAURI	3585	0.0259		VENUS	PROCYON	3587	0.0259
	SUN	EARTH	2097	0.0243		SUN	EARTH	2121	0.0243
		STRATEGY 3					STRATEGY 6		
0.30	SUN	SIRIUS			0.30	EARTH	A CENTAURI		
	SUN	A CENTAURI				EARTH	ARCTURUS		
	SUN	VENUS	4896	0.0263		VENUS	ARCTURUS	5251	0.0263
	VENUS	VEGA	4106	0.0259		SUN	EARTH	2868	0.0244
	VENUS	ARCTURUS	3585	0.0259		VENUS	SIRIUS	2182	0.0244
	SUN	EARTH	2097	0.0243		SUN	VENUS	1903	0.0236

TABLE 3-4

COMPARISON OF CELESTIAL FIX STRATEGIES

VENUS TRAJ. APRIL 19,1964 V_I = 37410 FT/SEC T_F = 0.45 YEARS V_{RV} = 18357 FT/SEC

TIME IN YEARS	FIRST BODY	SECOND BODY	RMS POSITION ERROR MILES	RMS TIME ERROR HOURS	TIME	FIRST BODY	SECOND BODY	RMS POSITION ERROR MILES	RMS TIME ERROR HOURS
		STRATEGY 1					STRATEGY 4		
0.40	VENUS	A CENTAURI			0.40	SUN	PROCYON		
	VENUS	ARCTURUS				SUN	B CENTAURI		
	VENUS	SUN	5821	0.0351		VENUS	PROCYON	5950	0.0351
	EARTH	CAPELLA	5347	0.0301		VENUS	CAPELLA	4797	0.0325
	EARTH	PROCYON	3889	0.0279		SUN	VENUS	4339	0.0325
	SUN	EARTH	2354	0.0277		SUN	EARTH	2701	0.0296
		STRATEGY 2					STRATEGY 5		
0.40	VENUS	A CENTAURI			0.40	SUN	PROCYON		
	VENUS	ARCTURUS				SUN	B CENTAURI		
	VENUS	SUN	5821	0.0351		SUN	VENUS	5367	0.0351
	SUN	PROCYON	4704	0.0350		VENUS	B CENTAURI	4869	0.0325
	SUN	B CENTAURI	4342	0.0325		VENUS	PROCYON	4306	0.0325
	SUN	EARTH	2701	0.0296		SUN	EARTH	2702	0.0296
		STRATEGY 3					STRATEGY 6		
0.40	SUN	PROCYON			0.40	EARTH	CAPELLA		
	SUN	B CENTAURI				EARTH	PROCYON		
	SUN	VENUS	5367	0.0351		VENUS	RIGEL	8474	0.0351
	VENUS	A CENTAURI	4873	0.0325		SUN	EARTH	4641	0.0299
	VENUS	ARCTURUS	4342	0.0325		VENUS	B CENTAURI	2497	0.0294
	SUN	EARTH	2701	0.0296		SUN	VENUS	2356	0.0278

TABLE 3-4

DECLASSIFIED

COMPARISON OF CELESTIAL FIX STRATEGIES

VENUS TRAJ. APRIL 19,1964 V_I = 37410 FT/SEC T_F = 0.45 YEARS V_{RV} = 18357 FT/SEC

TIME IN YEARS	FIRST BODY	SECOND BODY	RMS POSITION ERROR MILES	RMS TIME ERROR HOURS	TIME	FIRST BODY	SECOND BODY	RMS POSITION ERROR MILES	RMS TIME ERROR HOURS
		STRATEGY 1					STRATEGY 4		
0.40	VENUS	A CENTAURI			0.40	SUN	PROCYON		
	VENUS	ARCTURUS				SUN	B CENTAURI		
	VENUS	SUN	5821	0.0351		VENUS	PROCYON	5950	0.0351
	EARTH	CAPELLA	5347	0.0301		VENUS	CAPELLA	4797	0.0325
	EARTH	PROCYON	3889	0.0279		SUN	VENUS	4339	0.0325
	VENUS	DIAMETER	3888	0.0279		VENUS	DIAMETER	4339	0.0325
		STRATEGY 2					STRATEGY 5		
0.40	VENUS	A CENTAURI			0.40	SUN	PROCYON		
	VENUS	ARCTURUS				SUN	B CENTAURI		
	VENUS	SUN	5821	0.0351		SUN	VENUS	5367	0.0351
	SUN	RIGEL	4391	0.0349		VENUS	B CENTAURI	4869	0.0325
	SUN	EARTH	2741	0.0325		VENUS	PROCYON	4306	0.0325
	VENUS	DIAMETER	2741	0.0325		VENUS	DIAMETER	4305	0.0325
		STRATEGY 3					STRATEGY 6		
0.40	SUN	PROCYON			0.40	EARTH	CAPELLA		
	SUN	B CENTAURI				EARTH	PROCYON		
	SUN	VENUS	5367	0.0351		VENUS	RIGEL	8474	0.0351
	VENUS	A CENTAURI	4873	0.0325		SUN	EARTH	4641	0.0299
	VENUS	ARCTURUS	4342	0.0325		VENUS	B CENTAURI	2497	0.0294
	VENUS	DIAMETER	4342	0.0325		VENUS	DIAMETER	2497	0.0294

TABLE 3-4

COMPARISON OF CELESTIAL FIX STRATEGIES

VENUS TRAJ. APRIL 19,1964 V_I = 37410 FT/SEC T_F = 0.45 YEARS V_{RV} = 18357 FT/SEC

TIME IN YEARS	FIRST BODY	SECOND BODY	RMS POSITION ERROR MILES	RMS TIME ERROR HOURS	TIME	FIRST BODY	SECOND BODY	RMS POSITION ERROR MILES	RMS TIME ERROR HOURS
		STRATEGY 1					STRATEGY 4		
0.42	VENUS	A CENTAURI			0.42	SUN	SIRIUS		
	VENUS	RIGEL				SUN	CAPELLA		
	VENUS	SUN	6786	0.0368		VENUS	B CENTAURI	6407	0.0368
	MERCURY	PROCYON	2189	0.0309		VENUS	ARCTURUS	5422	0.0330
	MERCURY	B CENTAURI	2161	0.0300		SUN	VENUS	4839	0.0330
	VENUS	DIAMETER	2161	0.0300		VENUS	DIAMETER	4831	0.0329
		STRATEGY 2					STRATEGY 5		
0.42	VENUS	A CENTAURI			0.42	SUN	SIRIUS		
	VENUS	RIGEL				SUN	CAPELLA		
	VENUS	SUN	6786	0.0368		SUN	VENUS	5940	0.0368
	SUN	RIGEL	4854	0.0365		VENUS	B CENTAURI	5474	0.0330
	SUN	MERCURY	3114	0.0200		VENUS	PROCYON	4821	0.0330
	VENUS	DIAMETER	3111	0.0200		VENUS	DIAMETER	4812	0.0329
		STRATEGY 3					STRATEGY 6		
0.42	SUN	SIRIUS			0.42	MERCURY	PROCYON		
	SUN	CAPELLA				MERCURY	B CENTAURI		
	SUN	VENUS	5940	0.0368		VENUS	PROCYON	5035	0.0368
	VENUS	A CENTAURI	5479	0.0330		SUN	MERCURY	3439	0.0262
	VENUS	RIGEL	4862	0.0330		VENUS	CAPELLA	2305	0.0237
	VENUS	DIAMETER	4853	0.0329		VENUS	DIAMETER	2304	0.0237

TABLE 3-4

COMPARISON OF CELESTIAL FIX STRATEGIES

VENUS TRAJ. APRIL 19,1964 V_I = 37410 FT/SEC T_F = C.45 YEARS V_{RV} = 18357 FT/SEC

TIME IN YEARS	FIRST BODY	SECOND BODY	RMS POSITION ERROR MILES	RMS TIME ERROR HOURS	TIME	FIRST BODY	SECOND BODY	RMS POSITION ERROR MILES	RMS TIME ERROR HOURS
		STRATEGY 1					STRATEGY 4		
0.44	VENUS	CAPELLA			0.44	SUN	SIRIUS		
	VENUS	PROCYON				SUN	ARCTURUS		
	VENUS	SUN	8288	0.0386		VENUS	B CENTAURI	6768	0.0386
	MERCURY	PROCYON	3662	0.0373		VENUS	RIGEL	6227	0.0327
	MERCURY	B CENTAURI	3487	0.0361		SUN	VENUS	5434	0.0327
	VENUS	DIAMETER	3274	0.0356		VENUS	DIAMETER	4686	0.0314
		STRATEGY 2					STRATEGY 5		
0.44	VENUS	CAPELLA			0.44	SUN	SIRIUS		
	VENUS	PROCYON				SUN	ARCTURUS		
	VENUS	SUN	8288	0.0386		SUN	VENUS	6929	0.0386
	SUN	VEGA	5541	0.0377		VENUS	B CENTAURI	6226	0.0327
	SUN	MERCURY	4108	0.0322		VENUS	PROCYON	5421	0.0327
	VENUS	DIAMETER	3740	0.0322		VENUS	DIAMETER	4677	0.0314
		STRATEGY 3					STRATEGY 6		
0.44	SUN	SIRIUS			0.44	MERCURY	PROCYON		
	SUN	ARCTURUS				MERCURY	B CENTAURI		
	SUN	VENUS	6929	0.0386		VENUS	PROCYON	5483	0.0386
	VENUS	CAPELLA	6246	0.0327		SUN	MERCURY	4307	0.0330
	VENUS	PROCYON	5463	0.0327		VENUS	CAPELLA	3006	0.0330
	VENUS	DIAMETER	4703	0.0314		VENUS	DIAMETER	2858	0.0329

TABLE 3-4

COMPARISON OF CELESTIAL FIX STRATEGIES

VENUS TRAJ. APRIL 19,1964 V_I = 38826 FT/SEC T_F = 0.3 YEARS V_{RV} = 13339 FT/SEC

TIME IN YEARS	FIRST BODY	SECOND BODY	RMS POSITION ERROR MILES	RMS TIME ERROR HOURS	TIME	FIRST BODY	SECOND BODY	RMS POSITION ERROR MILES	RMS TIME ERROR HOURS
		STRATEGY 1					STRATEGY 4		
0.02	EARTH	CANOPUS			0.02	SUN	PROCYON		
	EARTH	RIGEL				SUN	B CENTAURI		
	EARTH	SUN	9039	0.0018		EARTH	SIRIUS	7946	0.0018
	MOON	A CENTAURI	2209	0.0018		EARTH	CAPELLA	6364	0.0018
	MOON	PROCYON	1241	0.0018		SUN	EARTH	5175	0.0018
	EARTH	DIAMETER	1238	0.0018		EARTH	DIAMETER	4978	0.0018
		STRATEGY 2					STRATEGY 5		
0.02	EARTH	CANOPUS			0.02	SUN	PROCYON		
	EARTH	RIGEL				SUN	B CENTAURI		
	EARTH	SUN	9039	0.0018		SUN	EARTH	7917	0.0018
	SUN	RIGEL	5216	0.0018		EARTH	PROCYON	6444	0.0018
	SUN	MOON	1073	0.0018		EARTH	VEGA	5134	0.0018
	EARTH	DIAMETER	1071	0.0018		EARTH	DIAMETER	4942	0.0018
		STRATEGY 3					STRATEGY 6		
0.02	SUN	PROCYON			0.02	MOON	A CENTAURI		
	SUN	B CENTAURI				MOON	PROCYON		
	SUN	EARTH	7917	0.0018		EARTH	SIRIUS	1331	0.0018
	EARTH	CANOPUS	6445	0.0018		SUN	MOON	1058	0.0018
	EARTH	RIGEL	5226	0.0018		EARTH	SIRIUS	884	0.0018
	EARTH	DIAMETER	5024	0.0018		EARTH	DIAMETER	883	0.0018

TABLE 3-5

ARISON OF CELESTIAL FIX STRATEGIES

VENUS TRAJ. APRIL 19, 1964 V_I = 38826 FT/SEC T_F = 0.3 YEARS V_{RV} = 13339 FT/SEC

TIME IN YEARS	FIRST BODY	SECOND BODY	RMS POSITION ERROR MILES	RMS TIME ERROR HOURS	TIME	FIRST BODY	SECOND BODY	RMS POSITION ERROR MILES	RMS TIME ERROR HOURS
		STRATEGY 1					STRATEGY 4		
0.04	EARTH	CANOPUS			0.04	SUN	A CENTAURI		
	EARTH	PROCYON				SUN	PROCYON		
	EARTH	SUN	9730	0.0035		EARTH	SIRIUS	8491	0.0035
	MOON	A CENTAURI	9333	0.0035		EARTH	CAPELLA	6787	0.0035
	MOON	PROCYON	3506	0.0035		SUN	EARTH	5539	0.0035
	EARTH	DIAMETER	3502	0.0035		EARTH	DIAMETER	5523	0.0035
		STRATEGY 2					STRATEGY 5		
0.04	EARTH	CANOPUS			0.04	SUN	A CENTAURI		
	EARTH	PROCYON				SUN	PROCYON		
	EARTH	SUN	9730	0.0035		SUN	EARTH	8332	0.0035
	SUN	RIGEL	5631	0.0035		EARTH	ACHERNAR	6976	0.0035
	SUN	MOON	5510	0.0035		EARTH	SIRIUS	5667	0.0035
	EARTH	DIAMETER	5495	0.0035		EARTH	DIAMETER	5651	0.0035
		STRATEGY 3					STRATEGY 6		
0.04	SUN	A CENTAURI			0.04	MOON	A CENTAURI		
	SUN	PROCYON				MOON	PROCYON		
	SUN	EARTH	8332	0.0035		EARTH	ARCTURUS	4397	0.0035
	EARTH	CANOPUS	6978	0.0035		SUN	MOON	4332	0.0035
	EARTH	PROCYON	5620	0.0035		EARTH	ACHERNAR	3689	0.0035
	EARTH	DIAMETER	5604	0.0035		EARTH	DIAMETER	3684	0.0035

TABLE 3-5

COMPARISON OF CELESTIAL FIX STRATEGIES

VENUS TRAJ. APRIL 19,1964 V_I = 38826 FT/SEC T_F = 0.3 YEARS V_{RV} = 13339 FT/SEC

TIME IN YEARS	FIRST BODY	SECOND BODY	RMS POSITION ERROR MILES	RMS TIME ERROR HOURS	TIME	FIRST BODY	SECOND BODY	RMS POSITION ERROR MILES	RMS TIME ERROR HOURS
		STRATEGY 1					STRATEGY 4		
0.06	EARTH	ARCTURUS			0.06	SUN	CAPELLA		
	EARTH	B CENTAURI				SUN	RIGEL		
	EARTH	SUN	10601	0.0053		EARTH	VEGA	8648	0.0053
	VENUS	A CENTAURI	5837	0.0053		EARTH	ARCTURUS	7311	0.0052
	VENUS	ARCTURUS	2811	0.0053		SUN	EARTH	6073	0.0052
	EARTH	DIAMETER	2811	0.0053		EARTH	DIAMETER	6069	0.0052
		STRATEGY 2					STRATEGY 5		
0.06	EARTH	ARCTURUS			0.06	SUN	CAPELLA		
	EARTH	B CENTAURI				SUN	RIGEL		
	EARTH	SUN	10601	0.0053		SUN	EARTH	8877	0.0053
	SUN	VEGA	6151	0.0053		EARTH	VEGA	7563	0.0053
	SUN	VENUS	3357	0.0053		EARTH	SIRIUS	5916	0.0052
	EARTH	DIAMETER	3356	0.0053		EARTH	DIAMETER	5913	0.0052
		STRATEGY 3					STRATEGY 6		
0.06	SUN	CAPELLA			0.06	VENUS	A CENTAURI		
	SUN	RIGEL				VENUS	ARCTURUS		
	SUN	EARTH	8877	0.0053		EARTH	ACHERNAR	3518	0.0053
	EARTH	ARCTURUS	7652	0.0052		SUN	VENUS	3048	0.0053
	EARTH	B CENTAURI	6113	0.0052		EARTH	SIRIUS	2377	0.0053
	EARTH	DIAMETER	6109	0.0052		EARTH	DIAMETER	2376	0.0053

TABLE 3-5

OMPARISON OF CELESTIAL FIX STRATEGIES

VENUS TRAJ. APRIL 19,1964 V_I = 38826 FT/SEC T_F = 0.3 YEARS V_{RV} = 13339 FT/SEC

TIME IN YEARS	FIRST BODY	SECOND BODY	RMS POSITION ERROR MILES	RMS TIME ERROR HOURS	TIME	FIRST BODY	SECOND BODY	RMS POSITION ERROR MILES	RMS TIME ERROR HOURS
		STRATEGY 1					STRATEGY 4		
0.10	EARTH	A CENTAURI			0.10	SUN	PROCYON		
	EARTH	PROCYON				SUN	ACHERNAR		
	EARTH	SUN	12502	0.0088		EARTH	A CENTAURI	9946	0.0088
	VENUS	CAPELLA	6945	0.0088		EARTH	ARCTURUS	9066	0.0087
	VENUS	ACHERNAR	1896	0.0088		SUN	EARTH	7551	0.0087
	SUN	VENUS	1554	0.0087		SUN	VENUS	2350	0.0087
		STRATEGY 2					STRATEGY 5		
0.10	EARTH	A CENTAURI			0.10	SUN	PROCYON		
	EARTH	PROCYON				SUN	ACHERNAR		
	EARTH	SUN	12502	0.0088		SUN	EARTH	10693	0.0088
	SUN	PROCYON	10351	0.0087		EARTH	A CENTAURI	8596	0.0088
	SUN	ACHERNAR	7553	0.0087		EARTH	ARCTURUS	7551	0.0087
	SUN	VENUS	2354	0.0087		SUN	VENUS	2350	0.0087
		STRATEGY 3					STRATEGY 6		
0.10	SUN	PROCYON			0.10	VENUS	CAPELLA		
	SUN	ACHERNAR				VENUS	ACHERNAR		
	SUN	EARTH	10693	0.0088		EARTH	ACHERNAR	2445	0.0088
	EARTH	A CENTAURI	8596	0.0088		SUN	VENUS	2134	0.0087
	EARTH	PROCYON	7553	0.0087		EARTH	RIGEL	1586	0.0087
	SUN	VENUS	2354	0.0087		SUN	EARTH	1545	0.0087

TABLE 3-5

COMPARISON OF CELESTIAL FIX STRATEGIES

VENUS TRAJ. APRIL 19,1964 V_I = 38826 FT/SEC T_F = 0.3 YEARS V_{RV} = 13339 FT/SEC

TIME IN YEARS	FIRST BODY	SECOND BODY	RMS POSITION ERROR MILES	RMS TIME ERROR HOURS	TIME	FIRST BODY	SECOND BODY	RMS POSITION ERROR MILES	RMS TIME ERROR HOURS
		STRATEGY 1					STRATEGY 4		
0.20	VENUS	RIGEL			0.20	SUN	CAPELLA		
	VENUS	B CENTAURI				SUN	RIGEL		
	VENUS	SUN	12484	0.0175		VENUS	SIRIUS	10217	0.0175
	EARTH	CAPELLA	1644	0.0175		VENUS	CAPELLA	9379	0.0166
	EARTH	PROCYON	1368	0.0175		SUN	VENUS	7229	0.0166
	SUN	EARTH	1067	0.0170		SUN	EARTH	1432	0.0166
		STRATEGY 2					STRATEGY 5		
0.20	VENUS	RIGEL			0.20	SUN	CAPELLA		
	VENUS	B CENTAURI				SUN	RIGEL		
	VENUS	SUN	12484	0.0175		SUN	VENUS	9215	0.0175
	SUN	CAPELLA	11251	0.0169		VENUS	ACHERNAR	8276	0.0171
	SUN	RIGEL	7257	0.0166		VENUS	PROCYON	7130	0.0167
	SUN	EARTH	1421	0.0166		SUN	EARTH	1910	0.0166
		STRATEGY 3					STRATEGY 6		
0.20	SUN	CAPELLA			0.20	EARTH	CAPELLA		
	SUN	RIGEL				EARTH	PROCYON		
	SUN	VENUS	9215	0.0175		VENUS	ARCTURUS	2293	0.0175
	VENUS	RIGEL	8298	0.0169		SUN	EARTH	1644	0.0171
	VENUS	B CENTAURI	7257	0.0166		VENUS	B CENTAURI	1161	0.0171
	SUN	EARTH	1421	0.0166		SUN	VENUS	1053	0.0170

TABLE 3-5

MPARISON OF CELESTIAL FIX STRATEGIES

VENUS TRAJ. APRIL 19,1964 V_I = 38826 FT/SEC T_F = 0.3 YEARS V_{RV} = 13339 FT/SEC

TIME IN YEARS	FIRST BODY	SECOND BODY	RMS POSITION ERROR MILES	RMS TIME ERROR HOURS	TIME	FIRST BODY	SECOND BODY	RMS POSITION ERROR MILES	RMS TIME ERROR HOURS
		STRATEGY 1					STRATEGY 4		
0.26	VENUS	RIGEL			0.26	SUN	PROCYON		
	VENUS	B CENTAURI				SUN	B CENTAURI		
	VENUS	SUN	7549	0.0228		VENUS	B CENTAURI	6592	0.0228
	EARTH	SIRIUS	3952	0.0223		VENUS	RIGEL	5643	0.0211
	EARTH	ARCTURUS	2335	0.0223		SUN	VENUS	4627	0.0211
	VENUS	DIAMETER	2334	0.0223		VENUS	DIAMETER	4616	0.0211
		STRATEGY 2					STRATEGY 5		
0.26	VENUS	RIGEL			0.26	SUN	PROCYON		
	VENUS	B CENTAURI				SUN	B CENTAURI		
	VENUS	SUN	7549	0.0228		SUN	VENUS	6343	0.0228
	SUN	B CENTAURI	4701	0.0228		VENUS	CAPELLA	5470	0.0211
	SUN	EARTH	3442	0.0201		VENUS	PROCYON	4701	0.0211
	VENUS	DIAMETER	3438	0.0201		VENUS	DIAMETER	4690	0.0211
		STRATEGY 3					STRATEGY 6		
0.26	SUN	PROCYON			0.26	EARTH	SIRIUS		
	SUN	B CENTAURI				EARTH	ARCTURUS		
	SUN	VENUS	6343	0.0228		VENUS	ACHERNAR	3558	0.0228
	VENUS	RIGEL	5474	0.0211		SUN	EARTH	2693	0.0216
	VENUS	B CENTAURI	4627	0.0211		VENUS	A CENTAURI	2194	0.0214
	VENUS	DIAMETER	4616	0.0211		VENUS	DIAMETER	2193	0.0214

TABLE 3-5

COMPARISON OF CELESTIAL FIX STRATEGIES

VENUS TRAJ. APRIL 19,1964 V_I = 38826 FT/SEC T_F = 0.3 YEARS V_{RV} = 13339 FT/SEC

TIME IN YEARS	FIRST BODY	SECOND BODY	RMS POSITION ERROR MILES	RMS TIME ERROR HOURS	TIME	FIRST BODY	SECOND BODY	RMS POSITION ERROR MILES	RMS TIME ERROR HOURS
		STRATEGY 1					STRATEGY 4		
0.28	VENUS	RIGEL			0.28	SUN	VEGA		
	VENUS	B CENTAURI				SUN	CAPELLA		
	VENUS	SUN	6375	0.0245		VENUS	B CENTAURI	5643	0.0245
	EARTH	RIGEL	2775	0.0240		VENUS	RIGEL	4685	0.0229
	EARTH	PROCYON	2775	0.0237		SUN	VENUS	3952	0.0229
	VENUS	DIAMETER	2740	0.0237		VENUS	DIAMETER	3851	0.0228
		STRATEGY 2					STRATEGY 5		
0.28	VENUS	RIGEL			0.28	SUN	VEGA		
	VENUS	B CENTAURI				SUN	CAPELLA		
	VENUS	SUN	6375	0.0245		SUN	VENUS	5599	0.0245
	SUN	B CENTAURI	4039	0.0245		VENUS	CAPELLA	4617	0.0229
	SUN	EARTH	3870	0.0228		VENUS	B CENTAURI	3944	0.0229
	VENUS	DIAMETER	3775	0.0227		VENUS	DIAMETER	3844	0.0228
		STRATEGY 3					STRATEGY 6		
0.28	SUN	VEGA			0.28	EARTH	RIGEL		
	SUN	CAPELLA				EARTH	PROCYON		
	SUN	VENUS	5599	0.0245		VENUS	ACHERNAR	4161	0.0245
	VENUS	RIGEL	4629	0.0229		SUN	EARTH	3369	0.0230
	VENUS	B CENTAURI	3952	0.0229		VENUS	B CENTAURI	2964	0.0229
	VENUS	DIAMETER	3851	0.0228		VENUS	DIAMETER	2920	0.0228

TABLE 3-5

CELESTIAL FIX POSITION AND TIME ERRORS

MARS TRAJECTORY NOV.5,1964

V_{RE} = 9968 FT/SEC V_{RM} = 9135 FT/SEC

TIME IN YEARS	RMS POS. ERROR MILES	RMS TIME ERROR HOURS	TIME IN YEARS	RMS POS. ERROR MILES	RMS TIME ERROR HOURS
0.001	10	0.0000	0.425	2926	0.0359
0.002	14	0.0002	0.450	3267	0.0380
0.003	20	0.0003	0.475	3742	0.0401
0.004	28	0.0004	0.500	4233	0.0419
0.005	39	0.0004	0.525	4950	0.0436
0.006	51	0.0005	0.550	5802	0.0452
0.007	67	0.0006	0.575	6689	0.0464
0.008	87	0.0007	0.600	6796	0.0500
0.009	112	0.0008	0.625	6812	0.0520
0.010	143	0.0009	0.650	6733	0.0543
0.025	1292	0.0022	0.675	5854	0.0586
0.050	2430	0.0044	0.700	5081	0.0594
0.075	2899	0.0066	0.725	4396	0.0589
0.100	3453	0.0088	0.750	3885	0.0571
0.125	4026	0.0109	0.775	3612	0.0545
0.150	3757	0.0129	0.800	6137	0.0670
0.175	6414	0.0151	0.825	6049	0.0689
0.200	5049	0.0170	0.840	2890	0.0617
0.225	7644	0.0200	0.841	2422	0.0607
0.250	NO 2ND PLANET		0.842	1964	0.0600
0.275	NO 2ND PLANET		0.843	1537	0.0594
0.300	2400	0.0254	0.844	1156	0.0590
0.325	2339	0.0274	0.845	837	0.0588
0.350	2382	0.0295	0.846	596	0.0587
0.375	2486	0.0316	0.847	444	0.0587
0.400	2633	0.0338	0.848	379	0.0586

TABLE 3-6

CELESTIAL FIX POSITION AND TIME ERRORS

MARS TRAJECTORY NOV.24.1964

V_{RE} = 13526 FT/SEC V_{RM} = 25261 FT/SEC

TIME IN YEARS	RMS POS. ERROR MILES	RMS TIME ERROR HOURS	TIME IN YEARS	RMS POS. ERROR MILES	RMS TIME ERROR HOURS
0.001	10	0.0001	0.250	NO 2ND PLANET	
0.002	9	0.0002	0.275	2719	0.0234
0.003	11	0.0003	0.300	2634	0.0255
0.004	21	0.0004	0.325	2799	0.0277
0.005	49	0.0004	0.350	2999	0.0298
0.006	119	0.0005	0.375	3326	0.0320
0.007	318	0.0006	0.400	3772	0.0341
0.008	564	0.0007	0.425	4373	0.0365
0.009	450	0.0008	0.450	5107	0.0382
0.010	376	0.0009	0.475	6019	0.0400
0.025	764	0.0022	0.490	6517	0.0420
0.050	3407	0.0044	0.491	6463	0.0421
0.075	3289	0.0066	0.492	6345	0.0421
0.100	3434	0.0087	0.493	6112	0.0422
0.125	4899	0.0109	0.494	5679	0.0423
0.150	6800	0.0130	0.495	4931	0.0423
0.175	6138	0.0149	0.496	3808	0.0424
0.200	8097	0.0174	0.497	2475	0.4248
0.225	NO 2ND PLANET		0.498	1318	0.0408

TABLE 3-7

CELESTIAL FIX POSITION AND TIME ERRORS

VENUS TRAJECTORY APRIL 19,1964

V_{RE} = 9688 FT/SEC V_{RV} = 18357 FT/SEC

TIME IN YEARS	RMS POS. ERROR MILES	RMS TIME ERROR HOURS	TIME IN YEARS	RMS POS. ERROR MILES	RMS TIME ERROR HOURS
0.001	19	0.0001	0.225	1870	0.0190
0.002	10	0.0002	0.250	1765	0.0208
0.003	9	0.0003	0.275	1793	0.0224
0.004	12	0.0004	0.300	1865	0.0238
0.005	17	0.0004	0.325	1962	0.0249
0.006	24	0.0005	0.350	3650	0.0285
0.007	33	0.0006	0.375	2939	0.0259
0.008	44	0.0007	0.400	2354	0.0277
0.009	55	0.0008	0.425	2143	0.0239
0.010	68	0.0009	0.440	2857	0.0329
0.025	604	0.0022	0.441	2902	0.0329
0.050	1990	0.0044	0.442	2856	0.0330
0.075	4337	0.0066	0.443	2729	0.0330
0.100	5531	0.0088	0.444	2486	0.0328
0.125	7301	0.0109	0.445	2103	0.0325
0.150	12768	0.0131	0.446	1607	0.0321
0.175	21517	0.0149	0.447	1090	0.0317
0.200	2272	0.0170	0.448	668	0.0300

TABLE 3-8

CELESTIAL FIX POSITION AND TIME ERRORS

VENUS TRAJECTORY APRIL 19,1964

V_{RE} = 14206 FT/SEC V_{RV} = 13339 FT/SEC

TIME IN YEARS	RMS POS. ERROR MILES	RMS TIME ERROR HOURS	TIME IN YEARS	RMS POS. ERROR MILES	RMS TIME ERROR HOURS
0.001	10	0.0001	0.150	1100	0.0129
0.002	14	0.0002	0.175	1026	0.0150
0.003	22	0.0003	0.200	1053	0.0170
0.004	34	0.0004	0.225	1343	0.0188
0.005	49	0.0004	0.250	1875	0.0203
0.006	68	0.0005	0.275	2596	0.0219
0.007	91	0.0006	0.290	2440	0.0241
0.008	116	0.0007	0.291	2266	0.0241
0.009	145	0.0008	0.292	2030	0.0241
0.010	177	0.0009	0.293	1733	0.0241
0.025	1675	0.0022	0.294	1389	0.0240
0.050	3817	0.0044	0.295	1032	0.0240
0.075	1983	0.0066	0.296	701	0.0239
0.100	1545	0.0087	0.297	439	0.0240
0.125	1277	0.0109	0.298	277	0.0241

TABLE 3-9

[redacted]

VARIABLE TIME OF ARRIVAL NAVIGATION

MARS TRAJECTORY NOV.5,1964

TIME OF FIX	RMS VEL CORR	FINAL VEL ERROR	FINAL POS ERROR
0.003	57		
0.425	3		
0.775	14		
0.843	20		
TOTAL=	94	109	48

TIME OF FIX	RMS VEL CORR	FINAL VEL ERROR	FINAL POS ERROR
0.002	57		
0.375	2		
0.775	11		
0.846	39		
TOTAL=	109	114	26

TIME OF FIX	RMS VEL CORR	FINAL VEL ERROR	FINAL POS ERROR
0.002	57		
0.400	2		
0.775	13		
0.844	24		
TOTAL=	96	110	41

TIME OF FIX	RMS VEL CORR	FINAL VEL ERROR	FINAL POS ERROR
0.005	58		
0.375	2		
0.775	11		
0.846	39		
TOTAL=	110	114	26

TIME OF FIX	RMS VEL CORR	FINAL VEL ERROR	FINAL POS ERROR
0.004	57		
0.375	2		
0.775	11		
0.845	31		
TOTAL=	102	112	33

TIME OF FIX	RMS VEL CORR	FINAL VEL ERROR	FINAL POS ERROR
0.005	58		
0.325	2		
0.775	13		
0.848	85		
TOTAL=	158	137	14

TIME OF FIX	RMS VEL CORR	FINAL VEL ERROR	FINAL POS ERROR
0.005	58		
0.400	3		
0.775	13		
0.845	29		
TOTAL=	102	111	33

TABLE 3-10

[redacted]

[redacted]

[redacted]

VARIABLE TIME OF ARRIVAL NAVIGATION

MARS TRAJECTORY NOV.24,1964

TIME OF FIX	RMS VEL CORR	FINAL VEL ERROR	FINAL POS ERROR
0.003	43		
0.025	5		
0.400	37		
0.494	34		
TOTAL=	118	74	93

TIME OF FIX	RMS VEL CORR	FINAL VEL ERROR	FINAL POS ERROR
0.004	43		
0.025	5		
0.425	51		
0.498	75		
TOTAL=	174	105	39

TIME OF FIX	RMS VEL CORR	FINAL VEL ERROR	FINAL POS ERROR
0.002	43		
0.025	4		
0.400	36		
0.496	50		
TOTAL=	133	82	61

TIME OF FIX	RMS VEL CORR	FINAL VEL ERROR	FINAL POS ERROR
0.003	43		
0.075	8		
0.400	47		
0.498	101		
TOTAL=	198	123	39

TIME OF FIX	RMS VEL CORR	FINAL VEL ERROR	FINAL POS ERROR
0.001	43		
0.025	4		
0.425	45		
0.497	51		
TOTAL=	143	86	46

TABLE 3-11

[redacted] 60 WWRN - 5337

[redacted]

DECLASSIFIED

[redacted]

VARIABLE TIME OF ARRIVAL NAVIGATION

VENUS TRAJECTORY APRIL 19,1964

TIME OF FIX	RMS VEL CORR	FINAL VEL ERROR	FINAL POS ERROR	TIME OF FIX	RMS VEL CORR	FINAL VEL ERROR	FINAL POS ERROR
0.006	59			0.002	58		
0.225	4			0.200	6		
0.400	22			0.400	38		
0.443	28			0.447	57		
TOTAL=	113	62	117	TOTAL=	159	85	44

TABLE 3-12

[redacted]

[redacted]

[redacted]

VARIABLE TIME OF ARRIVAL NAVIGATION

VENUS TRAJECTORY APRIL 19,1964

TIME OF FIX	RMS VEL CORR	FINAL VEL ERROR	FINAL POS ERROR	TIME OF FIX	RMS VEL CORR	FINAL VEL ERROR	FINAL POS ERROR
0.003	41			0.006	42		
0.175	4			0.150	6		
0.250	7			0.250	9		
0.293	24			0.297	56		
TOTAL=	77	55	63	TOTAL=	113	73	26

TIME OF FIX	RMS VEL CORR	FINAL VEL ERROR	FINAL POS ERROR	TIME OF FIX	RMS VEL CORR	FINAL VEL ERROR	FINAL POS ERROR
0.002	41			0.003	41		
0.150	4			0.075	7		
0.250	9			0.250	37		
0.294	28			0.298	90		
TOTAL=	82	57	51	TOTAL=	176	94	18

TIME OF FIX	RMS VEL CORR	FINAL VEL ERROR	FINAL POS ERROR	TIME OF FIX	RMS VEL CORR	FINAL VEL ERROR	FINAL POS ERROR
0.005	42			0.005	42		
0.150	5			0.075	8		
0.250	9			0.250	38		
0.295	34			0.298	90		
TOTAL=	90	59	41	TOTAL=	178	94	18

TABLE 3-13

[redacted] 60WWRN - 5337

[redacted]

[redacted]

FIXED TIME OF ARRIVAL NAVIGATION

MARS TRAJECTORY NOV.5,1964

TIME OF FIX	RMS VEL CORR	FINAL VEL ERROR	FINAL POS ERROR	TIME OF FIX	RMS VEL CORR	FINAL VEL ERROR	FINAL POS ERROR
0.003	70			0.002	70		
0.425	8			0.375	6		
0.775	32			0.775	28		
0.843	120			0.846	195		
TOTAL=	230	113	62	TOTAL=	298	186	44

TIME OF FIX	RMS VEL CORR	FINAL VEL ERROR	FINAL POS ERROR	TIME OF FIX	RMS VEL CORR	FINAL VEL ERROR	FINAL POS ERROR
0.004	70			0.005	70		
0.300	6			0.400	8		
0.775	42			0.775	30		
0.843	117			0.847	263		
TOTAL=	235	113	61	TOTAL=	371	254	40

TIME OF FIX	RMS VEL CORR	FINAL VEL ERROR	FINAL POS ERROR	TIME OF FIX	RMS VEL CORR	FINAL VEL ERROR	FINAL POS ERROR
0.002	70			0.005	70		
0.400	7			0.325	6		
0.775	30			0.775	35		
0.844	135			0.848	401		
TOTAL=	241	127	55	TOTAL=	512	392	36

TIME OF FIX	RMS VEL CORR	FINAL VEL ERROR	FINAL POS ERROR	TIME OF FIX	RMS VEL CORR	FINAL VEL ERROR	FINAL POS ERROR
0.005	70			0.001	69		
0.300	6			0.425	10		
0.775	42			0.840	237		
0.844	132			0.848	342		
TOTAL=	250	126	54	TOTAL=	658	367	34

TABLE 3-14

[redacted]

CHAPTER 4

A CENTAUR INTERPLANETARY SPACECRAFT GUIDANCE AND CONTROL SYSTEM*

by
John M. Dahlen
Milton B. Trageser
Philip N. Bowditch
Harold H. Seward
William E. Toth

*Note: System is often referred to as "CIGS" for brevity.

TABLE OF CONTENTS

LIST OF FIGURES

LIST OF TABLES

CHAPTER 4

A CENTAUR INTERPLANETARY SPACECRAFT GUIDANCE AND CONTROL SYSTEM

Introduction

The objective of this study has been to formulate practicable techniques and equipment for the guidance and control of interplanetary spacecraft to be launched by Centaur boosters beginning in 1964. It is clear that two fundamental conditions prevail, and these have directed the course of this investigation. First, a detailed description of spacecraft missions and configurations does not at present exist. Secondly, it is known that accomplishment of the navigation and stabilization function will require the development of a well-integrated guidance and control system which is designed in harmony with the mother spacecraft.

We have therefore focused our attention upon a self-contained system which would be packaged in a small cylindrical container*. Little or no adaption of this system would be required to permit integration with a wide variety of Centaur payload configurations.

The interplanetary guidance and control system presented here would be suitable for a large number of space missions, typical among which are the atmospheric probe, planetary satellite and television reconnaissance pass for either Mars or

*The system will be referred to as CIGS (Centaur Interplanetary Guidance System) for brevity.

Venus discussed in Chapter 1. As already described in detail, navigation studies have shown that, given a modest spacecraft velocity correction capability, CIGS has very respectable performance.

For the most part, this system is derived from the extensive investigations documented in MIT/IL Report R-235, and therefore largely relies upon that report for a justification of the techniques and equipment proposed. Certain changes in the manner of accomplishing guidance and control over that proposed for the complete space vehicle in R-235 have been introduced here either to improve performance or to permit the construction of a package which can be applied to a wide variety of spacecraft configurations. One example of this is the replacement of the solar vanes by a sublimating iodine jet for angular momentum control. Such departures from the functional operation in R-235 have been studied and documented below.

I. General System Description

The CIGS is a self-contained, fully-automatic system designed to carry out the tasks of guidance and attitude control for Centaur-boosted interplanetary spacecraft. Each of these tasks is performed by means of complex sequences of operations which involve the functioning of many CIGS components and mobility of the complete spacecraft. Control of these operations is exerted by a general purpose digital computer which is used for time sequencing and logical decision making in addition to its obvious arithmetic function. The computer is also available to the mother spacecraft for timing signals, arithmetic computations and logical decision-making.

A. Attitude Control

Attitude control is required to achieve a variety of necessary ends:

1. During normal "quiescent" operation the "sunny" end of the space vehicle is kept facing the sun by torquing control flywheels so as to null the sun-finders' signals. By using the "dead zone mode" of operation described in Chapter 6 of R-235 and later in Chapter 5, the flywheel duty cycles can be kept below one percent thus conserving the bearings and reducing power consumption.
2. Tracking of celestial objects with the body-fixed sun/star tracker or the mobile star/planet tracker is accomplished by torquing the control flywheels to null tracker error signals.
3. Spatial re-orientations of the vehicle about the x, y and z axes are performed by spinning up and later stopping appropriate control flywheels. The x and y wheels are monitored by two torqued single-degree-of-freedom integrating gyros used to provide the necessary angular measurements. Rotation about the z axis, being less critical, is monitored by counting flywheel revolutions.
4. Attitude control during the application of velocity-correcting rocket thrust would be achieved by gimballing the spacecraft engine or otherwise directing the thrust vector so as to provide corrective torques computed on the basis of gyro-measured attitude deviations.
5. Control of angular momentum, which tends to build up over extended time periods due to unwanted external torques, is accomplished by operating the iodine jet through an iterative procedure which persistently acts to reduce angular momentum.

Mechanization of these attitude control functions including descriptions of specific hardware and system analyses are covered by R-235 or later sections of this report.

B. Guidance

Control of the spacecraft's path through space is accomplished by several operations requiring, in general, mobility of the spacecraft and the application of rocket thrust in addition to the expected usage of all CIGS elements.

1. A navigational fix is obtained by converting precise measurements of the angles between several pairs of visible objects into an accurate estimate of position and time. This computation is made by the digital computer. The desired angles may be subtended at the space sextant by:

    (a) the sun and a planet;
    (b) the sun and our moon;
    (c) the sun and a star; and
    (d) a planet and a star.

    In addition, the space sextant is sometimes used to determine the apparent diameter of planets when they subtend more than one milliradian.

    The object-pairs are chosen to minimize errors and eliminate unprofitable sightings. A redundancy of data (i. e., a measurement of more than four angles) is used to minimize errors in the statistical sense.
2. Velocity corrections would be calculated by the computer and carried out by means of the spacecraft rocket engine and CIGS control components. A computer-commanded spatial re-orientation would establish the spacecraft and hence the thrust vector in the proper attitude for firing. This attitude would be held during firing by the CIGS gyros. The computer would then control the magnitude of velocity change by commanding cut-off when the accelerometer indicates completion of the desired correction.

A full explanation of the navigation scheme and the equipment and techniques by which it is implemented in the CIGS can be found in R-235 and elsewhere in this report.

C. Physical Description

The CIGS proposed here is packaged in a cylindrical can weighing approximately 70 pounds and measuring 11 inches in diameter by 22 inches in length. Its size and weight are largely independent of the navigational accuracy requirements and mission types prescribed. However, the physical size and mass of the spacecraft do determine the size of the control flywheels and iodine jets; hence, for the sake of definiteness in the preliminary layout, the spacecraft weight and inertia were assumed to be 1000 pounds and 50 slug-ft^2, respectively. We have also anticipated a possible 50% increase in the moments of inertia due to the use of solar cell panels extending to large distances from the center of mass.

CIGS design criteria were as follows:

1. component simplicity and reliability;
2. minimum component interface complexity; and
3. minimum total volume and weight.

The resulting preliminary layout is shown in Fig. 4-1 and 4-2.

In essence the guidance and control system is a right circular cylinder containing the space sextant, inertial component group, computer, and associated electronics. This combination, together with a semi-passive thermal environment control, constitutes the entire self-contained system requiring only primary power and engine control lead ties to the mother ship. The following paragraphs describe the CIGS sub-assemblies.

The thermal control system may best be described as a twelve-bladed reflecting surface fan rotating through approximately 30 degrees of arc co-axial with a fixed similar 12-bladed

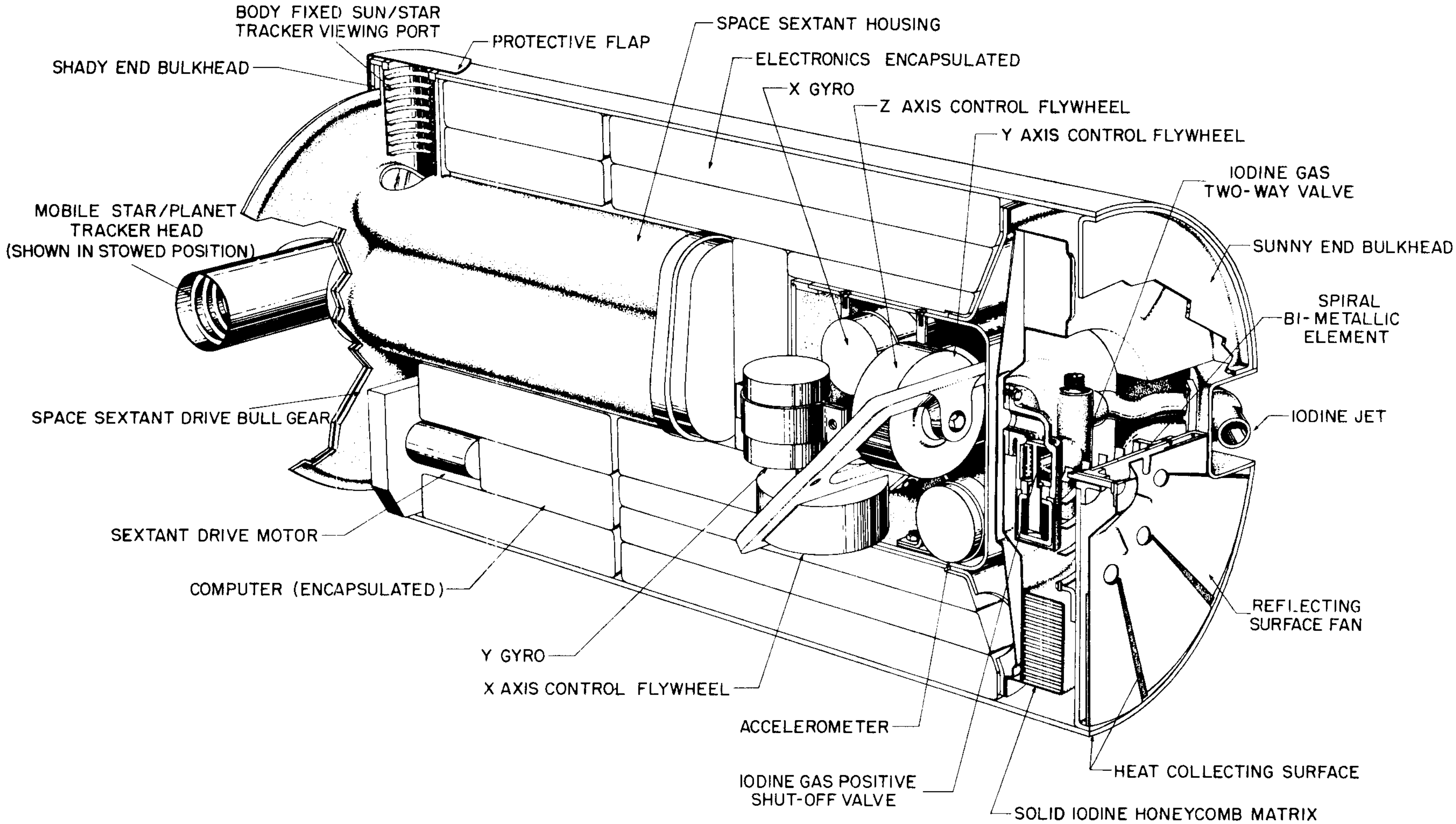

Fig. 4-1 CIGS cutaway view with callouts.

collector surface on the end closure of the cylinder. The rotation is supplied by a passive bi-metallic spiral element with demand over-ride. This system allows for modulation of collected thermal energy which is transferred to the components of the guidance system by conduction and/or radiation. The remaining surfaces of the cylinder have low emissivity to minimize radiative heat loss.

Placed next to the fine angular momentum reduction system (i. e., iodine jets) we see a toroidal storage tank providing maximum evaporative surface for the iodine in conjunction with a centrally-located two-stage valve. The first stage of the valve is a positive shut-off spring-loaded solenoid, power being supplied to the solenoid only when the jets are in use. The second stage is a ball-seated electro-magnet providing choice of nozzle. In its quiescent state this valve is centered by a permanent magnet to prevent any minor leakage from the positive shut-off valve from imparting angular momentum to the spacecraft. The iodine in the system is a solid entrapped in a honeycomb matrix to prevent breakage during booster firing and is covered with a fine mesh screen.

The inertial component group has three attitude control flywheels, two single-degree-of-freedom gyros, and a velocity cut-off torqued pendulum accelerometer packaged in one hermetically sealed canister above the iodine tank. The flywheels are mounted with their spin axes along principal axes of the complete spacecraft. The gyros are mounted with opposed spin axes to prevent imparting angular momentum during their operation. The velocity cut-off accelerometer is mounted with its sensitive direction parallel to the rocket thrust vector.

The computer and other electronics are packaged as two welded-wire totally encapsulated entities filling the majority of the remaining volume of the guidance container. These components are connected to the structure mechanically and thermally by long rods extending to the iodine tank mounting plane.

The remaining component of the system, namely the space sextant, described more fully in another section of this report, provides the closure for the other end of the guidance cylinder.

In summary, the design attempt has been to provide a self-contained, minimum volume system with its own space environment controls requiring only primary electrical power from the mother ship.

Table 4-1 provides a breakdown of the expected component weights.

TABLE 4-1

WEIGHT BREAKDOWN FOR CIGS

ITEM		WEIGHT(lbs)
Computer		20
Electronics		20
Inertial Group		7.3
Space Sextant		5.1
Iodine Jet System		3.24
Thermal Control System		1.35
Structure Group		12.58
Cylindrical Shell	7.60	
Sunny End Bulkhead	0.95	
Shady End Bulkhead	0.80	
Inertial Grp Canister	2.0	
Other	1.23	
TOTAL CIGS WEIGHT		70 lbs.

II. System/Spacecraft Integration and Functional Operation

A. Physical Mating

So far as the CIGS is concerned for its own operation, interface requirements are extremely simple, it being necessary only to furnish the CIGS with direct current unregulated power and an attachment which provides:

(a) a clear 180° field of view for the space sextant; and

(b) orientation of the heat-collecting end of the system with the result that it will normally be facing the sun, like the spacecraft solar battery.

Fig. 4-3 illustrates the general configuration which might prevail with a spacecraft of "conventional" form, where the longitudinal axis is at once the direction of applied thrust and the axis which is normally oriented parallel to the sun's rays.

The body-fixed sun/star tracker line of sight is placed parallel to one of the vehicle's transverse axes which will now be termed the x-axis. The center line of the can is then located parallel to the vehicle's longitudinal axis, which can now be called the z-axis. This places the heat-collecting face on the CIGS with its thermal control vanes at the "sunny" end, and aligns the accelerometer input axis with the thrust vector. The y-axis is then defined perpendicular to the other two. The mobile star tracker head protrudes from the "shady" end of the can and rotates 180 degrees about the z-axis in order to sweep the mobile tracker line of sight through its minimum field of view. The head is turned in toward the vehicle for stowage in order to protect the objective and mirror from unnecessary exposure to the environment. Rotation of the mobile tracker head to this stowage position also positions a protective flap in front of the body-fixed sun/star tracker viewing port. The iodine jet is oriented so as to constrain its thrust vector to the y-z plane while at the same time maximizing its torque about the x-axis. The external torque from this jet can only have a compo-

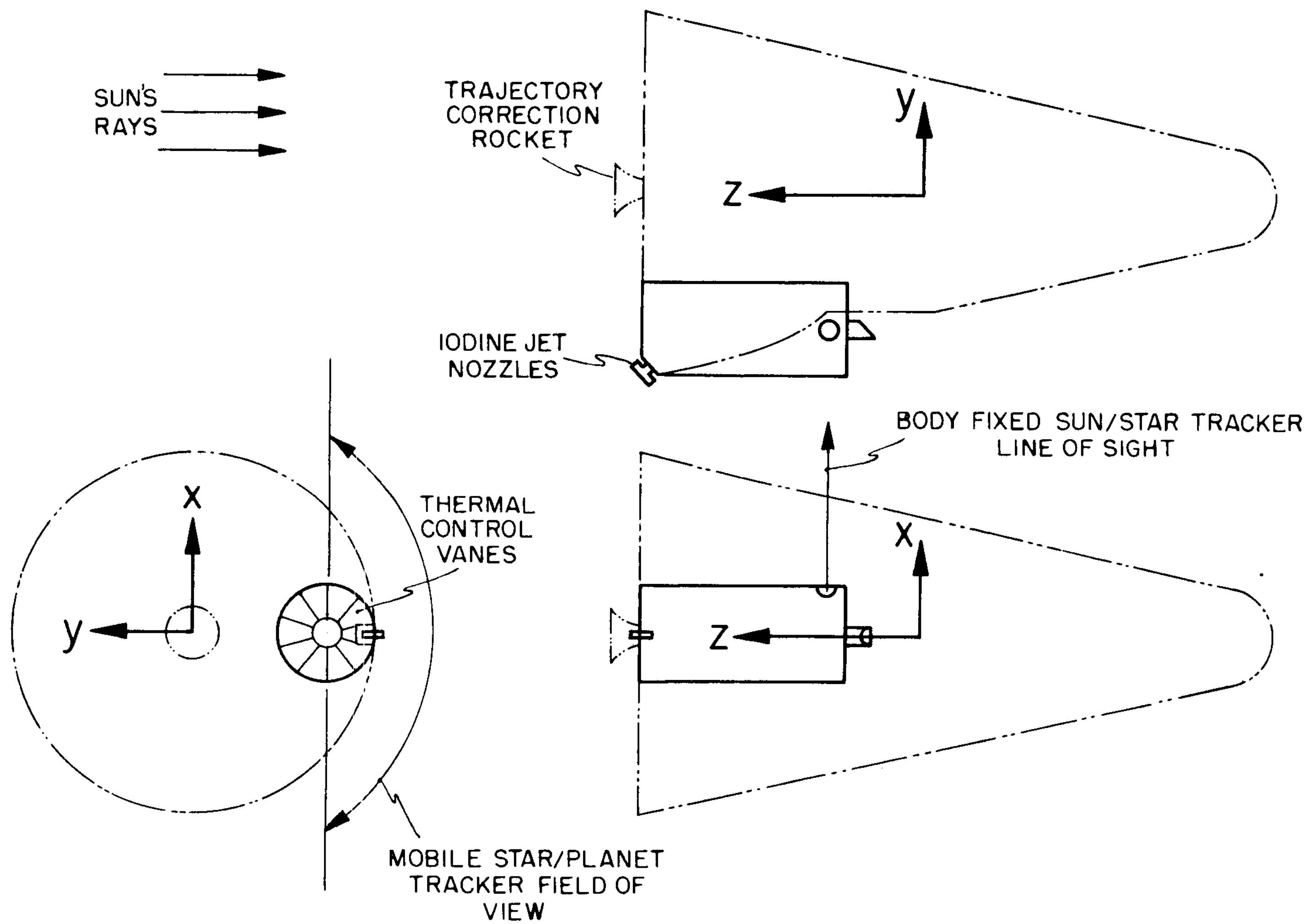

Fig. 4-3 Typical spacecraft--CIGS configuration.

nent about the y or z axes when the center of mass shifts parallel to the x-axis, or when the thrust is not properly aligned.

B. Functional Operation

The over-all operation of the integrated CIGS spacecraft system toward achieving its guidance and control objectives would be in close conformance to that described in R-235 for the recoverable interplanetary reconnaissance probe. The R-235 description with appropriate modifications is repeated here in order to lend a reasonable degree of self-sufficiency to this chapter.

The basic computer program would cause most procedures to be initiated at times prescribed before launch. The necessary time reference would be established by the clock which would be started at some fixed date and time chosen to occur during the launch countdown. It is in terms of this time reference that most of the data in the fixed (core rope) storage are prepared. Several procedures including at least the first angular momentum reduction and the first navigational correction will be required at some prescribed times after lift-off. Hence the computer will require an index signal from the booster at launch on the basis of which the early procedures will be initiated and certain data corrections will be computed. It is expected that holds of several days may be taken into account in this way.

The navigation and control procedures which, as stated above, are sequenced by the basic computer program are only six in number. They may be thought of as basic routines which have many sub-routines in common. Hence computer storage capacity is minimized by reducing the navigation and control function to a number of simple tasks which are repeated a great many times. A description of the six basic routines along with their occurrence in time should provide a picture of the over-all mission.

1. Coarse Angular Momentum Reduction Routine

This procedure is required only once, shortly after separation of the spacecraft from the booster rocket, in order to remove the expected tumbling motion. A tumbling rate greater than 1 deg/sec would exceed the control flywheel capacity, hence the torque available from the navigation rocket is employed. Perhaps twenty minutes after the launch index signal (allowing a generous period for separation) this routine would be initiated by firing the rocket for some fraction of a minute. Because the rocket would be gimballed to null gyro outputs, this firing would reduce the x and y components of angular velocity to less than 0.1 deg/sec, but would leave a substantial spin about the z axis. The vehicle would now be rotated 90 deg about the x axis (using the x control flywheel) and the rocket fired again to reduce the spin (now about the x and y axes) to less than 0.1 deg/sec. The residual angular velocity is determined by the moderate performance characteristics of the rocket control loops, and is sufficiently small to be within the capacity of the fine momentum reduction scheme.

2. Fine Angular Momentum Reduction

This routine which controls the application of iodine jet torques is used approximately once per week to reduce spacecraft angular velocities to about 0.001 deg/sec. During the week between reductions, spacecraft angular rates may build-up to 0.025 deg/sec due to iodine gas leakage and other unwanted external torques. Suppression of angular momentum in this way allows the control flywheels to operate at very low duty cycles, below 1%, while keeping the spacecraft heat-collecting end sun-oriented. Other routines which require accurate spatial orientations of the vehicle, such as the radio transmission and velocity change routines, would best be performed shortly after this fine momentum reduction. The details of the manner in which the iodine jet is applied to reduce angular momentum are covered below in section III, A of this chapter.

3. Radio Transmission

The purpose of this routine is to orient spacecraft antennae or directional instrumentation in prescribed spatial attitudes for data gathering or transmission. A reference attitude is first obtained by tracking the sun and a star with the body-fixed sun/star tracker and mobile star/planet tracker respectively. Starting from the quiescent condition with the z axis sun-oriented, the vehicle is slewed 90 degrees about the y axis using the y control flywheel under the monitorship of the y gyro. This places the sun in the body-fixed sun/star tracker field of view after which time it is tracked. Now the vehicle, which knows its approximate position in the Solar System and the approximate location of six bright stars and thirty stars of secondary brightness, chooses one of the bright stars which will be unambiguous with the 30 intermediate stars during a search about the sun line. This search about the sun line is performed by setting the mobile star tracker at the angle (sextant drive angle) expected between the sun and the selected star and then slewing the x flywheel until the star is picked up in the mobile tracker.

Starting from this attitude, which is unambiguous, the spacecraft can now be oriented in any desired direction by slewing appropriate amounts about the x and y axes. Use of the x and y gyros to monitor these attitude changes will limit errors to less than 1/2 degree. Gyro calibration described later in Chapter 5, Section VII, may under certain conditions be worthwhile in reducing errors.

4. Navigational Fix

The routine for making a navigational fix also begins by assuming the unambiguous orientation required while tracking the sun and a star. By sweeping around the sun-line while holding the sun in the body-fixed sun tracker, several objects are acquired and tracked by the mobile star/planet tracker. Typically these objects might be: the nearest planet, a second planet, and Sirius. If either planet has an apparent diameter greater than one milliradian, its center and possibly its apparent diameter would be determined using the disc scanning procedures. Thus the following navigational angles might be determined in order by noting sextant drive angles:

(a) sun to nearest planet center;

(b) apparent diameter of nearest planet;

(c) sun to second planet; and

(d) sun to Sirius.

Now Sirius might be transferred to the body-fixed sun/star tracker by the Transfer Tracking Mode of operation described in R-235. A planet is then located in the mobile tracker by slewing about the Sirius line. The angle between this planet and Sirius is then found. These five angles might constitute a representative case which is sufficient to complete the fix. Using these angle measurements the computer determines the required velocity increment and a correction to the clock.

5. Velocity Change

This routine begins by orienting the rocket engine thrust line in accordance with computer commands by using the same sequence of operations already described for the radio transmission. The engine is fired for a sufficient duration to provide the impulse called for by the computer monitored by the pendulous float accelerometer. During the thrusting period, attitude control is maintained by gimballing the engine or otherwise directing the thrust vector in order to null the CIGS gyro outputs. This routine, like all the others, is completed by returning the vehicle to its quiescent, energy-collecting mode of operation.

6. Mission Objective Routines

These routines will control the sequence of events required to accomplish the spacecraft's ultimate missions. It will most likely be initiated on the basis of observed positional data as well as clock time. Some of the sub-routines which may be involved are:

(a) spatial re-orientation to accomplish TV photography, probe ejection, etc;

(b) velocity change to accomplish atmospheric entry, transfer to satellite orbit, etc; and

(c) planetary disc scanning to monitor altitude above planet's surface.

It is perhaps true that, in addition to its primary role, the CIGS could profitably be used for other spacecraft functions. This is particularly true with regard to the digital computer which will be available most of its useful life for timing and sequencing signals, arithmetic computations, logical decision making, and malfunction analysis.

The final section of this chapter which follows is intended to support by engineering analyses the functional changes in guidance and control made over those methods proposed in R-235.

III. Revisions to System Functions Proposed in Report R-235

A. Use of Iodine Jet for Fine Angular Momentum Control

1. Background

Report R-235 proposed the use of solar vanes to provide the corrective torques necessary for fine angular momentum reduction (recall the assumption that course angular momentum reduction would be accomplished with the ship's rocket). Though the use of the solar vanes appears to permit efficient, reliable performance of the desired operation, further study into means for obtaining small external torques has resulted in at least a tentative preference for the sublimating iodine jet (described fully in Chapter 7). It will be seen that a single source of iodine vapor feeding two nozzles so as to provide a positive or negative torque about a single axis (the x-axis) is simpler and more adaptable to a multitude of vehicle configurations than the solar vane system, both with respect to electro-mechanical design and speed of application.

2. Mode of Operation

It is assumed that fine angular momentum reduction will be accomplished once per week, probably immediately prior to a radio transmission routine. In addition, fine momentum reduction will be accomplished promptly following course angular momentum reduction and immediately before and after each navigational velocity correction. This momentum reduction schedule permits the attainment of maximum accuracy in spatial orientation during radio transmission and velocity correction. Also by limiting the build-up of angular momentum the control flywheel duty cycle can be held below 1% during the major portion of the vehicle's voyage when it is tracking the sun and collecting solar energy. The proposed jet configuration, illustrated in Fig. 4-3, consists of two opposing nozzles which thrust in the y-z plane, thereby providing positive or negative torque about the x-axis only. This configuration results in a simple procedure and has the advantage that torques about the other axes can only result from thrust misalignments and center of mass shifts in the direction of the x-axis. Another advantage is that leakage thrusts tend to cancel each other. Other configurations, including a single nozzle design, were also studied and later discarded.

The first step in fine angular momentum $(\overline{H})$ reduction consists of measuring and reducing the component of $\overline{H}$ parallel to the sun-line. This is accomplished by sampling revolutions of the x-axis control flywheel over a time interval of approximately 30 seconds while the vehicle tracks the sun and a star (with the body-fixed sun tracker and mobile star tracker respectively). Wheel revolutions are measured by accumulating bits from digital pickoffs, as described in R-235 Chapter 6. The number of wheel revolutions during the sampling interval is an accurate indication of the desired $\overline{H}$ component ($H_{sun\ line}$), since the vehicle is not rotating and the time interval is sufficiently long to subdue the effects of unwanted bits (such as those due to noise and small vehicle oscillations). Through calibration data already stored, the computer commands the appropriate jet valve to open so as to exert a torque about the x-axis directed opposite to $H_{sun\ line}$. At the end of a computed thrusting interval, valve closure is commanded.

Because the jet thrust and vehicle inertia may have changed significantly since the previous calibration, much of the measured sun-line component of $\overline{H}$ may remain. Another measurement of this momentum component is therefore made to determine if it is yet below a specified criteria and to permit the computation of a calibration factor for the next reduction period. This factor is merely the ratio of positive torque duration to the measured reduction of wheel speed. It is expected that one or two repetitions of this step will render the sun-line component of $\overline{H}$ less than 0.4 bit/sec (or 0.001 deg/sec). The calibration procedure described effectively provides for the expected slow variations of jet thrust and vehicle momentum such as those due to temperature changes and fuel exhaustion.

The <u>second step</u> consists of measuring and reducing the component of $\overline{H}$ perpendicular to the sun-line. To accomplish this, the vehicle, which has been tracking the sun and a star, is turned -90 degrees about the y-axis so as to point the energy-collecting face (and z-axis) toward the sun. The sun is tracked with the sun finders in control of the x and y control flywheels in the damped, no-dead-zone mode of operation. The spacecraft is now stationary because sun tracking eliminates any average velocity about the x or y axes, and the previous step has resulted in negligible velocity about the z axis.

The x and y wheel revolutions are now sampled over a time interval of about 30 seconds, providing a measurement of H_x and H_y which is sufficiently free from errors due to unwanted bits. Since the jets can provide torque only about the x-axis, the vehicle is rotated through the angle, $\tan^{-1} H_y/H_x$, about the z-axis and the appropriate valve is actuated to provide torque directed opposite to the measured $\bar{H}$ component. The computer shuts off the jet upon the completion of a thrusting interval calculated proportional to $\sqrt{H_x^2 + H_y^2}$. As in the reduction of the sun-line $\bar{H}$ component, a test and calibration is then performed followed by another torque application if necessary.

The first step is now repeated to eliminate any momentum component in the sun-line direction which may have been introduced by the second step due to center of mass shifts in the x direction or thrust misalignments. After the first step is repeated, the total angular momentum should be less than that corresponding to 0.001 deg/sec of vehicle rotation. This can be checked by sampling all wheels to see that H_x, H_y and H_z are each sufficiently small. The spacecraft is now in the correct position (tracking the sun and a star) to initiate accurate spatial re-orientations.

It is obvious by reference to R-235 that the above procedure requires less time than the procedure employing solar vanes. The electro-mechanical simplicity and reliability of the iodine jet system system should be equally apparent.

3. Selection of Thrust Level

Several factors limit the range of suitable iodine jet thrust levels. A thrust level above this limiting band would have at least the following undesirable features:

(a) Interference with control flywheels: Since the jet will operate while the vehicle is held motionless by the control flywheels, it is important that its torque not be so large as to interfere with the stabilizing torque of the wheels (2.7×10^5 dyne-cm).

This consideration limits jet thrust to less than about 1000 dynes (assuming a moment arm of 60 cm).

(b) Excessive leakage: Reference to Chapter 7 will show that higher thrust levels are obtained using larger pressures and exit areas which would result in greater difficulties in restraining leakage. This leakage, if large enough, can result in very high propellant consumption rates and, possibly more important, the build-up of excessive angular momentum during the week between momentum reduction. If one makes a pessimistic assumption of leakage thrust one might expect a leakage torque to rated torque ratio of 1/100,000. Therefore, a reasonable requirement that weekly angular velocity build-up be less than 0.025 deg/sec limits thrust below 700 dynes.

(c) Value closure errors: The iodine jet control valve is of extremely simple construction in order to help achieve the necessary reliability and light weight. For this valve, an uncertainty in closure time of 0.01 sec is anticipated; thus, to maintain angular velocity below 0.001 deg/sec, thrust must be below 10,000 dynes.

Satisfactory thrust levels are also bounded at the lower extreme by several factors. For example, thrust below a certain level would be impractical because of fabrication tolerances, lack of repeatability, contamination problems, etc. Very small thrusts would also require excessive time for angular momentum reduction and hence would result in excessive power consumption and wear of equipment. It is evident that one should design as close as possible to the upper limit.

A thrust level of 400 dynes, at the maximum expected iodine temperature of $90^{\circ}F$, has therefore been selected for the proposed system. A lower internal temperature would result in lower thrusts; for example, thrust would be about 70 dynes at $50^{\circ}F$. The selection of 400 dynes also gives a safety factor of about two to allow for very high temperatures, in-flight reductions of moments of inertia, etc.

The following table lists some of the principal design features of the Iodine Jet system.

Thrust at 90^{o}F	400 dynes
Nozzle exit area	1.0 cm^2
Moment arm	60 cm
Vehicle inertia	6×10^8 gm-cm^2
Thrust duration to eliminate 0.1 deg/sec at 90^{o}F	45 seconds
Residual angular velocity	0.001 deg/sec
Weekly angular velocity build-up due to jet leakage	0.025 deg/sec
Angular velocity sampling interval (minimum)	30 sec
Design tolerance on thrust misalignment	±1 deg
System weight including 2 lbs iodine	3.2 lbs

Refer to Chapter 7 for a detailed description of the iodine jet.

B. Use of Gyros for Control of Spatial Attitude Changes

1. Summary

It appears that the CIGS gyros, already required for attitude control during rocket operation, should also be used to control spatial re-orientation about the transverse (x and y) axes. Errors less than 1/2% seem reasonable even without calibration. The amount of additional equipment required to utilize the gyros in this way is very small, being represented almost entirely by the pulse modulating circuit described below.

2. Background

Report R-235 proposed that spatial re-orientations be measured and therefore controlled by counting momentum control flywheel revolutions. It will be recalled that this operation would be controlled by the digital computer in the Counter Control Mode through which the vehicle is rotated about one axis at a time until prescribed wheel rotations are accumulated. The errors made in this mode of operation are primarily attributable to uncertainities in the knowledge of vehicle moments of inertia and the disturbing torques due to rotating equipment and propellant sloshing. Use of gyros for controlling spatial attitude changes would circumvent these problems, thereby making greater accuracy available. They would also make the system operation more independent of the particular spacecraft characteristics.

3. Mode of Operation

The system configuration studied is illustrated in Fig. 4-4 for either the x or y channel. It is not proposed to use a gyro for control about the longitudinal (z) axis because accuracy requirements are sufficiently relaxed not to warrant the addition of another gyro. Torque (T) is applied to the vehicle as before by acceleration or deceleration of the appropriate control flywheel. The gyro, being rigidly attached to the vehicle, senses changes in attitude (θ). Null operation of each gyro is maintained by using gyro output (displacement of the gimbal from null, A_g) to admit either positive or negative current pulses of amplitude I to the gyro torque microsyn so as to restore the float to its null position. The average current is just sufficient to provide the torque needed to balance the precessional moment due to vehicle rotation. Hence, accumulation of these pulses in a computer storage register provides a continuous knowledge of vehicle rotation. The computer then controls the flywheels in a fashion similar to that described in R-235 for the Counter Control Unit. The essential change over the system in R-235 is that rotation is measured by a gyro rather than by counting wheel revolutions. Note that the Counter Control Unit will no longer be required, for it has been found that the computer has sufficient speed to perform

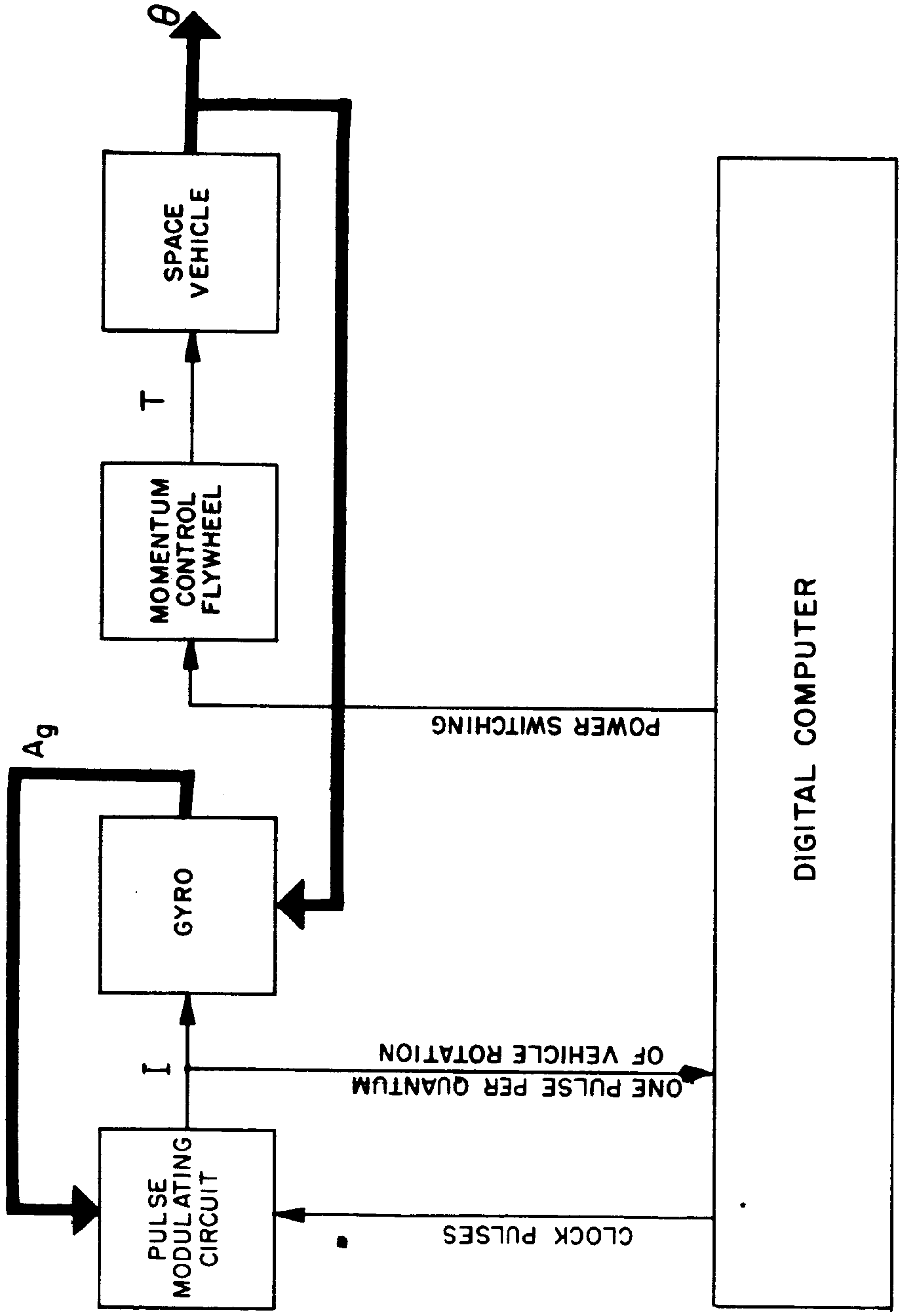

Fig. 4-4 Gyro-controlled spatial attitude control system.

the function of simultaneously counting the rotations and outputs of all space vehicle accessories.

4. Description of the Gyro

The MIT 16 IG gyro is proposed for use in the space vehicle guidance system. It would be modified by the use of a new flotation fluid, "Flouro-chem", which remains liquid in the expected ambient environment. It has been suggested in R-235 and in this report to mount the gyros, momentum wheels, and accelerometer in a hermetically sealed container inside of which an ambient temperature of 50-70°F is expected. In this environment the power dissipation within the gyro (2.5 watts) would maintain the unit at about 90°F without a temperature control system. In this crude application the gyro can be expected to have a drift rate of about 3 deg/hr. The unit weighs 5 oz and measures 1.600 in. diameter by 1.925 in. long.

5. Description of the Pulse Modulating Circuit

The pulse-modulating circuit is illustrated in Fig. 4-5. It is used to control the flow of precisely regulated current pulses to the gyros and accelerometer. The three inertial units, two single-degree-of-freedom gyros, and one pendulous accelerometer are restrained about their null positions. The restraining torques are either positive or negative as determined by the position of the flip-flop associated with the particular unit. With the flip-flop in one position, the current through the microsyn winding is in a direction to create a negative torque on the floated unit; the other flip-flop position creates a positive torque.

The secondary windings of the microsyn are connected in series to a constant-current source I_{DC}, as shown in Fig. 4-5. Besides providing the reference current for each microsyn, the secondary winding is also used to indicate the displacement of the float (A_g). Clock pulses, displaced in phase 1.0 milliseconds, sample each inertial unit in turn, leaving the torque in such a

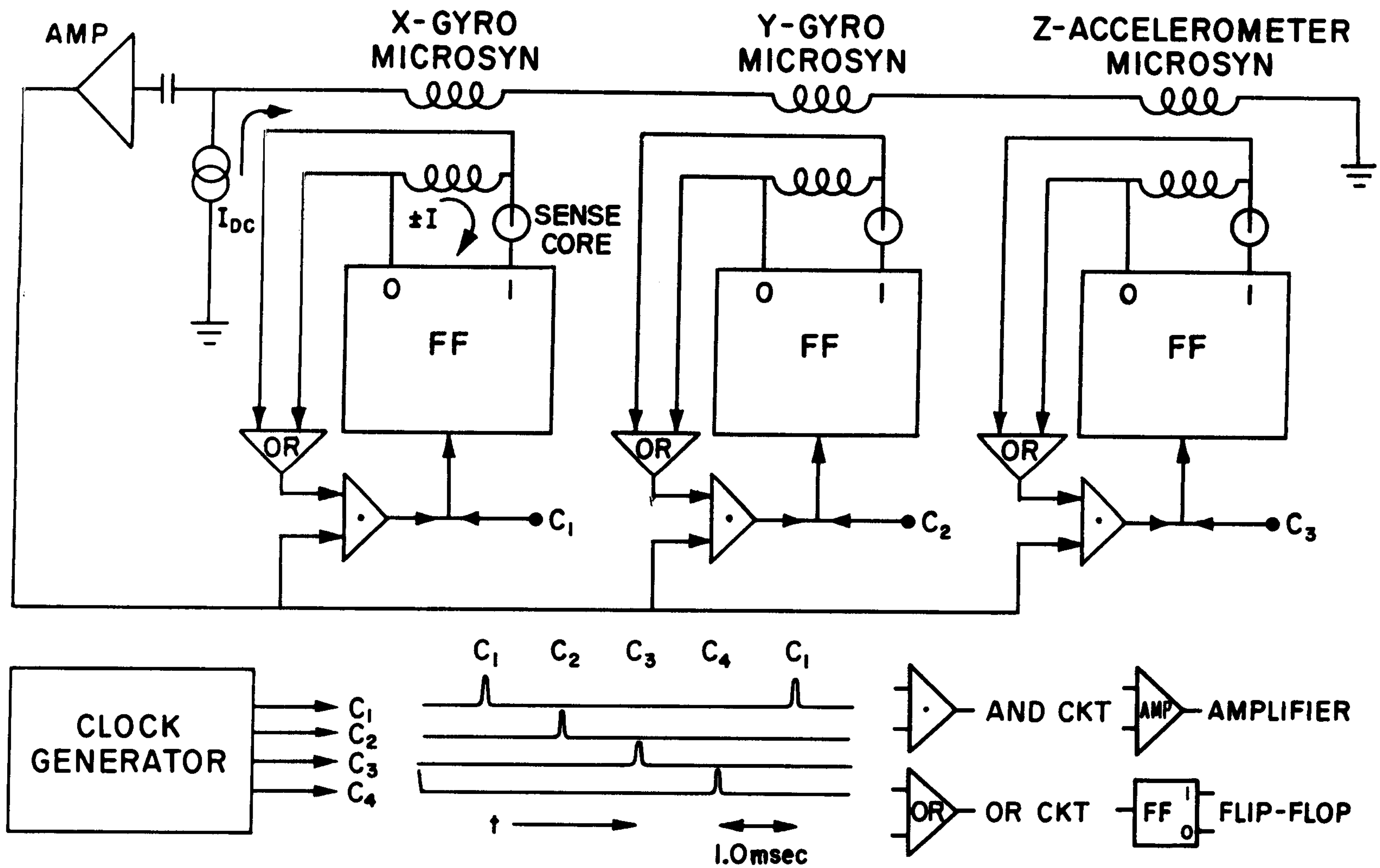

Fig. 4-5 Pulse-modulating circuit.

direction to drive the float towards null until the next sampling time. Sensing cores, shown in series with the microsyn windings, are available for interrogation by the computer which counts (integrates) the net torque pulses applied to each unit.

The total pulses for each gyro represent the total angle of vehicle rotation applied about the x and y axes, respectively. The total accelerometer pulses represent z-axis velocity change.

Operation sequence: Initially, clock pulse C_1 switches the state of the x-gyro flip-flop. This causes a large inductive voltage to appear across the primary winding of the x-gyro microsyn and the current starts decreasing. At the same time, a voltage is induced in the secondary winding which is proportional to the product of this large primary voltage and the error angle of the float, A_g. This effect is identical in operation to that of the ordinary signal-generator microsyn, with the exception that voltage steps, rather than sine waves, are applied to the primary of the microsyn.

The a-c amplifier senses the secondary output immediately after the flip-flop switches. Since the other microsyns have not been switched on C_1, no conflicting outputs occur from their respective secondaries.

The amplifier output following clock pulse C_1 is arbitrarily positive if the previous torque pulse did not succeed in driving the float through null. This positive output is directed to the "and" gates associated with each flip-flop of Fig. 4-5. Since only the x-gyro microsyn has a high induced voltage feeding the "or" gate, only the x-gyro "and" gate will pass the amplifier pulse. This pulse switches the flip-flop back to its previous position, thereby continuing torquing of the unit towards null until the next C_1 pulse.

In the alternate instance, where the float has been driven past null during the previous period, a zero or negative output

$$\Delta\theta = \frac{S_{tg}}{H} \int I \, dt = \frac{S_{tg}}{H} I \, \Delta t \, N,$$

where N is the net number of current pulses (number of positive pulses minus the number of negative pulses) of amplitude I and duration Δt. For the system under consideration one pulse corresponds to 0.008 degrees of vehicle rotation.

Fig. 4-6 illustrates the operation of the system when the vehicle is being rotated at 1 deg/sec. The following parameters have been used:

$$\frac{S_{tg}}{H} I = 2 \text{ deg/sec};$$

$$H = 10^4 \text{gm-cm}^2/\text{sec};$$

$$\frac{H}{C_d} = 1;$$

$$T_g = 0.001 \text{ sec; and}$$

$$\Delta t = 0.004 \text{ sec.}$$

These parameters can be obtained using the MIT 16 IG gyro unheated at the expected ambient temperatures.

7. System Errors

The precision current pulses will be regulated within about 1/2%. All other errors would then be negligible and spatial attitude changes should be accomplished with over-all errors of about 1/2%. It should be noted that coupling effects (due to rotations about the z-axis) are only negligible if fine angular momentum reduction has been accomplished prior to spatial reorientations. More accuracy can be achieved by calibrating the gyro.

C. Use of Torqued Floated Pendulum for Velocity Change Measurements

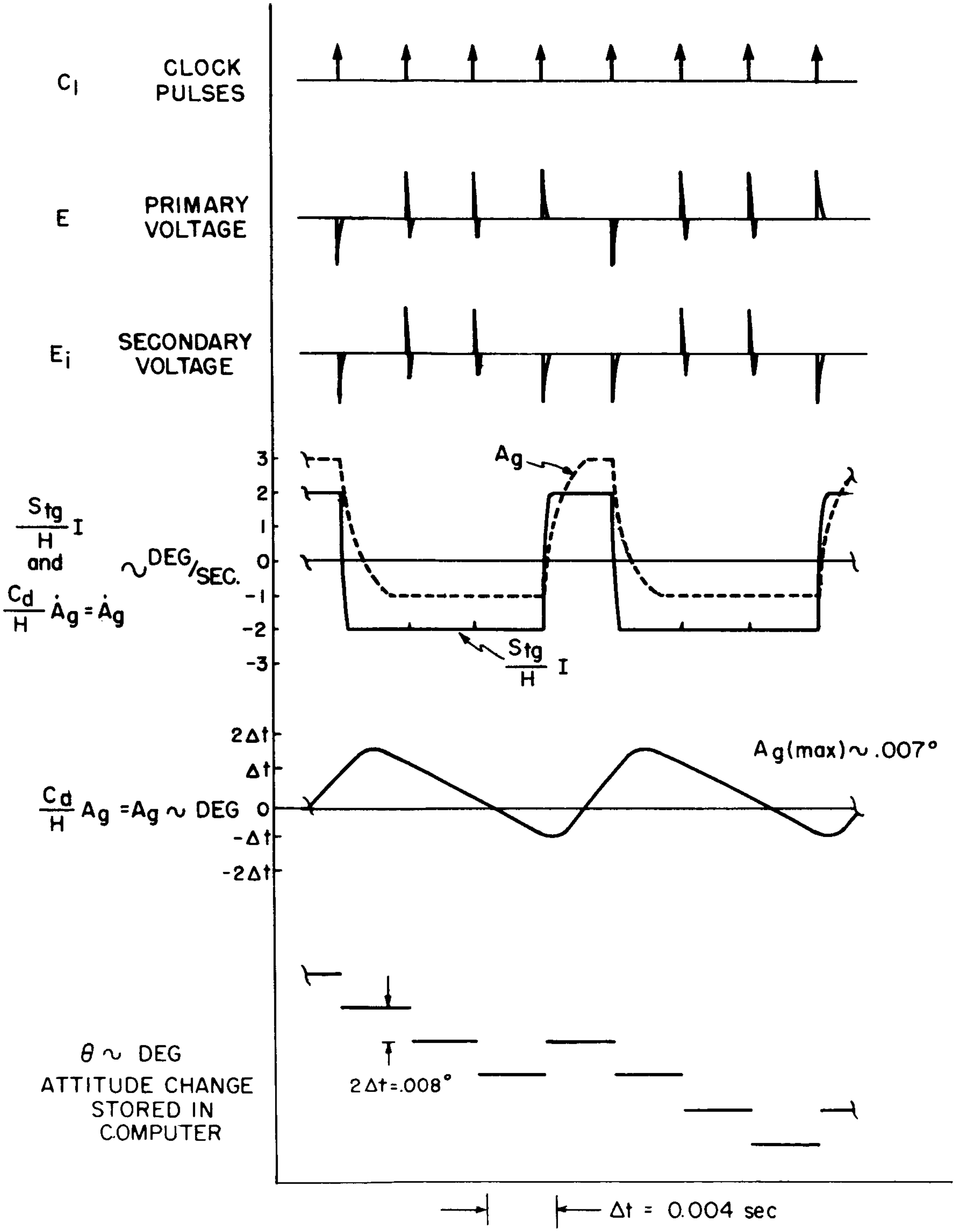

Fig. 4-6 Operation of the attitude control system during spatial re-orientation. Vehicle turning rate, $\dot{\theta}$, equals -1 deg/sec.

1. Summary

The extreme similarity between the floated integrating gyro and the floated pendulum (which is simply the former instrument without the spinning gyroscope wheel but with a small unbalance about the output axis) would almost seem to dictate their use together if at all. The economy of external circuitry thus permitted is amply shown in the preceding section where the pulse modulating circuit is described. Furthermore, the pulse-torqued floated pendulum is a proven component contrasted to the pendulous watch-movement accelerometer proposed in R-235. Therefore, it is felt that, should the pulse-torqued gyro be used for measuring spatial re-orientations, the pulse-torqued pendulum should be used also. If this does not turn out to be the case, experimental work would be required precedent to an intelligent selection.

2. Mode of Operation

The pulse-torqued floated pendulum would be used in a fashion completely similar to that already described for the pulse-torqued floated gyro. That is, in the presence of the torque due to acceleration on the unbalance mass, the instrument torque generator is supplied with positive or negative pulses as required to maintain the float at its null position. The average input current is then proportional to vehicle acceleration. Then the net quantity of current pulses is proportional to the velocity imparted by the spacecraft rocket engine.

3. System Dynamics

If we define ml as the unbalance about the instrument output axis, and use the other terms already defined, we obtain for the instrument equation:

$$T_g \ddot{A}_g + \dot{A}_g = \frac{S_{tg}}{C_d} I - \frac{ml}{C_d} \dot{V}.$$

Thus the pendulum responds in angular velocity about the output axis as a first order lag behind the input current and vehicle acceleration.

If the equation is integrated over a "long" period of time so that changes in $\dot{A}_g$ and $\ddot{A}_g$ are negligible, one obtains:

$$\Delta V = \frac{S_{tg}}{ml} \int I \, dt = \frac{S_{tg}}{ml} I \, \Delta t \, N,$$

where N is the net number of current pulses of amplitude I and duration Δt.

Response of the accelerometer to a constant input acceleration is exactly of the form shown in Fig. 4-6 for the pulsed gyro response to steady vehicle angular velocity.

By adjusting the instrument pendulosity, a wide range of scale factors are made available. Even if one uses a torque microsyn gain identical to that used in the gyros, one obtains a maximum available torque of 350 dyne-cm. For a reasonable pendulosity range of 0.1 to 10 gram-cm, the system is then capable of measuring peak accelerations of 3.57 to 0.0357 "g's" respectively. The corresponding current pulses would then represent 14 cm/sec to 0.14 cm/sec. The range of scale factors can be widened further by changing microsyn gain and current.

4. Velocity Measurement Error

This error is essentially determined by the regulation of current pulses and should therefore be about 1/2%, which is sufficiently small.

D. Thermal Control

A thermal control system is required to maintain acceptable temperature for the guidance equipment because of the large variation of incident solar energy during flight. Since the thermal-mechanical interface between the guidance system and spacecraft is unknown at this time, we have done no more

Thus the pendulum responds in angular velocity about the output axis as a first order lag behind the input current and vehicle acceleration.

If the equation is integrated over a "long" period of time so that changes in $\dot{A}_g$ and $\ddot{A}_g$ are negligible, one obtains:

$$\Delta V = \frac{S_{tg}}{ml} \int I \, dt = \frac{S_{tg}}{ml} I \, \Delta t \, N,$$

where N is the net number of current pulses of amplitude I and duration Δt.

Response of the accelerometer to a constant input acceleration is exactly of the form shown in Fig. 4-6 for the pulsed gyro response to steady vehicle angular velocity.

By adjusting the instrument pendulosity, a wide range of scale factors are made available. Even if one uses a torque microsyn gain identical to that used in the gyros, one obtains a maximum available torque of 350 dyne-cm. For a reasonable pendulosity range of 0.1 to 10 gram-cm, the system is then capable of measuring peak accelerations of 3.57 to 0.0357 "g's" respectively. The corresponding current pulses would then represent 14 cm/sec to 0.14 cm/sec. The range of scale factors can be widened further by changing microsyn gain and current.

4. Velocity Measurement Error

This error is essentially determined by the regulation of current pulses and should therefore be about 1/2%, which is sufficiently small.

D. Thermal Control

A thermal control system is required to maintain acceptable temperature for the guidance equipment because of the large variation of incident solar energy during flight. Since the thermal-mechanical interface between the guidance system and spacecraft is unknown at this time, we have done no more than lay out in a preliminary way what might be suitable system. This system, which assumes that one end of the guidance container will be sun-oriented most of the time, regulates the amount of collected solar power by controlling the ratio of heat-reflecting to heat-collecting area. Refer to Fig. 4-7 for a schematic diagram.

1. Temperature Control System

The temperature control system consists of a passive bi-metallic element as an actuator for "fan blade" shutters which move over and beneath heat collecting surfaces. The fan blades are reflecting surfaces with the same pitch as the corresponding heat collecting surfaces. For maximum heat input, the reflecting surfaces are completely under the collecting surfaces. For minimum heat input the reflecting surfaces are completely over the collecting surfaces. The bi-metallic actuator is located centrally in a position which adequately senses collecting plate temperature. The fan blades are supported only by the bi-metallic element, with limit stops at strategic places to prevent damage during booster operation.

Heat is conducted from the collecting surfaces to the guidance equipment through welds around the outer edge to the cylindrical case and through welds at one edge of each collecting surface to the end bulkhead.

2. Thermal Data

The following data describe the thermal properties of the cylindrical guidance package.

Material	aluminum
Cylinder length	22 in
Cylinder diameter	11 in
Cylinder wall thickness	0.1 in
Sunny end bulkhead thickness	0.1 in
Heat collector surface thickness	0.1 in

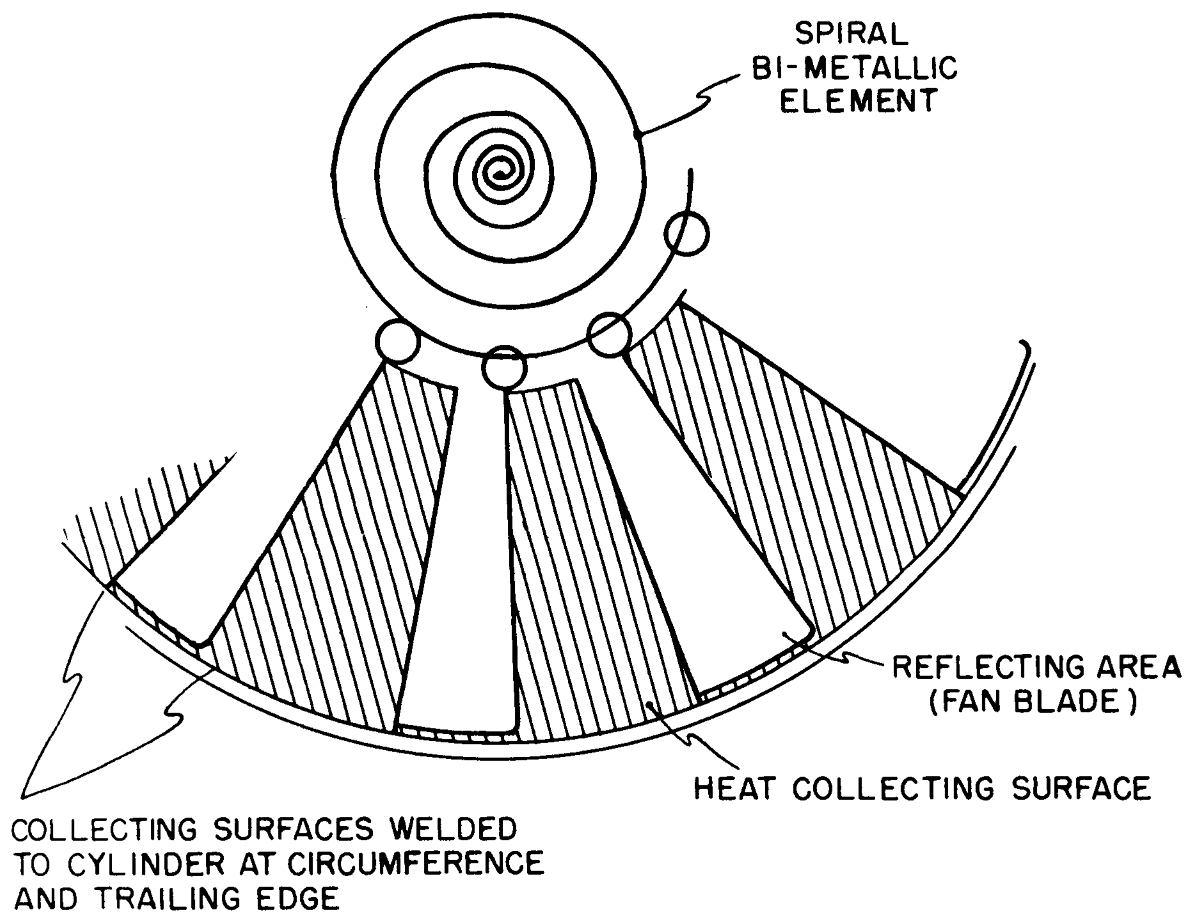

Fig. 4-7 Thermal control mechanism.

Surface Characteristics of thermal control surfaces:

Absorptivity of reflecting surface,	$\alpha_r = 0.1$
Absorptivity of collecting surface,	$\alpha_c = 0.9$
Emissivity of reflecting surface,	$\epsilon_r = 0.1$
Emissivity of collecting surface,	$\epsilon_c = 0.3$
Emissivity of surface areas not facing the sun,	$\epsilon = 0.05$

This configuration results in an average internal temperature of about 70°F at any point in space between Venus and Mars. The temperature difference between hot and cold sides will be about 12°F.

E. Control Flywheel Re-scaling

1. Summary

The control flywheels selected for the CIGS have an angular momentum of 10^7 gm-cm^2/sec at a synchronous speed of 12,000 rpm. Their hysteresis motors are sized to develop synchronous speed in 40 seconds which is just twice the run-up time proposed in R-235 for the interplanetary probe. Each wheel will then consume 50 watts of 400 cps power (75 watts of dc power before conversion) and develop 2.7×10^5 dyne-cm of torque.

2. Selection of Wheel Momentum

Each flywheel must have sufficient angular momentum to balance the spacecraft's momentum about the same axis while slewing. Spacecraft moments of inertia of 6×10^8 gm-cm^2 and slewing speeds of 1 deg/sec therefore set the wheel momentum at 10^7 gm-cm^2/sec. The preference for a hysteresis motor is justified in R-235, Chapter 9. The MIT 10 FG gyro rotor which develops 10^7 gm-cm^2/sec at 12,000 rpm was then selected as representative for the CIGS application.

Several factors lead to the requirement for a slewing speed of 1 deg/sec. Smaller slewing speeds would result in longer slewing times and therefore more stringent requirements for gyro drift rate during spatial re-orientations and planetary disk scanning. Slewing at 1 deg/sec permits us to accept a drift rate of about 3 deg/hr, which can be achieved without closed-loop temperature control and precise compensation of the gyro. Also, 1 deg/sec is an order of magnitude larger than the spacecraft angular velocities which, without the flywheels, would result from the reaction to rotating equipment, the influence of unwanted external torques and the unrefined performance of the attitude control system during rocket operation. Thus a 1 deg/sec slewing speed leaves a comfortable margin of safety in flywheel momentum-balancing capacity.

On the other hand a higher slewing speed does not appear to be warranted because more momentum-balancing capacity would be superfluous, and because the reduction of gyro drift errors would probably not justify the high price paid in terms of greater wheel size and power and increased computer sampling and counting speeds.

At least for the present purpose, a slewing speed of 1 deg/sec appears to be reasonable. A different wheel momentum might, of course, prove to be more suitable in real application.

3. Selection of Motor Torque

The determination of wheel run-up time or net torque leads to a consideration of the required electrical energy and power. For the motor size and type applicable here, power-to-torque ratios of the order of 2×10^{-4} watts per dyne-cm can be expected. A probable upper limit is about 10^6 dyne-cm, because of the space available for stator copper. Another general consideration is that high torques and consequently "large" spacecraft angular accelerations lead to "fast" dynamics, which in turn assure rapid completion of spatial re-orientations and quick settling of tracking oscillations. Thus, only a weak dependence of total energy requirements on selected torque might be expected.

Starting with the angular acceleration selected for the R-235 interplanetary probe it can be seen that 1/20 deg/sec^2 would necessitate a motor torque of 5.4×10^5 dyne-cm, which is approaching the upper limit on motor size. The required power would also be high - about 100 watts at the wheel or 150 watts delivered to the 400 cps power supply per wheel. Further examination leads to the selection of 1/40 deg/sec^2 and 2.7×10^5 dyne-cm for angular acceleration and torque respectively. These appear to be reasonable figures which lead to a comfortable motor size and only half the power levels just described. Slewing times are only slightly larger than for the higher torque case, being 130 sec for a 90 degree attitude change instead of 110 sec. Compared to the results shown in R-235, large tracking oscillations will require twice the damping times and will have steady-state periods $\sqrt{2}$ times as long for equivalent amplitudes.

Total energy needed for spacecraft mobility is then a little less than would be required at higher torques. Even smaller torque levels might be preferable, but, without more information on spacecraft characteristics, we are reluctant to consider smaller torques which might not be sufficiently large in comparison with interfering torques generated within the spacecraft.

F. Revised Power Estimates

The original power estimates in R-235 generally apply to the proposed guidance system except for the deletion of certain accessories and the increase in control flywheel power requirements.

Table 8-1 of R-235 is shown in revised form in Table 4-2. The control flywheel power has increased from 30 to 75 watts for each axis.

Table 4-3 is a revision of Table 8-II in R-235. The principal differences are due to the increased control flywheel power. The average monthly power required is 1.3 watts.

TABLE 4-3 ESTIMATED ENERGY BUDGET FOR ACTIVE GUIDANCE AND CONTROL

ROUTINE

Accessory	Power Watts	Course Angular Momentum Reduction: Time Minutes	Course Angular Momentum Reduction: Energy Watt-Min	Fine Angular Momentum Reduction: Time Minutes	Fine Angular Momentum Reduction: Energy Watt-Min	Navigational Fix: Time Minutes	Navigational Fix: Energy Watt-Min	Velocity Change: Time Minutes	Velocity Change: Energy Watt-Min	Radio Transmission: Time Minutes	Radio Transmission: Energy Watt-Min
Duration of Activity	—	7	—	40	—	72	—	46	—	30	—
Computer Medium Speed	0.7	7	5	40	28	72	50	46	32	30	21
x flywheel slew	75	2.2	165	4	300	35	2625	7	525	7	525
x flywheel damped	38			24	912	4	152	4	152	4	152
x flywheel undamped	75					15	1125	1	75	1	75
y flywheel slew	75			6	450	6	450	12	900	12	900
y flywheel damped	38			32	1216	32	1216	16	608	16	608
y flywheel undamped	75					20	1500	1	75	1	75
z flywheel slew	75			2	150	6	450	4	300	4	300
z flywheel damped	38			24	912	32	1216	14	532	14	532
z flywheel undamped	75					20	1500				
Sextant Drive	10			6	60	27	270	6	60	6	60
Tracker Motors and Circuitry	40			26	1040	50	2000	8	320	8	320
Sensing and Command	5	3	15	40	200	72	360	46	230	30	150
Gyros (incl circuitry)	10	5	50	40	400	65	650	46	460	30	300
Accelerometer	2.5							20	50		
Iodine Jet Valve	10			4	40						
Total Energy (Watt-Min)		235		5708		13,564		4,319		4018	
Times Used Per Month		—		4		1		1		4	

Total Monthly Energy Requirement: 57,000 Watt-Min or Approx 1 KWH

TABLE 4-2

ESTIMATED POWER REQUIREMENTS

Operation	Watts
Clock	0.1
Leakage in holding switches	0.15
Computer	
Low speed	0.01
Medium speed	0.7
High speed	50
Sunfinders	0.005
Control flywheels, each	75
Sextant drive	10
Tracker motors and circuitry	40
Sensing pickoffs	5
Gyros (2 wheels and circuitry)	10
Accelerometer	2.5
Iodine jet valve	10

TABLE 4-4

DORMANT POWER DISSIPATION

Operation	Watts
x-wheel 1/2% duty cycle	0.375
y-wheel 1/2% duty cycle	0.375
Sunfinders	0.001
Clock	0.10
Computer, standby	0.01
Leakage for holding switches	0.15
Total Average Power	1.01

Table 4-4 shows the revised dormant power consumption. This is essentially the same as Table 8-III of R-235 except that the flywheel power is higher and the power required for the clock and sunfinders is reduced.

The average power for both the dormant functions and the high-power functions of the vehicle is about 2.3 watts.